# IMPACT OF SOIL AND WATER CONSERVATION MEASURES ON IRRIGATION WATER QUALITY AND LULC CHANGES IN PERUMATTY PANCHAYATH

**BY**

**MIDHUN S (2020-02-033)**

**ANN MARIA PETER (2021-02-014)**

**MEENAKSHI MADHUMOHAN (2021-02-031)**

**NASLA SHARIN P (2021-02-035)**

**PROJECT REPORT**

Submitted in partial fulfilment of the requirement for the degree of

***BACHELOR OF TECHNOLOGY IN AGRICULTURAL ENGINEERING***

**Faculty of Agricultural Engineering and Technology**


**Kerala Agricultural University**

**DEPARTMENT OF SOIL AND WATER CONSERVATION ENGINEERING**

**KELAPPAJI COLLEGE OF AGRICULTURAL ENGINEERING AND FOOD TECHNOLOGY**

**Tavanur-679573, Malappuram**

**Kerala, India**

**2025**

## DECLARATION

We hereby declare that this Project entitled **"IMPACT OF SOIL AND WATER CONSERVATION MEASURES ON IRRIGATION WATER QUALITY AND LULC CHANGES IN PERUMATTY PANCHAYATH"** is a Bona fide record of the project work done by us during the course of study and that the report has not previously formed the basis for the award to us of any degree, diploma, associateship, fellowship or other similar title of another university or society.

Date: 31/05/2025

Place: Tavanur

**Midhun S**
**(2020-02-033)**

**Ann Maria Peter**
**(2021-02-014)**

**Meenakshi Madhumohan**
**(2021-02-031)**

**Nasla Sharin P**
**(2021-02-035)**

## CERTIFICATE

This is to certify that the project entitled **"IMPACT OF SOIL AND WATER CONSERVATION MEASURES ON IRRIGATION WATER QUALITY AND LULC CHANGES IN PERUMATTY PANCHAYATH"** is a record of the project work done jointly by **Mr. MIDHUN S (2020-02-033), Ms. ANN MARIA PETER (2021-02-014), Ms. MEENAKSHI MADHUMOHAN (2021-02-031)** and **Ms. NASLA SHARIN P (2021-02-035)** under my guidance and supervision and that it has not been previously formed the basis for the award of any degree, diploma, fellowship or associateship or other similar title of any other university or society to them.

Place: Tavanur

Date: 31/05/2025

**Guide**
Dr. Abdul Hakkim V M
Professor and Head
Dept. of SWCE
KCAEFT, Tavanur

**Co-Guide**
Er. Namitha M R
Assistant Professor (C)
Dept. of SWCE
KCAEFT, Tavanur

## ACKNOWLEDGEMENT

First of all, we offer million gratitude to God, the Almighty who made us to do this task and made every job a success for us.

Our diction would be inadequate to express our deepest sense of gratitude and heartfelt thanks to our project guide, Dr. Abdul Hakkim V. M., Professor and Head, Department of Soil and Water Conservation Engineering, KCAEFT, Tavanur. His level of guidance, constructive criticism and generous assistance at every stage of our project work is beyond measure, in fact it was the new idea and smooth dealing with the thing which motivated us to work under his guidance. It is our proud privilege to express our heartfelt indebtedness and deepest sense of gratitude for laying out the guidelines of project work. We have real admiration and regard for his whole hearted support and untiring help.

It is our pleasure to pay tribute to Dr. Jayan P R., Dean of Faculty and Professor & Head, Department of Farm Machinery and Power Engineering, KCAEFT, Tavanur, for his valuable advices and help rendered during this study.

We are highly indebted to our co-guide, Er. Namitha M R, Assistant Professor (C), Department of Soil and Water Conservation Engineering, KCAEFT, Tavanur for providing us with all the guidance and support during the entire project. We sincerely thank Dr. Shaheemath Suhara, Assistant Professor (C), Department of Soil and Water Conservation Engineering, KCAEFT, Tavanur for her valuable guidance and unwavering support throughout this project.

Our words of thanks to Dr. Dhalin D, Professor, Department of Farm Machinery and Power Engineering, KCAEFT, Tavanur and drivers of college vehicles for their timely support to arrange vehicle for doing the field work of our project work.

One last word, since it is practically impossible to list all contributions to our work, it seems proper to issue a blanket of thanks for those who helped us directly or indirectly during the course of our study.

Midhun S
Ann Maria Peter
Meenakshi Madhumohan
Nasla Sharin P

# DEDICATED TO OUR AGRICULTURAL ENGINEERING PROFESSION

**CONTENTS**

## LIST OF FIGURES

## LIST OF TABLES

## LIST OF PLATES

# INTRODUCTION

# CHAPTER I

# INTRODUCTION

Soil is at the interface between the atmosphere and lithosphere (the mantle of rocks making up the Earth's crust). It also has an interface with bodies of fresh and salt water (collectively called the hydrosphere). The soil sustains the growth of many plants and animals, and so forms part of the biosphere (White, 2005).

Nutrient deficiencies, soil acidity, structural instability or a soil's susceptibility to erosion can affect the growth of natural vegetation and agricultural crops. Other conditions that can severely limit the productivity of agricultural land are a high concentration of soluble salts, salinity and excess soil water, waterlogging. An excess of precipitation over evaporation for several months each year, impermeable subsurface layers and high groundwater tables, separately or combined, induce soil waterlogging and the attendant problems of inadequate aeration for root growth and soil microbial activity, poor trafficability of the soil for machinery and animals with the danger of surface structural collapse and 'poaching', invasion by flood-tolerant weeds e.g. sedges and rushes and an increase in animal parasites and diseases favoured by wet conditions and slow warming of the soil in spring (White, 2005).

The causal climatic factors are beyond control, but an improvement in soil drainage does much to mitigate these ill effects. On the other hand, in areas of high evaporation, serious problems occur when the water table rises to within 2 m of the soil surface and salinization occurs due to the upward movement and evaporation of saline groundwater. Such a situation may arise when the steady-state equilibrium of a soil's hydrology is disturbed by natural events, such as earth movements (faulting) or long-term climatic change (usually over a time span of centuries), or by man's intervention through changing the land use or supplying irrigation (usually a time span of decades). Problems associated with hydrological disturbances, and their solutions, fall into two main categories; soils not initially saline, with deep water tables, which become saline under irrigation or due to a change in land use and soils already salinized and of limited cropping potential, but requiring careful management to avoid chemical and physical deterioration under irrigation (White, 2005).

Access to the world's water resources is largely governed by the dynamics of the water cycle. Approximately 40% of the water that reaches the Earth's surface flows

into creeks, rivers, aquifers, wetlands, lakes, and reservoirs before eventually evaporating or transpiring back into the atmosphere. Human consumption patterns show that around 70% of this accessible freshwater is used for agriculture, 20% for industrial activities including energy production, and only 10% for direct domestic use (UNEP, 2011).

Given that irrigated agriculture alone contributes to 40% of the global food supply, improving water productivity in this sector is essential. This would help reallocate water for other crucial needs without harming food security or the environment. However, the diversity of water bodies—from large transboundary river systems to small local catchments—requires context-specific management strategies. Effective water governance is further complicated as water is reused and transferred across regions. For example, when efficient irrigation technologies are promoted, decision-makers must determine whether the saved water should be used to expand agricultural activities or be returned to its source, such as a river or aquifer. If not properly managed, this can lead to reduced water availability and quality for other users and ecosystems (Kılıç Z, 2020).

Additionally, rising global population and increased per capita water use are exerting pressure on freshwater resources and biodiversity. Factors like rainfall patterns, temperature, evaporation, soil type, vegetation, and surface runoff significantly influence water availability at local and regional levels. Water use has surged nearly sevenfold over the last century, while potable water availability continues to decline due to pollution, unplanned urban expansion, population growth, and unsustainable practices (Kılıç Z, 2020). Misuse in agriculture, poor recycling systems, pesticide overuse, and the effects of climate change all contribute to this growing crisis. Furthermore, unconscious water consumption habits deprive ecosystems and future generations of this vital resource. Thus, ensuring sustainable and efficient water use—especially in agriculture—must remain a top global priority to meet the needs of both people and the planet.

The ultimate goal of soil and water conservation is to ensure maximum sustainable productivity from a given land area while maintaining soil loss below the threshold limit. This threshold represents the equilibrium between the natural rate of soil formation and soil erosion (Suresh, 2012). Conservation practices aim not only to

minimize erosion and nutrient loss from agricultural land but also to protect water quality by preventing sediment and agrochemical runoff into nearby water bodies. Furthermore, reducing sedimentation in reservoirs, rivers, canals, and drainage ditches plays a vital role in maintaining the capacity and function of these water resources.

On arable lands, conservation strategies are implemented to prevent both water and wind erosion, while also ensuring adequate soil moisture for sustainable crop production. The design and selection of these measures depend on factors such as soil type, topography, rainfall intensity, and wind characteristics. Conservation approaches are broadly classified into biological and mechanical measures. Biological measures involve using vegetation, crops, and agronomic practices to control erosion and enhance soil health, while mechanical measures involve engineering structures designed to reduce runoff, control erosion, and promote water infiltration. Typically, mechanical measures serve as the first line of defence by immediately arresting soil erosion and managing surface water, while biological measures complement these by providing long-term stability and ecological balance (Singh, 2023).

Four land capability classes namely V, VI, VII and VIII have one or more limitations of slope, erosion, stoniness, rockiness, shallow soils, wetness, flooding, etc. which make them usually unsuited for crop production. Their use is mainly limited to pasture, forest, wildlife and recreation. These lands are generally confined to the upper reaches of watershed and have an undulating topography and are foci for soil erosion. In lands with steep slopes and subjected to soil erosion, vegetative covers do not establish. Due to lack of vegetative cover soil erosion is accelerated transporting large amounts of sediment into the streams below. The uncontrolled runoff from the sloping lands also causes extensive damage in lower reaches of watersheds. In order to prevent degradation of these lands, vegetative and mechanical measures are employed together and are complimentary to each other. Mechanical measures act like the foundation of a building whereas the vegetative measures act like a superstructure which helps in improving the productivity of non-arable lands. These lands have a great potential for producing fodder, fuel, minor forest produce, fruits and low-quality timber. It is essential to treat these lands with suitable location specific soil and water conservation measures. The practices such as contour trenching, grading, installation of temporary and permanent structures for gully control, construction of sediment retention structures and retaining walls, reclamation of ravine lands, improvement and management of

grasslands and rehabilitation of mined lands can be adopted for soil and water conservation measures in non-arable areas of watershed (Singh, 2023).

The last half century has seen the development and use of different remotely sensed vegetation indices. The basic assumption behind the development and use of these indices is that some algebraic combination of remotely-sensed spectral bands can reveal valuable information such as vegetation structure, state of vegetation cover, photosynthetic capacity, leaf density and distribution, water content in leaves, mineral deficiencies and evidence of parasitic shocks or attacks (Jensen 2009, Liang 2005). NDVI is one of the standard and frequently used methods of estimating C-factor through satellite remote sensing (RS) for estimation of soil erosion at regional scale.

NDVI is a satellite product that measures the vigour and greenness of vegetation on the earth's surface. It is calculated as the ratio of visible spectral wave bands to near infrared spectral wave bands. Healthy, green vegetation has a high presence of chlorophyll pigment, which causes low reflectance in visible wave bands and high reflectance in near-infrared wave bands. The reverse is true in vegetation under stress. NDVI is a unitless index, with values ranging from -1 to 1. Healthy vegetation has the highest positive values, while bare soil, water, snow, ice, or clouds have NDVI values of zero or that are slightly negative. Vegetation under stress or with a small leaf area has lower positive NDVI values. Typically, the NDVI values from healthy vegetation will increase as plant cover in-creases at the beginning of the growing season, reach a peak sometime during the middle of the growing sea son, and will then decrease as the season comes to its end (Mkhabela *et al.,* 2011).

In addition to evaluating land and vegetation conditions, a comprehensive assessment of conservation effectiveness also requires attention to water-related parameters. Water plays a vital role in sustaining agricultural productivity and ecological balance, particularly in areas where soil and water conservation measures are implemented. Assessing the quality of water resources is crucial for understanding their suitability for irrigation, domestic use, and environmental health. The Water Quality Index (WQI) serves as an effective tool to simplify complex water quality data into a single numerical value, making it easier to interpret and communicate findings to policymakers and stakeholders (Brown *et al*., 1970).

The Water Quality Index (WQI) model has emerged as a widely used tool for evaluating surface water quality. This model aggregates a range of water quality parameters and transforms them into a single value or index, making the interpretation of data more straightforward. The process generally involves four key stages: selecting relevant water quality parameters, generating sub-indices for each, assigning weights to each parameter, and finally aggregating these sub-indices to compute the overall water quality index. WQI effectively combines different parameters such as pH, dissolved oxygen, and turbidity into a single value that represents the overall condition of a water source. This unified score helps assess whether water is suitable for specific purposes including drinking, swimming, irrigation, or supporting aquatic life. It simplifies complex technical data into a more accessible form for a variety of stakeholders, including policymakers, environmental agencies, and the general public. The index also facilitates monitoring of changes in water quality over time and allows comparisons across different water bodies or geographic regions. Furthermore, WQI supports decision-making by helping to identify polluted areas, plan water management strategies, implement pollution control measures, and evaluate the effectiveness of environmental regulations (Arab *et al.*, 2019)

In rural areas, the significance of WQI is particularly noteworthy. Many rural communities depend on untreated water sources such as wells, rivers, and ponds. WQI offers a practical means to determine whether these sources are safe for consumption, thereby preventing waterborne diseases like diarrhoea, cholera, and typhoid. Since rural regions often lack the technical infrastructure to conduct detailed assessments, the simplified output of WQI proves especially beneficial. It helps local health workers, villagers, and community leaders understand water quality and make informed decisions. Farmers also benefit, as they can determine whether water is safe for crops and livestock, thus preventing soil degradation and animal health issues. Additionally, WQI can serve as an early warning system, detecting contamination from septic systems, agricultural runoff, or industrial waste before major health problems arise. It supports planning and policymaking by enabling local authorities and NGOs to prioritize areas for treatment and sanitation. Importantly, WQI results can also be used for community education, raising awareness about the value of clean water and encouraging efforts to protect water sources (Uddin *et al.,* 2022).

The rural areas of Perumatty Panchayat, in particular, are experiencing challenges related to clean water availability. A study was therefore initiated to analyse water quality in this region. Thirteen water samples were collected from four micro-watersheds Sarkarpathi, Mullanthodu, Kambalathara- Kalyanappetta, and Muthuswamy to assess the quality of both irrigation and drinking water. The community in Perumatty primarily relies on a method called "Kokkarni," which involves extracting groundwater and pumping it into open wells using external motors. This water is used both for irrigation and, to some extent, for drinking purposes. The main objectives of the study are to evaluate the water quality in this area using the WQI method and to provide a comprehensive understanding of the issues faced by local residents. The WQI will help identify which regions have cleaner water sources, free from excessive mineral deposits or pollutants that could potentially harm human health or vegetation. Based on the collected data, appropriate solutions can be recommended to address the challenges and ensure stable irrigation conditions for the people of Perumatty. The present study was carried out to assess the impact of soil and water conservation measures on irrigation water quality and LULC changes in Perumatty Panchayath. The specific objectives of the study are:

1. To determine the morphometric parameters of the study area.
2. To assess the impact of soil and water conservation measures on LULC and NDVI in the study area using Remote Sensing and GIS.
3. To assess the water quality of the study area based on Irrigation Water Quality Index using various interpolation methods in ArcGIS.
4. To analyse the effect of LULC on IWQI of the study area.

# REVIEW OF LITERATURE

# CHAPTER II

# REVIEW OF LITERATURE

## 2.1 WATERSHED

The word watershed is used for a small basin or a small catchment representing a hydrological unit which drains all its rainwater into a stream. A watershed containing large amounts of vegetation is considered as a healthy watershed. It is also called a well-managed or a green watershed. It has no or very limited soil erosion and also it has large reserves of groundwater as well as surface water. In general, it has most of its natural resources conserved.

Vegetation or plants play a vital role in conserving the natural resources of a watershed such as soil and water. The underground components of the plants such as roots spread within the soil and thereby stabilize and reinforce the soil. This generally leads to soil conservation. The water infiltrates below the ground through the voids in the soil as well as through the interface between the root surface and the soil.

The scope of watershed management involves all the actions and programs aimed at achieving an overall balance between utilization and conservation of natural resources in a watershed. It represents a sustainable approach for resource conservation through watershed management (Kato *et al*., 2009).

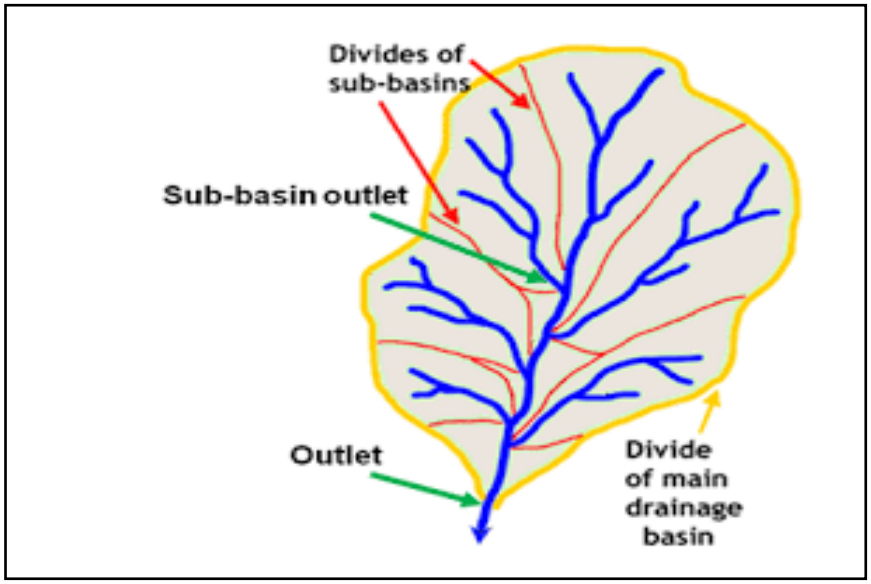


**Fig. 2.1. Watershed and its components**

### 2.1.1 Watershed management programs in India

Organized watershed development in India began in the 1950s with the establishment of Soil Conservation Research Demonstration and Training Centers (SCRDTCS) under the First Five-Year Plan. Key initiatives followed, including small experimental watersheds (1956) and the River Valley Project (1961-62) to prevent reservoir siltation. The 1970s-80s saw major programs like DPAP (1973-74), DDP (1977-78), and the Sukhomajri model in Haryana. In 1987-88, the Planning Commission adopted the watershed approach for WGDP and HADP. During the 1990s, international support boosted programs like NWDPRA (1991) and IWDP (1995). The 2000s saw further expansion with Haryali guidelines (2003), NRAA (2006), and MGNREGA-based projects. By 2005, 28.53 M ha of degraded land had been restored. In 2008, NRAA introduced common watershed guidelines. Watershed management remains vital for India's land restoration, water conservation, and sustainable rural development (Kato *et al*., 2009)

#### *2.1.1.1 Problems and constraints in watershed management*

Watershed management in India faces several challenges, including land degradation and soil erosion, which have worsened due to uncertain rainfall and poor economic conditions, limiting farmers' investments. Inequitable benefit sharing affects women, marginal farmers, and landless laborers, while upstream water harvesting often reduces downstream availability. Poor management leads to water shortages, seasonal droughts, and inadequate re-vegetation of common lands, affecting livestock and ecosystems. Additionally, conflicts among government ministries, lack of impact assessment data, and neglect of tribal areas further hinder effective watershed development. Addressing these issues is crucial for sustainable water and land resource management in India (Kato *et al*., 2009)

#### *2.1.1.2 Opportunities in watershed management*

Despite challenges, watershed management offers significant opportunities for sustainable development. It enables better food production while preserving the environment through organic farming, afforestation, and efficient irrigation. Regulating groundwater extraction and ensuring balanced upstream-downstream water use can prevent resource depletion. Cost-effective, low-cost traditional technologies and community participation can enhance long-term sustainability. Scaling up successful

small-scale projects, investing in research and technology, and preserving common resources like water, forests, and agriculture can improve rural livelihoods. Additionally, reducing migration by boosting rural employment and agricultural resilience can further strengthen watershed management efforts in India (Kato *et al*., 2009).

### 2.1.2 Methods to measure the effectiveness of soil and water conservation measures

Evaluating the effectiveness of soil and water conservation (SWC) measures is essential for assessing their impact on soil erosion control, water retention, and agricultural productivity. Various methods are employed, ranging from direct field measurements to modeling and socioeconomic assessments. The following are some key approaches used to measure the effectiveness of SWC interventions.

#### *2.1.2.1 Sediment yield measurement*

Sediment yield measurement is one of the most reliable ways to assess the effectiveness of SWC measures in reducing soil erosion. This method involves comparing sediment loads in runoff from treated and untreated areas using tools such as sediment traps, erosion pins, silt fences, and weirs. Araya *et al*. (2015) conducted a study in Ethiopia and found that the installation of check dams resulted in a 68% reduction in sediment yield, demonstrating the effectiveness of these structures in reducing soil loss and enhancing land stability.

#### *2.1.2.2 Runoff measurement*

Runoff measurement helps determine how SWC measures influence water movement across landscapes by assessing differences in runoff volume between conserved and non-conserved areas. Instruments such as rain gauges, runoff plots, and water level recorders are commonly used for this purpose. Kato *et al*. (2009) investigated the impact of terracing in Japan and found that it significantly reduced peak flow rates, thereby preventing excessive runoff and improving water retention in agricultural fields.

#### *2.1.2.3 Soil moisture monitoring*

Soil moisture monitoring evaluates how SWC measures improve water retention in the soil, which is crucial for plant growth and drought resilience. This

method involves the use of tensiometers, neutron probes, and time-domain reflectometry (TDR) devices. Rockström *et al*. (2003) found that contour bunds increased soil moisture by 30% in semi-arid regions of Africa, leading to improved crop yields and reduced vulnerability to dry conditions. This highlights the role of SWC measures in enhancing soil water availability and sustaining agricultural productivity.

#### *2.1.2.4 Soil erosion modeling*

Soil erosion modeling is an advanced method used to predict and evaluate the impact of SWC interventions under different land management scenarios. Various models, including the Revised Universal Soil Loss Equation (RUSLE), the Water Erosion Prediction Project (WEPP), and the Soil and Water Assessment Tool (SWAT), are widely used. García-Ruiz *et al.* (2015) applied RUSLE to assess the effectiveness of stone bunds in Spain and found that these structures significantly reduced soil loss, reinforcing the value of modeling approaches in erosion control planning.

#### *2.1.2.5 Remote sensing and GIS-based assessment*

Remote sensing and Geographic Information System (GIS) techniques provide spatial and temporal analysis of SWC measures' effectiveness across large landscapes. These methods utilize satellite imagery, aerial photography, and GIS tools to assess land cover changes, vegetation dynamics, soil moisture variations, and erosion patterns. Studies such as those by Zerihun *et al*. (2018) have demonstrated how remote sensing and GIS help in monitoring SWC impacts, identifying erosion-prone areas, and evaluating land management interventions. The integration of high-resolution satellite data and GIS-based modeling offers a cost-effective and scalable approach to assessing SWC performance over time.

## 2.2 WATERSHED DELINEATION AND MORPHOMETRIC ANALYSIS FOR HYDROLOGICAL INSIGHTS

### 2.2.1 Watershed delineation

All the points that drain water into the outlet defines the watershed’s boundary. In hydrologic design, a watershed’s delineation is important. Understanding which locations within the watershed contribute water to the outlet is essential. A watershed’s boundary is delineated by the most extreme of these points. Therefore, it is essential to

show how a watershed's boundary is defined. Using the Survey of India's toposheets and identifying the ridge lines, watershed can be delineated.

The drainage network of the Ithikkara River Basin, a sixth-order tropical river basin, was retrieved from a variety of sources, including digital elevation data from the Advanced Spaceborne Thermal Emission and Reflection Radiometer (ASTER) (30 m) and Shuttle Radar Topography Mapping Mission (SRTM) (90 m), as well as topographic maps from the Survey of India (1: 50,000; TOPO). The accuracy of drainage networks obtained from digital elevation models (DEMs) for hydrologic applications and terrain characterization was assessed by estimating basin morphometric features. With a small overestimation of lower order streams, the stream networks obtained from ASTER and SRTM DEMs exhibit a high degree of agreement with TOPO's. According to the study, SRTM outperforms ASTER in drainage delineation and basin morphometry, even with its coarser spatial resolution. Additionally, spatial variance in elevation, raster grid size, and vertical precision of the DEMs, as well as the incapacity of the surface hydrologic analysis algorithms in the GIS platform, may be responsible for the variability of basin morphometry among the data sources (Thomas & Prasannakumar, 2015).

Watershed delineation is a crucial step in hydrological studies, enabling effective water resource management, flood control, and land-use planning. Geographic Information Systems (GIS) and Remote Sensing (RS) have significantly improved the accuracy and efficiency of watershed boundary identification and morphometric analysis. Studies have demonstrated the effectiveness of using Digital Elevation Models (DEMs) for extracting watershed characteristics, including stream networks, drainage basins, and hydrological parameters. Advanced GIS-based tools, such as Arc Hydro and HEC-HMS, facilitate the automatic delineation of watersheds, reducing manual errors and increasing precision in hydrological modelling (Visharolia *et al.,* 2017). Research has shown that the integration of DEM, hydrological models, and morphometric analysis can provide insights into surface runoff, erosion susceptibility, and groundwater recharge potential, making watershed delineation a fundamental aspect of sustainable water management.

Using 30 m SRTM DEM, 150 sub-watersheds were created for the Bangalore South region. First, raster elevation data is used to extract the outflow sites. A modified

D8 method is used to determine the flow direction. Using a position matching technique, the outlets and flow direction are integrated to extract the stream network. Strahler's algorithm is used to determine the stream order. The stream linkages are taken into consideration while creating the sub-watersheds for certain mouth sites. When compared to the conventional D8 algorithm, the flow direction accuracy is 95.45 %. The suggested method's overall stream order accuracy, when compared to the accuracy of the Arc hydro and SWAT tools, is 91.83 % (Sowmya *et al.,* 2020).

Using ArcGIS software, Ping *et al*. (2024) sought to determine how well three different DEMs (Contour-based DEM, SRTM DEM, and IFSAR (Interferometric Synthetic Aperture Radar) DEM) defined catchment regions in different places. With less than a 3.5% variation in the defined catchment regions across all tested locations, the study found that both contour-based DEM and SRTM DEM were good substitutes for IFSAR DEM. When compared to the Contour-based DEM, the SRTM DEM performed better than the other options, demonstrating more accuracy as seen by lower Root Mean Square Error (RMSE) values.

### 2.2.2 Characterization of watershed using morphometry

Morphometric analysis is a fundamental approach for watershed characterization, as it provides quantitative insights into the hydrological and geomorphological behaviour of a basin. Rekha *et al*. (2011) conducted a detailed morphometric study of the Peruvanthanam sub-watershed in the Manimala River Basin, Kerala, using GIS and remote sensing techniques to assess linear, relief, and aerial morphometric parameters. Their analysis revealed that the watershed exhibits high drainage density (3.36), high stream frequency (6.15), and a low elongation ratio (0.58), indicating high runoff, steep slopes, and low infiltration capacity. Additionally, bifurcation ratio (3.18) suggested minimal structural disturbances, while ruggedness number (3.02) highlighted the watershed's complex topography. The study prioritized nine micro-watersheds based on their water-holding capacity and erosion susceptibility, identifying zones requiring conservation interventions. Their findings emphasize the critical role of morphometric analysis in watershed management, aiding in soil erosion control, groundwater recharge planning, and flood mitigation strategies.

Morphometric analysis is essential for understanding the hydrological behaviour of watersheds, influencing runoff potential, infiltration capacity, and

drainage network development. Sukristiyanti *et al*. (2018) conducted a comprehensive review on watershed-based morphometric analysis, emphasizing its significance in watershed planning and management. Their study highlighted that parameter such as drainage density, bifurcation ratio, elongation ratio, circularity ratio, and relief ratio help in classifying watersheds based on their shape and hydrological response. They found that elongated watersheds, which have high relief and high drainage density, tend to be more prone to erosion, while circular watersheds with lower relief are more susceptible to flooding. The study also pointed out the lack of a standardized classification for certain morphometric parameters, leading to inconsistencies in interpretation. Additionally, they emphasized the importance of input data quality, noting that variations in DEM resolution and mapping scales can significantly impact morphometric analysis accuracy. Their findings suggest that integrating morphometric analysis with GIS and remote sensing techniques enhances watershed characterization, aiding in hydrological modelling, flood management, and conservation planning.

Morphometric analysis is an essential tool for understanding watershed characteristics, influencing hydrological responses, erosion potential, and flood susceptibility. Bajirao *et al*. (2019) reviewed the application of remote sensing and GIS in morphometric analysis, emphasizing their efficiency in delineating watershed boundaries, drainage networks, and topographical features. Their study highlighted the significance of linear, areal, and relief parameters, including stream order, drainage density, elongation ratio, and relief ratio, in assessing watershed behaviour. They found that high drainage density and relief ratios indicate regions prone to higher surface runoff and erosion, while elongated watersheds tend to have longer peak times, reducing flood risks. The study also underscored the advantages of DEM-based GIS analysis over conventional methods, allowing for highly accurate and time-efficient morphometric assessments. Their findings support the integration of morphometric parameters with hydrological modelling, aiding in watershed prioritization, soil conservation planning, and artificial recharge site identification.

Morphometric analysis is a key tool in understanding the hydrological behaviour of a watershed, aiding in flood risk assessment, soil erosion control, and groundwater potential evaluation. Mangan *et al*. (2019) conducted a morphometric study of the Nanganji River Basin in Tamil Nadu, India, using remote sensing and GIS techniques to assess various linear, relief, and aerial parameters. Their study employed

Strahler's stream ordering system and analysed 16 morphometric parameters across 35 sub-basins. A factor analysis approach was used to classify these sub-basins based on three dominant factors: basin magnitude, runoff potential, and shape characteristics. The findings indicated that sub-basins influenced by basin magnitude exhibited larger drainage areas and stream lengths, while sub-basins controlled by runoff parameters showed higher drainage density and lower infiltration capacity, making them more prone to erosion and flash floods. Additionally, the study found a strong negative correlation between drainage density and channel maintenance, emphasizing the role of geological and climatic conditions in shaping watershed hydrology. These insights demonstrate the effectiveness of GIS-based morphometric analysis in watershed characterization, providing valuable information for sustainable water resource management and conservation planning.

Morphometric analysis is a fundamental approach for understanding the hydrological response of watersheds and their influence on hydrograph parameters. Tunas *et al*. (2020) conducted a study on eight watersheds in Central Sulawesi, Indonesia, to analyse the relationship between key morphometric parameters—watershed area, main river length, main river slope, and form factor—and hydrograph characteristics such as peak time ($T_P$), peak discharge ($Q_P$), and base time ($T_B$). Their findings indicated that watershed area (A) had a strong positive correlation with peak discharge ($Q_P$) ($r = 0.98$), demonstrating that larger watersheds generate higher peak flows. Similarly, main river length (L) was found to have a significant correlation with peak time ($T_P$) ($r = 0.99$), suggesting that longer river networks delay the time to peak discharge. However, main river slope (S) and form factor ($F_B$) showed weak correlations with hydrograph parameters, indicating that their influence might be less significant or dependent on other factors. The study emphasized the role of GIS and DEM data in accurately extracting morphometric attributes, allowing for a better understanding of watershed behaviour in runoff generation and flood risk assessment. These findings contribute to the refinement of synthetic unit hydrograph models, enhancing watershed management strategies.

## 2.3 ANALYSIS OF LAND USE LAND COVER (LULC) CHANGES AND NORMALIZED DIFFERENCE VEGETATION INDEX (NDVI)

### 2.3.1 Land use land cover (LULC)

Land Use/Land Cover (LULC) refers to the physical characteristics of the Earth's surface and how humans utilize these lands. LULC changes have significant environmental, climatic, and socio-economic implications, often driven by urbanization, agricultural expansion, and deforestation. These changes influence land-atmosphere interactions, impacting climate change, biodiversity, and water resources. Over the years, research on LULC has focused on understanding these changes through remote sensing, GIS mapping, and classification systems. However, challenges such as inconsistent datasets, classification ambiguities, and the need for high-resolution satellite imagery remain critical areas for improvement. As an essential source of data, satellite remote sensing, has been widely utilized, in order to produce LULC. Landsat images have been commonly utilized, in order to produce high-quality multispectral images with medium spatial resolution and time resolution for scientific research since 1972. Since Landsat images are available for long-term series image storage and free access, they still continue to be one of the most commonly used essential sources of data, even today. Landsat 8, the fourth generation Landsat sensor is widely used in a variety of LULC classification studies.

For example, Sharma *et al.* (2019) conducted LULC classification research based on Landsat 8 images by employing the wavelet transform. According to the results, the highest obtainable accuracy of the five-level wavelet transform is 95.03%. Gupta and Shukla (2020) studied the influence of terrain correction on the LULC classification based on Landsat 8 images, and the classification results before and after the terrain correction process were 65.60% and 82.40%, respectively. According to the above-mentioned studies, it is evident that Landsat 8 images are suitable for LULC classification studies. Huan *et al.* (2020) also conducted a LULC classification study based on Landsat 8 images via the object-oriented method. The object-oriented support vector machine, based on texture, was found to be the most accurate, with an accuracy of 85.67%. Jiang *et al.* (2020) conducted LULC classification research based on Landsat 8 images by using the mixed decomposition of multi-seasonal spectrum and a decision tree classification method, and the accuracy was 90.94%.

Land resources can provide material, energy, ecological, and other services for human survival and well-being. The change in LULC (land use and land cover) is the most obvious manifestation of the human impact on the environment. Due to its close relationship with regional natural factors and socio-economic factors, LULC serves as the basis of regional sustainable development. At the same time, regional sustainable development could, in turn, enhance the LULC change. With the development of population and society, the extent and magnitude of land use are constantly increasing, resulting in a series of environmental issues, such as greenhouse gases emissions, biodiversity loss, soil erosion, desertification, and so on. The effects of LULC changes on the environment are evaluated to determine the primary driving factors affecting LULC and environmental changes, and the targeted prevention and improvement measures are implemented to achieve regional sustainable development. Therefore, how to realize the precise classification of LULC and long-term dynamic change monitoring is the central issue to be solved, in order to realize regional sustainable development (You *et al.,* 2022). Further, Ren *et al.* (2023) conducted LULC classification research based on Landsat 8 images. The results indicate that the highest obtainable classification accuracy, based on the combination of pixel and object-oriented methods, is 92.99%.

### 2.3.2 LULC classification and change detection

The LULC can be broadly categorized into two major domains: land cover and land use (Masoumi & Van Genderen, 2020). Land cover pertains to the existing natural and human factors on Earth's surface, constituting objects that form a covering. This encompasses the natural states of the Earth's surface, such as forests, grasslands, farmland, soil, and roads. On the other hand, land use refers to the process of transforming the natural ecosystem of land into an artificial ecosystem – a comprehensive process influenced by natural, economic, and social factors. Examples include areas designated for transportation, commerce, residential use, and so forth.

LULC classification systems play a crucial role in categorizing and mapping land changes at local, regional, and global scales. Various classification approaches exist, including the CORINE system for Europe, the National Land Cover Database (NLCD) in the U.S., and the FAO's Land Cover Classification System (LCCS). These systems help standardize LULC data and facilitate cross-regional comparisons. Despite

these advances, inconsistencies in classification methods and data quality issues hinder accurate LULC assessments. Ensuring reliable classification frameworks with updated datasets and integrating machine learning techniques for automated land classification are potential solutions to enhance accuracy in LULC mapping. However, challenges such as inconsistent datasets, classification ambiguities, and the need for high-resolution satellite imagery remain critical areas for improvement (Nedd *et al.,* 2021).

The LULC classification and change detection in the study Ananthapuramu region in Andhra Pradesh, India were carried out using remote sensing and GIS techniques. The research employed multi-temporal Landsat satellite images from 1978 and 2018 to classify and analyse changes in land cover over four decades. Accuracy assessment was performed using error matrices, and classification results showed an overall accuracy of 81.25% for 1978 and 87.46% for 2018, confirming the reliability of the classification results. For change detection, a post-classification comparison technique was employed, where LULC maps from 1978 and 2018 were compared pixel-by-pixel to quantify land use changes. The results revealed a significant expansion of built-up areas, which increased from 6.81 km² in 1978 to 31.55 km² in 2018, a 454.33% rise, mainly due to urbanization and infrastructure development. Conversely, agriculture land shrank from 47.83 km² to 18.25 km² (a 61.84% decrease), while forest cover also declined by 31%, indicating environmental degradation. Water bodies reduced drastically by 73.04% due to declining rainfall and urban encroachment. The increase in barren land/other land, from 17.27 km² to 35.35 km², suggests that agricultural land is being abandoned. These findings highlight the rapid urban expansion and associated environmental consequences in the region (Vivekananda *et al.,* 2021).

A Study by You *et al.* 2022 presents a comprehensive methodology for LULC classification and change detection. The study utilized Landsat 8 and Landsat 9 satellite imagery, both processed through the Google Earth Engine (GEE) platform with geometric, radiometric, and atmospheric corrections. Various spectral reflectance bands and vegetation indices, such as the Normalized Difference Vegetation Index (NDVI) and Normalized Difference Water Index (NDWI), were extracted to enhance classification accuracy. The results indicated that Landsat 9, with its higher radiation resolution, provided better classification accuracy, especially for water bodies and tree species, improving overall accuracy by 6.01% compared to Landsat 8. To assess LULC

changes, the study analysed classification results across 40 test areas in China, comparing differences in land cover categories such as water and forests. The findings revealed that discrepancies between Landsat 8 and Landsat 9 classifications were most notable in water detection, where Landsat 9 demonstrated superior sensitivity. These findings underscore the impact of improved radiation resolution on LULC classification and highlight the potential for using Landsat 9 data to enhance regional sustainable development and long-term environmental monitoring.

LULC classification using hyperspectral images is an essential aspect of remote sensing, enabling detailed mapping of various land cover types and their transitions over time. Traditional classification techniques such as K-Nearest neighbour (KNN) and Support Vector Machines (SVM) often struggle to process hyperspectral images effectively due to their high dimensionality and the complexity of spatial features. To address these limitations, advanced machine learning methods, including deep learning (DL), have been extensively employed. Deep learning models, particularly Convolutional Neural Networks (CNNs) and Recurrent Neural Networks (RNNs), have significantly improved classification accuracy by leveraging both spectral and spatial information. Recent studies have also explored hybrid approaches, integrating spectral unmixing with classification algorithms to enhance performance. Furthermore, feature extraction techniques such as Principal Component Analysis (PCA) and Independent Component Analysis (ICA) have been used to reduce dimensionality and improve computational efficiency (Lou *et al.,* 2024).

Change detection in LULC classification involves comparing images from different time periods to analyse land cover transitions, such as deforestation, urbanization, or agricultural expansion. Traditional change detection methods rely on pixel-based classification, which often results in misclassification due to spectral variations. Recent advancements have introduced object-based image analysis (OBIA) and machine learning-driven methods that incorporate spatial context, improving detection accuracy. Supervised classifiers like Random Forest (RF) and deep neural networks have been widely adopted for change detection, demonstrating superior performance over conventional approaches. Additionally, techniques like Spectral Angle Mapper (SAM) and Spectral Correlation Mapper (SCM) have been applied to hyperspectral images to quantify spectral differences over time. These methods help in

accurately identifying LULC changes and assist in sustainable land management practices (Lou *et al.,* 2024).

### 2.3.3 Normalized difference vegetation index (NDVI)

One of the most widely used vegetation indices in remote sensing applications, especially for tracking the density and health of vegetation, is the NDVI. It is predicated on the concept that healthy vegetation absorbs visible light (Red) for photosynthesis while reflecting near-infrared (NIR) light, which is less absorbed by the plants. The health and strength of the vegetation can be measured by measuring the difference in the reflectance level of these two wavelengths (Red and NIR) (Rouse *et al.,* 1973).

NDVI is formed using satellite photography, a form of remote sensing technology that provides a spatially continuous image of land cover, including vegetation. The basis for NDVI operation is the variation in how plant tissues react to the red and near-infrared wavelengths. In healthy plants, the chlorophyll absorbs the majority of the red light (approximately 660 nm), while the leaf structure reflects a sizable portion of the near-infrared light (about 850 nm). By computing the difference in reflectance between these two bands, NDVI enables a quantitative evaluation of vegetation health and productivity (Gitelson *et al.,* 2003).

The NDVI value is computed using the following formula;

$$NIR = \frac{[NIR - Red]}{[NIR + Red]}$$

Where;

NIR = Reflectance in the Near-Infrared (NIR) spectrum (typically around 850 nm)

Red = Reflectance in the Red spectrum (typically around 660 nm)

The value of NDVI ranges from -1 to +1. Bhandari *et al.* (2012) used vegetation cover and its connection to soil erosion to show that the NDVI is a useful tool for assessing soil and water conservation. Vegetation is necessary to stop soil erosion, and indices derived from the NDVI help determine how dense and widely distributed vegetation is. By utilizing multi-spectral remote sensing data, NDVI is able to differentiate between a variety of geographical features, including arid regions, water bodies, and agricultural lands. Since values close to zero indicate bare soil and higher

values indicate denser vegetation, the study concludes that NDVI is a useful indicator for assessing soil stability and moisture retention. The study also demonstrated how NDVI variations, which reflect changes in soil, aid in conservation planning and sustainable land management strategies.

NDVI is also vital for evaluating soil conservation measures. By understanding its guiding principles, interpreting the NDVI values, and using a variety of data sources, researchers, land managers, and policymakers can more accurately monitor and evaluate sustainable soil management techniques. As remote sensing technology advance, the significance and efficacy of NDVI in agriculture, soil conservation, and sustainable land management will only grow (Pettorelli *et al.,* 2014). The NDVI is often used to evaluate soil conservation capabilities as a measure of vegetation cover, which is crucial for lowering soil erosion. In the Jhagrabaria watershed study, the NDVI was used to calculate the Crop Management Factor (C factor) in the Revised Universal Soil Loss Equation (RULSE). The results demonstrated that areas with high NDVI values imply dense vegetation connected with lower rates of soil erosion due to enhanced soil retention and less surface runoff. Conversely, regions with bare ground or minimal vegetation have a higher risk of soil loss. The study emphasizes the importance of vegetation cover in planning for sustainable soil conservation and the efficiency of C factor mapping based on NDVI in assessing the risks of soil erosion (Rawat & Singh, 2018).

The study by Rahmi *et al*. (2024) analyses land use/land cover (LULC) classification and change detection in Sumedang Regency, West Java, Indonesia, using NDVI. Landsat-7 ETM and Landsat-8 OLI/TIRS images from 2003 to 2023 were processed to compute NDVI values, allowing for the classification of different vegetation densities. Over the study period, the high greenness index initially declined, with a reduction in area from 144,793.17 ha in 2003 to 122,392.08 ha in 2018. However, from 2018 to 2023, the greenness index showed an increasing trend, indicating some vegetation recovery. By integrating NDVI with LULC classification, the research provides insights into spatiotemporal vegetation dynamics in Sumedang Regency. Image processing techniques, including radiometric and atmospheric corrections, were employed to enhance the accuracy of NDVI calculations. The study found that areas with dense vegetation showed a positive trend in recent years, but urban expansion in regions like Jatinangor sub-district led to a significant increase in non-vegetated land,

rising from 48.42 ha in 2003 to 3,507.12 ha in 2023. This suggests ongoing land use transformation, necessitating sustainable environmental planning. The research emphasizes role of NDVI in identifying vegetation loss hotspots and guiding conservation efforts.

## 2.4 IRRIGATION WATER QUALITY INDEX (IWQI)

### 2.4.1 Concept and methodology

The Irrigation Water Quality Index (IWQI) is a vital tool designed to assess the suitability of water sources for agricultural use. This index integrates several critical physicochemical parameters into a single numerical value that reflects the potential impact of irrigation water on soil properties and crop health. Unlike general WQI, which focuses on human consumption and ecological impact, IWQI targets parameters influencing salinity hazards, sodicity, and long-term soil sustainability. The index typically includes measurements such as electrical conductivity (EC), sodium adsorption ratio (SAR), sodium percentage (Na%), residual sodium carbonate (RSC), and chloride levels. Each parameter is weighted according to its significance in determining irrigation suitability, and a composite score is generated to classify water into categories ranging from “no restriction” to “unsuitable” for irrigation. According to Ayers and Westcot (1985), the use of indices like IWQI is crucial in regions where agriculture depends heavily on groundwater and surface water resources, especially under variable climatic conditions and intensive farming practices.

The IWQI methodology has gained attention for its ability to condense complex water quality data into an accessible format, thus enabling planners, farmers, and policymakers to make informed decisions. Various computational frameworks are used, ranging from simple arithmetic weighting to fuzzy logic and GIS-based spatial analyses, depending on the scope and precision required. Parameters are normalized and rated against irrigation-specific standards such as those established by the U.S. Salinity Laboratory or FAO guidelines. The final IWQI score facilitates comparative assessments across regions and seasons, supporting long-term irrigation planning and water resource sustainability (Ramesh & Elango, 2012).

### 2.4.2 Parameters and analysis

The selection of parameters for IWQI evaluation is based on their direct influence on soil permeability, crop yield, and salinity buildup (Ramesh & Elango, 2012). The most commonly used parameters include:

#### *2.4.2.1 Electrical conductivity (EC)*

EC is a primary indicator of salinity hazard, reflecting the total concentration of soluble salts in irrigation water. High EC levels can lead to osmotic stress in plants and salt accumulation in soil, thereby reducing crop productivity.

#### *2.4.2.2 Sodium adsorption ratio (SAR)*

SAR measures the relative concentration of sodium to calcium and magnesium in water. Elevated SAR values are indicative of potential sodicity problems, which can deteriorate soil structure and reduce water infiltration.

#### *2.4.2.3 Residual sodium carbonate (RSC)*

RSC assesses the combined effect of carbonate and bicarbonate ions relative to calcium and magnesium. High RSC values may result in calcium and magnesium precipitation, enhancing sodium hazard and negatively affecting soil permeability.

#### *2.4.2.4 Sodium percentage (Na%)*

Na% quantifies the proportion of sodium ions in total cations. High sodium levels can lead to soil dispersion and reduced aeration, impacting plant root health and nutrient uptake.

#### *2.4.2.5 Chloride ($Cl^-$)*

Chloride is a toxic element for many crops when present in excess. It also contributes to soil salinity and can be detrimental to salt-sensitive plant species if irrigation water contains high $Cl^-$ levels.

#### *2.4.2.6 Total dissolved solids (TDS)*

TDS represents the cumulative concentration of all inorganic and organic substances dissolved in water. High TDS levels are associated with increased salinity, affecting plant growth and soil function.

These parameters collectively provide insights into the chemical nature of irrigation water and its long-term effects on soil health. Proper evaluation and monitoring ensure the safe and sustainable use of available water resources for agriculture.

### 2.4.3 Case studies on IWQI

Subba Rao (2006) conducted a detailed seasonal evaluation of groundwater in the Guntur District, Andhra Pradesh, focusing on parameters such as EC, TDS, SAR, Na%, and RSC across pre- and post-monsoon periods. Post-monsoon water exhibited elevated levels of sodium and nitrate due to leaching and runoff, rendering much of the groundwater unsuitable for irrigation. The study concluded that dynamic monitoring and seasonal adjustments in water management practices are essential for maintaining soil health and crop productivity. In the study of the Tamiraparani River Basin in Southern India, Kumarasamy *et al*. (2014) assessed irrigation water suitability using a multi-parameter index including SAR, Na%, and RSC. Most upstream regions showed excellent irrigation potential, while downstream estuarine areas had salt accumulation issues, leading to "doubtful to unsuitable" ratings. The study highlights the need for region-specific irrigation strategies and regular water quality monitoring.

A comprehensive IWQI-based evaluation by Al Obaidy *et al*. (2016) in the Tigris River Basin of Iraq revealed that only 25% of the sampled sites were considered suitable for irrigation without restrictions. Parameters like EC and SAR often exceeded standard thresholds, with RSC values contributing significantly to classification shifts during dry seasons. Their findings stress the importance of understanding seasonal dynamics in river-fed irrigation systems to avoid salinization and degradation of arable land. In a study by Abbasnia *et al*. (2019), groundwater samples from Sistan and Baluchistan province, Iran, were evaluated using IWQI to assess irrigation suitability. Among 40 samples analysed, nearly 47.5% were categorized under “high restriction,” while only 2.5% were deemed suitable without any limitations. Parameters like EC and SAR showed values as high as 14,506 µS/cm and 44.25, respectively, indicating severe salinity and sodicity hazards. GIS-based spatial mapping highlighted that the eastern and southeastern parts of the region had the most degraded groundwater quality. The authors emphasized the importance of adopting localized water treatment and sustainable irrigation practices to mitigate long-term agricultural impacts.

In a recent GIS-supported study, Kiran *et al*. (2022) examined the spatial distribution of groundwater quality using IWQI. The study found that nearly 60% of groundwater samples required moderate to severe restrictions for irrigation due to high salinity and Na% values. The visual outputs from interpolation methods such as IDW and Kriging enabled the identification of critical zones, guiding targeted intervention and infrastructure planning.

## 2.4 COMPARATIVE ANALYSIS OF IDW AND KRIGING INTERPOLATION METHODS

Interpolation techniques are essential tools in spatial analysis, enabling the estimation of unknown values at unsampled locations based on known data points. Among the various interpolation methods, Inverse Distance Weighting (IDW) and Kriging are widely used in environmental studies, particularly for groundwater and irrigation water quality assessment.

Kriging is a geostatistical method that incorporates both the distance and the degree of variation between known data points. It uses a semi variogram model to estimate spatial correlation and provides a measure of prediction uncertainty. Robeson (1997) emphasized Kriging's advantage in producing more reliable estimates by accounting for spatial structure. IDW is a deterministic interpolation technique that assumes that points closer to the prediction location have more influence than those further away. According to Yalcin and Akyurek (2004), increasing the power parameter often improves accuracy but may lead to overfitting in areas with sparse data.

On the other hand, Goovaerts (2008) compared interpolation techniques and found that while Kriging generally provides better accuracy, IDW may perform equally well or better under certain conditions, such as when sample points are evenly distributed or spatial autocorrelation is minimal. Li and Heap (2008) studied the comparative performance between IDW and Kriging often depends on the dataset, spatial distribution, and heterogeneity of the study area. While Kriging tends to yield higher accuracy, IDW can perform comparably in some conditions.

Lu and Wong (2008) noted that IDW is suitable when spatial autocorrelation is weak and the sample point distribution is relatively uniform. However, the accuracy of IDW is sensitive to the choice of power parameter, which controls the rate at which influence decays with distance. Hengl (2009) noted that Kriging's success heavily relies

on selecting an appropriate semi variogram model, with common options being spherical, exponential, Gaussian, and linear models. Knotters and Brus (2010) emphasized the importance of cross-validation techniques, including leave-one-out cross-validation (LOOCV) and random data splitting, to assess interpolation reliability and minimize prediction errors.

Zhou *et al*. (2016) demonstrated that Kriging is especially beneficial when data are clustered or when there is a significant spatial trend. Wang *et al*. (2017) used both IDW and Kriging for irrigation suitability mapping. Their findings showed that although Kriging offered better spatial consistency, IDW was simpler to calibrate and interpret. Nedd *et al*. (2021) emphasized the ongoing challenges in interpolation, such as data inconsistency and spatial resolution limitations, reinforcing the need for proper model selection and validation.

In a study by Baseri *et al*. (2023) in the Neyshabur Plain, Iran, IDW and Kriging were evaluated for irrigation water quality mapping using IWQI derived from EC, $Na^+$, and $Cl^-$ concentrations. The results indicated that Kriging, particularly with a Gaussian semi variogram, provided more accurate spatial representations by effectively incorporating spatial structure. Gautam *et al*. (2024) investigated groundwater fluoride and nitrate concentrations in the Bist-Doab region of Punjab, India, using both IDW and Kriging. Their findings revealed that Kriging performed better in regions with high variability and data clustering, while IDW was effective in areas with uniform data distribution.

Given these findings, recent studies recommend using both methods in parallel and conducting rigorous cross-validation to identify the optimal approach for a given application. In the context of irrigation water quality mapping, comparing IDW and Kriging provides insights into spatial interpolation performance and ensures better spatial representation of Irrigation Water Quality Index (IWQI) values.

## 2.6 EFFECT OF LULC ON IWQI

Several studies have explored the intricate relationship between Land Use/Land Cover (LULC) changes and water quality, often employing remote sensing (RS) and geospatial techniques alongside Irrigation Water Quality Index (IWQI) frameworks to quantify and visualize impacts.

Zhang *et al*. (2022) expanded this understanding by evaluating seasonal in-stream water quality responses to LULC and landscape patterns across small watersheds. Their findings stressed the seasonal variability of LULC impacts on water quality, with urban and agricultural areas contributing more pollutants during rainy seasons due to runoff. Landscape metrics (e.g., patch density, edge density) were used to assess spatial configurations of LULC classes, reinforcing the importance of spatial pattern analysis in IWQI studies.

Gani *et al*. (2023) investigated the impact of LULC changes on river water quality using WQI and RS tools. Their study emphasized how increasing urbanization and agricultural expansion significantly degrade water quality, particularly increasing turbidity and nutrient loads. They used satellite imagery to classify LULC patterns and linked these with in-situ water quality parameters to calculate the IWQI. The integration of GIS facilitated spatial correlation and visualization of degradation hotspots.

The study by Pandey *et al*. (2023), gives a comprehensive evaluation of how land use dynamics influence water quality across five key dam reservoirs in Jharkhand, India. Utilizing remote sensing and GIS techniques, the authors performed supervised classification to assess LULC changes between 2016 and 2021 and correlated these with seasonal IWQI values derived from both field data and secondary sources. The findings revealed that vegetation cover significantly improves water quality, while increased urbanization and agricultural expansion contribute to degradation through runoff and sedimentation. The study also highlights alarming trends in vegetation loss, growing drought conditions, and reduced surface water areas, emphasizing the need for sustainable land and water management practices. The integration of NDVI, NDWI, and IWQI in the analysis adds robustness and spatial insight, making this paper a valuable reference for environmental monitoring and policy-making in water-stressed regions.

# MATERIALS AND METHODS

# CHAPTER III

# MATERIALS AND METHODS

The objectives of the present study are;

1. To determine the morphometric parameters of the study area.
2. To assess the impact of soil and water conservation measures on LULC and NDVI in the study area using Remote Sensing and GIS.
3. To assess the water quality of the study area based on Irrigation Water Quality Index using various interpolation methods in ArcGIS.
4. To analyse the effect of LULC on IWQI of the study area.

## 3.1 DESCRIPTION OF THE STUDY AREA

Paddy fields and palmyrahs can be seen plenty at Palakkad (Palghat). And one of the state's main paddy-growing regions is Palakkad. It is frequently referred to as the "Gateway of Kerala". Over the past five years, the district's farming and land use patterns have changed significantly. Farmers are shifting their cropping patterns to cash crops including sugarcane, vegetables, and flower cultivation as a result of the low income from rice and coconut. The districts over reliance on groundwater for industrial, agricultural, and residential uses has caused the water table to drop and there is now a shortage of water, particularly in the eastern regions. Water level declines in most places, particularly in the eastern portion of the district, require deepening already-existing dug wells and installing deep bore wells, which raises pumping costs and degrades quality. According to a local investigation, farmers have borrowed money from banks to install irrigation pump sets and bore wells. Every year, the region receives 2362 mm of rain on average. The district had a good rainfall total of 2407 mm in 1998, however since then, the rainfall has significantly fallen.

The Perumatty Panchayath is located in the Chittur Block, which borders Tamil Nadu, on the eastern side of the Palakkad district. Nestled between latitudes 100 37'53" N and 100 41'29" N and longitudes 760 43'28" E and 760 53'05" E, the research area spans 60.91 km2 and is part of the Bharathapuzha river basin's Chitturpuzha sub-basin. It has been determined that the Perumatty panchayat and the entire Chittur block are overexploited in terms of groundwater, meaning that more groundwater is extracted than is recharged. The primary cause of this unreasonable over-extraction is the

excessive reliance on groundwater for industrial, agricultural, and residential uses. It eventually caused the area to become dry and barren.

For a number of reasons, the evaluation of groundwater, water quality, and vegetation changes during a specific time period within Perumatty Panchayath are very important. To ensure effective resource use and develop sustainable management plans, a thorough understanding of groundwater availability and quality is essential. Analyzing groundwater potential becomes essential for proactive planning because of the possibility of changes in water demand brought on by things like population increase and changes in land use. Notably, not every region has the same level of groundwater accessibility and quality, therefore it's critical to distinguish between resource-rich and resource-poor areas. Additionally, this type of study helps prevent groundwater reserves from being overused. Consequently, a comprehensive examination encompassing both traditional and geophysical investigative methods is undertaken to ascertain groundwater availability and depths accurately. Given the inherent limitations of conventional approaches, the preference leans towards geophysical investigations for their ability to yield more precise outcomes.

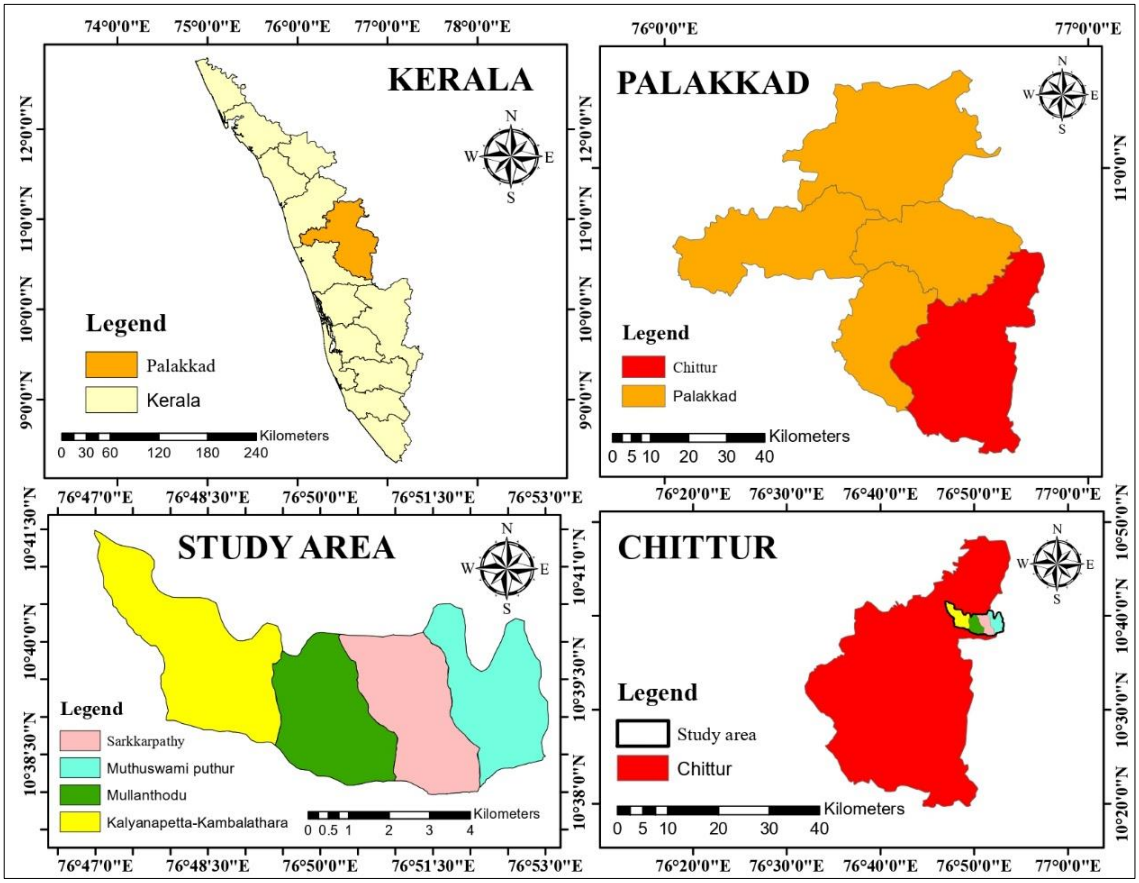


**Fig. 3.1 Location map of the study area**

## 3.2 DATA AND SOFTWARE USED

### 3.2.1 Data and sources

In this study, the major problems experienced and watershed interventions implemented in the study area were collected from the Department of Soil Survey and Soil Conservation (DSSSC), Palakkad. Survey of India (SOI) Toposheet at a 1:50000 scale was used for verification of stream networks. An open-source Shuttle Radar Topography Mission Digital Elevation Model (SRTM DEM) data with a spatial resolution of 30m was downloaded from United States Geological Survey (USGS) Earth Explorer website (http://earthexplorer.usgs.gov/) to delineate watershed boundaries, define the stream network and determine morphometric parameters. Landsat 8-9 Operational Land Imager and Thermal Infrared Sensor (OLI/TIRS) satellite images of the study area downloaded from USGS Earth Explorer has been used in this study for LULC mapping, change analysis and NDVI classification for the year 2015 and 2023 as pre- and post-treatment period.

### 3.2.2 Software and platforms

**Table 3.1 Data and software used**

| SI. No | Data and Software | Utility | Source |
|---|---|---|---|
| 1 | Perumatty report | Details of watershed and management measures taken | Department of Soil Survey and Soil Conservation (DSSSC), Palakkad |
| 2 | Topographic map with scale 1:50000 | Validation of drainage networks | Survey of India (SOI) |
| 3 | SRTM DEM data | Watershed delineation and morphometric analysis | USGS Earth Explorer |
| 4 | Landsat 8-9 (OLI/TIRS) data | LULC and NDVI mapping | USGS Earth Explorer |
| 5 | ArcGIS 10.8 | Image processing | ESRI |
| 6 | Google Earth Pro | Validation-Accuracy assessment | Google |
| 7 | Microsoft Excel | Data pre-processing and visualization | Microsoft |

ArcGIS (Version 10.8) Software was used for watershed delineation, image pre-processing, LULC classification, change analysis and computation of irrigation water quality index. Google Earth Pro was used for ground truth verification of the LULC maps. Microsoft Excel used for data preparation, data analysis and visualization. All the data, software and platform used for this study, their purpose and source were presented in Table 3.1.

## 3.3 SOIL AND WATER CONSERVATION MEASURES IN PERUMATTY

### 3.3.1 Earthen bunds

**Plate 3.1 Earthen bund**

Earthen bunds are small, low-height embankments or ridges constructed using compacted soil to conserve water and prevent soil erosion in agricultural fields. They are commonly used in rainfed farming, terraced fields, and watershed management. Its major purpose and beneficial for water conservation, slow down runoff, allowing water to infiltrate the soil, increase soil moisture for crops, especially in dry regions, soil erosion control reduce soil loss by preventing water flow from carrying away topsoil

cost-effective & simple, made using locally available soil, requiring minimal machinery, suitable for small and marginal farmers, crop productivity, improve water availability, supporting better crop growth.

### 3.3.2 Farm ponds

A farm pond is a small, dug-out water storage structure constructed on agricultural land to harvest rainwater, store runoff, and provide irrigation. It helps farmers manage water scarcity and improve crop productivity. Its major purpose and beneficial for water storage, collects rainwater and runoff for use during dry spells, reduces dependency on wells and groundwater, irrigation support, provides a reliable water source for crops, livestock, and fish farming, soil & moisture conservation, prevents soil erosion by controlling runoff, recharges groundwater in the surrounding area, supports drought-proofing in rainfed agriculture.

**Plate 3.2 Farm pond**

### 3.3.3 Centripetal terrace

Centripetal terrace are long, narrow excavations dug into the soil to manage water flow, conserve moisture, and improve soil health. They are commonly used in contour farming, agroforestry, and erosion control. Its major purpose and beneficial for water management, slow down runoff, allowing water to infiltrate the soil, recharge groundwater by directing water deep into the subsoil. Soil conservation, prevent

erosion by trapping sediment and reducing surface flow, improve soil fertility by capturing organic matter and nutrients, moisture retention increases water availability for crops, especially in drylands, support deep-rooted plants (e.g., trees in agroforestry), drainage Improvement, prevent waterlogging in heavy soils by diverting excess water.

**Plate 3.3 Centripetal terrace**

## 3.4 MORPHOMETRIC ANALYSIS OF WATERSHED

### 3.4.1 Watershed delineation

In this study, ArcGIS 10.8 was employed to analyse the DEM data, with all datasets projected to the UTM Zone 43N coordinate system. A 30-meter resolution SRTM DEM was utilized to delineate the watersheds within the Perumatty Grama Panchayat of Palakkad district, Kerala. The study area encompasses micro-watersheds such as Kambalathara- Kalyanappetta, Mullanthodu, Sarkkarpathy, and Muthuswamy.

The major steps involved in the process of watershed delineation are given below:

a) Fill

The Fill operation is used to eliminate depressions or sinks in the DEM, ensuring continuous flow across the terrain surface. This step is critical for creating a hydrologically correct DEM that supports accurate watershed and stream network delineation (Choudhari *et al*., 2023).

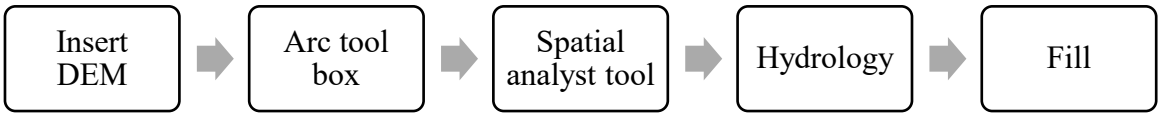


**Fig. 3.2 Steps for fill**

b) Flow direction

The Flow Direction tool assigns a flow direction to each cell in the DEM based on the steepest descent method, where water flows towards the neighbouring cell with the highest slope. Newer models, like the hydrological object-based flow direction model, have been developed to better represent flow dynamics, particularly around complex features such as lakes (Choudhari *et al*., 2023).

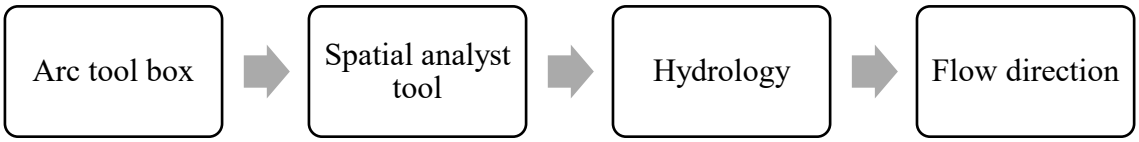


**Fig. 3.3 Steps for flow direction**

c) Flow accumulation

The Flow Accumulation process calculates the cumulative number of upstream cells draining into a particular cell, helping in identifying stream networks and drainage basins. Recent approaches advocate for adaptive thresholds based on topography and land cover, enhancing the accuracy of stream extraction from DEMs (Zhang *et al*., 2022).

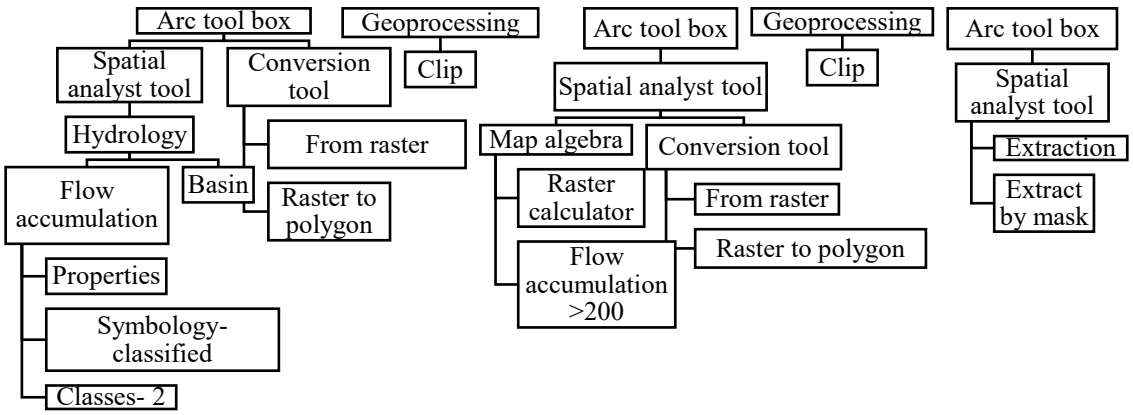


**Fig. 3.4 Steps for flow accumulation**

### 3.4.2 Morphometric analysis

**Table 3.2 Morphometric parameters of watershed**

| Linear Aspects | Areal Aspects | Relief Aspects |
|---|---|---|
| Stream order | Circularity ratio | Basin relief |
| Stream length | Elongation ratio | Relief ratio |
| Bifurcation ratio | Form factor | Gradient ratio |
| Stream length ratio | Shape factor | |
| Texture ratio | Compactness constant | |
| Length of overland flow | Constant of channel maintenance | |
| Mean stream length | Drainage texture | |
| Drainage density | Drainage frequency | |

Morphometric parameters were evaluated to identify various characteristics of the watershed, establishing quantitative relationships and patterns within it. This analysis provided a deeper understanding of the watershed's behaviour and hydrological response. The parameters were classified into three categories: Linear Aspects, Areal Aspects, and Relief Aspects, as presented in Table 3.2. The watershed area, perimeter, elevation, and slope were determined using ArcGIS 10.8 software. Stream ordering was carried out following Strahler's method (Strahler, 1964) using the Hydrology tool in ArcGIS 10.8, while other morphometric parameters were calculated using mathematical formulas provided in Table 3.3.

**Table 3.3 Mathematical formulas used to calculate morphometric parameters**

| Sl. No. | Category | Parameter | Formula / Definition | Reference |
|---|---|---|---|---|
| 1 | Basin parameter | Area (A) | GIS Analysis | |

| | | | | |
|---|---|---|---|---|
| 2 | Basin parameter | Perimeter (P) | GIS Analysis | |
| 3 | Basin parameter | Basin length ($L_b$) | $Lb = 1.312 \times A^{0.568}$ | Schumm (1956) |
| 4 | Basin parameter | Mean basin width ($W_b$) | $W_b = \frac{A}{L_b}$ | Horton (1945) |
| 5 | Basin parameter | Stream order (u) | Ranking hierarchically | Strahler (1964) |
| 6 | Basin parameter | Stream number ($N_u$) | $N_u = N_1 + N_2 + \cdots + N_n$ | Horton (1945) |
| 7 | Linear parameter | Stream length ($L_u$) | $L_u = L_1 + L_2 + \cdots + L_n$ | Horton (1945) |
| 8 | Linear parameter | Mean stream length ($L_{sm}$) | $L_{sm} = \frac{L_u}{N_u}$ | Strahler (1964) |
| 9 | Linear parameter | Stream Length Ratio ($R_L$) | $R_L = \frac{L_{sm}}{L_{sm-1}}$ | Schumm (1956) |
| 10 | Linear parameter | Bifurcation ratio ($R_b$) | $R_b = \frac{N_u}{N_{u+1}}$ | Schumm (1956) |
| 11 | Linear parameter | Rho coefficient (ρ) | $\rho = \frac{R_L}{R_b}$ | Horton (1945) |
| 12 | Linear parameter | Drainage density ($D_d$) | $D_d = \frac{L_u}{A}$ | Horton (1932) |

| | | | | |
|---|---|---|---|---|
| 13 | Linear parameter | Stream frequency ($F_S$) | $F_S = \frac{N_u}{A}$ | Horton (1932) |
| 14 | Linear parameter | Drainage texture / Texture ratio ($D_t$) | $D_t = \frac{N_u}{P}$ | Horton (1945) |
| 15 | Linear parameter | Infiltration number ($I_f$) | $I_f = F_s \times D_d$ | Faniran (1968) |
| 16 | Linear parameter | Length of overland flow ($L_0$) | $L_o = \frac{1}{(2 \times D_d)}$ | Horton (1945) |
| 17 | Linear parameter | Drainage intensity ($D_i$) | $D_i = \frac{F_S}{D_d}$ | Strahler (1964) |
| 18 | Shape parameter | Circularity ratio ($R_c$) | $R_c = \frac{4\pi A}{P^2}$ | Miller (1953) |
| 19 | Shape parameter | Elongation ratio ($R_e$) | $R_e = \frac{D}{L}$ $or$ $1.128 \times \sqrt{\frac{A}{L}}$ | Schumm (1956) |
| 20 | Shape parameter | Form Factor ($F_f$) | $F_f = \frac{A}{L^2}$ | Horton (1945) |
| 21 | Shape parameter | Compactness constant ($C_c$) | $C_c = 0.282 \times \frac{P}{\sqrt{A}}$ | Horton (1945) |
| 22 | Shape parameter | Lemniscate's ratio ($K$) | $K = \frac{{L_b}^2}{4A}$ | Chorley (1967) |

| | | | | |
|---|---|---|---|---|
| 23 | Shape parameter | Shape factor ($B_s$) | $B_s = \frac{L^2}{A}$ | Horton (1945) |
| 24 | Shape parameter | Constant of channel maintenance ($C$) | $C = \frac{1}{Dd}$ | Schumm (1956) |
| 25 | Relief parameter | Elevation of basin outlet (h) | GIS Analysis | |
| 26 | Relief parameter | Maximum elevation of the basin (H) | GIS Analysis | |
| 27 | Relief parameter | Basin relief ($R$) | $R = H - h$ | Strahler (1964) |
| 28 | Relief parameter | Relief ratio ($R_h$) | $R_h = \frac{R}{L_b}$ | Schumm (1956) |
| 29 | Relief parameter | Relative relief ($R_r$) | $R_r = \frac{R}{P}$ | Melton (1957) |
| 30 | Relief parameter | Ruggedness number ($H_d$) | $H_d = D_d \times R$ | Strahler (1964) |

1. Linear aspects

These parameters describe the linear features of a watershed, reflecting its drainage network's structure and pattern.

a. Stream order ($N_u$): A hierarchical classification of streams based on their branching complexity. Higher orders indicate more complex drainage networks (Strahler, 1964).

b. Stream length ($L_u$): The total length of streams within each order, providing insights into the watershed's hydrological characteristics (Kannan & Venkateswaran, 2020).
c. Stream length ratio ($R_l$): The ratio of the average length of streams of a given order to that of the next lower order, indicating changes in slope and topography (Kannan & Venkateswaran, 2020).
d. Bifurcation ratio ($R_b$): The ratio of the number of streams of a given order to the number in the next higher order. It reflects the degree of branching and can indicate structural control over the drainage pattern (Tiwari & Kushwaha, 2021).
e. Rho coefficient (ρ): A dimensionless parameter representing the ratio between the stream length ratio and the bifurcation ratio, indicating the drainage network's development stage (Waikar & Nilawar, 2014).
f. Drainage density ($D_d$): The total length of all streams per unit area, signifying the closeness of spacing of channels. High values suggest impermeable subsurface material and high runoff (Gautam, 2023).
g. Stream frequency ($F_s$): The number of stream segments per unit area, indicating the drainage texture and potential runoff (Gautam, 2023).
h. Drainage texture (T): The total number of stream segments of all orders per perimeter of the basin, reflecting the underlying lithology and infiltration capacity (Gautam, 2023).
i. Infiltration number ($I_f$): The product of drainage density and stream frequency, indicating the infiltration characteristics of the basin (Waikar & Nilawar, 2014).
j. Length of overland flow ($L_o$): The average length of water flow over the ground before it becomes concentrated in streams, inversely related to drainage density (Gautam, 2023).
k. Drainage intensity ($D_i$): The ratio of stream frequency to drainage density, indicating the runoff potential and drainage efficiency (Waikar & Nilawar, 2014).

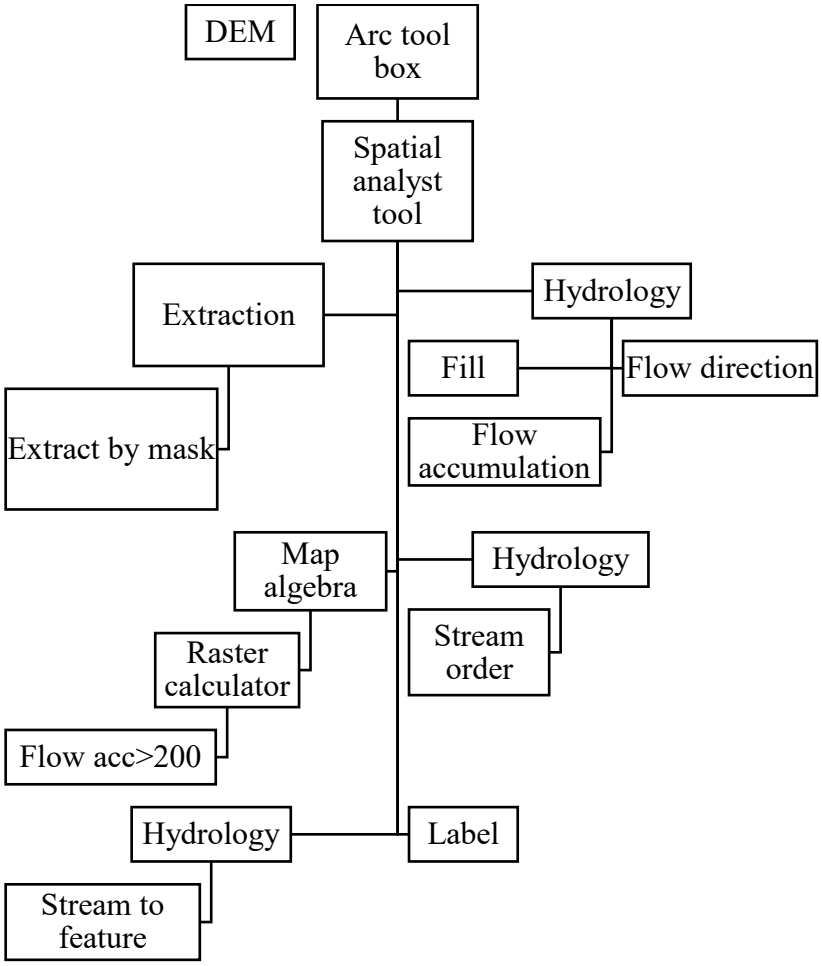


**Fig. 3.5 Steps for determining stream order**


**Fig. 3.6 Steps for determining slope**

**2.** Areal Aspects

These parameters assess the two-dimensional properties of the watershed, providing insights into its shape and form.

a. Circularity ratio ($R_c$): A dimensionless ratio of the area of the basin to the area of a circle having the same perimeter, indicating the basin's shape and potential for erosion (Kannan & Venkateswaran, 2020).

b. Elongation ratio ($R_e$): The ratio of the diameter of a circle with the same area as the basin to the maximum basin length, indicating the basin's shape and flow characteristics (Kannan & Venkateswaran, 2020).
c. Form factor ($F_f$): The ratio of the basin area to the square of the basin length, indicating the flow intensity of a basin (Kannan & Venkateswaran, 2020).
d. Compactness ratio ($C_c$): A measure comparing the basin perimeter to the circumference of a circle with the same area, indicating the basin's shape and potential for erosion (Kannan & Venkateswaran, 2020).
e. Lemniscate's ratio (K): A dimensionless parameter indicating the basin's shape, calculated using the square of the basin length divided by four times the area (Kannan & Venkateswaran, 2020).
f. Shape factor ($S_f$): The ratio of the square of the basin length to the area, indicating the basin's elongation and potential for peak flows (Kannan & Venkateswaran, 2020).
g. Constant of channel maintenance (C): The reciprocal of drainage density, indicating the area required to sustain a unit length of stream channel (Kannan & Venkateswaran, 2020).

3. Relief aspects

These parameters evaluate the vertical characteristics of the watershed, reflecting its topography and potential energy.

a. Relief (H): The elevation difference between the highest and lowest points in the basin, indicating the potential energy of the drainage system (Kannan & Venkateswaran, 2020).
b. Relief ratio ($R_r$): The ratio of basin relief to basin length, indicating the overall steepness of the basin (Kannan & Venkateswaran, 2020).
c. Relative relief ($R_{hp}$): The ratio of basin relief to perimeter, expressed as a percentage, indicating the basin's ruggedness (Kannan & Venkateswaran, 2020).
d. Ruggedness number ($R_n$): The product of basin relief and drainage density, indicating the structural complexity of the terrain (Gautam, 2023).

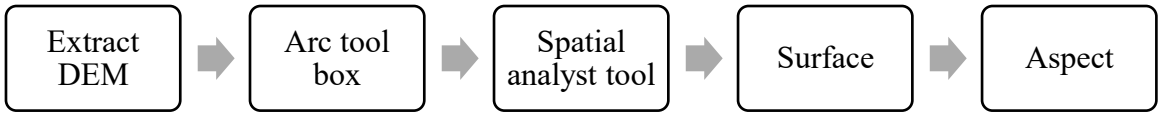


**Fig. 3.7 Steps for making aspect map**

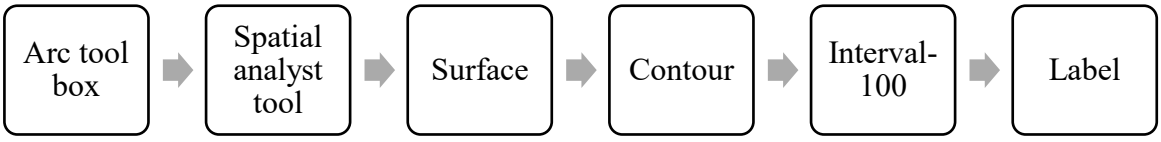


**Fig. 3.8 Steps for making contour map**

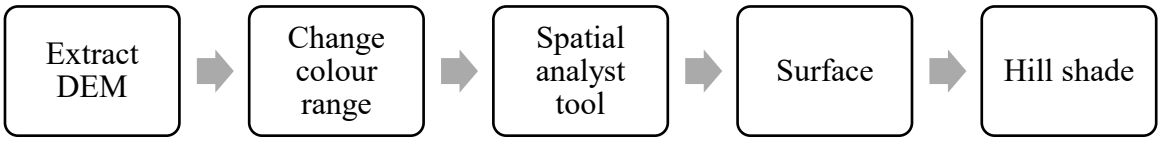


**Fig. 3.9 Steps for making elevation map**

3.5 IMPACT ASSESSMENT OF SWCE STRUCTURES

### 3.5.1 Based on LULC change detection

This study used Remote Sensing (RS) techniques to analyse changes in Land Use/Land Cover (LULC) between the years 2014 (pre-treatment) and 2024 (post-treatment). Cloud-free Landsat 8-9 (OLI/TIRS) satellite imagery was used for both years. LULC mapping methodology shown in Fig.3.10. Image processing and analysis were carried out using ArcGIS 10.8 software to fulfil the study's objectives. The LULC classification included five major classes vegetation, agricultural field, water bodies, barren land, and built-up areas.

#### *3.5.1.1 Description of LULC classification*

1. Vegetation: Includes Forest, stunted trees, bushes, and plantation crops such as coconut, rubber, cashew, pepper, and banana.
2. Agricultural fields: Encompasses all agricultural fields, including current fallow land, grasslands, and croplands.
3. Water Bodies: Comprises rivers, open water, lakes, reservoirs, and ponds.
4. Barren Land: Refers to land surfaces without vegetation, such as bare soil, open spaces, vacant land, sand, and landfill sites. Barren land may also include fallow land.
5. Built-up: Includes commercial, residential, and institutional buildings, transportation networks, roads, and mixed urban areas.

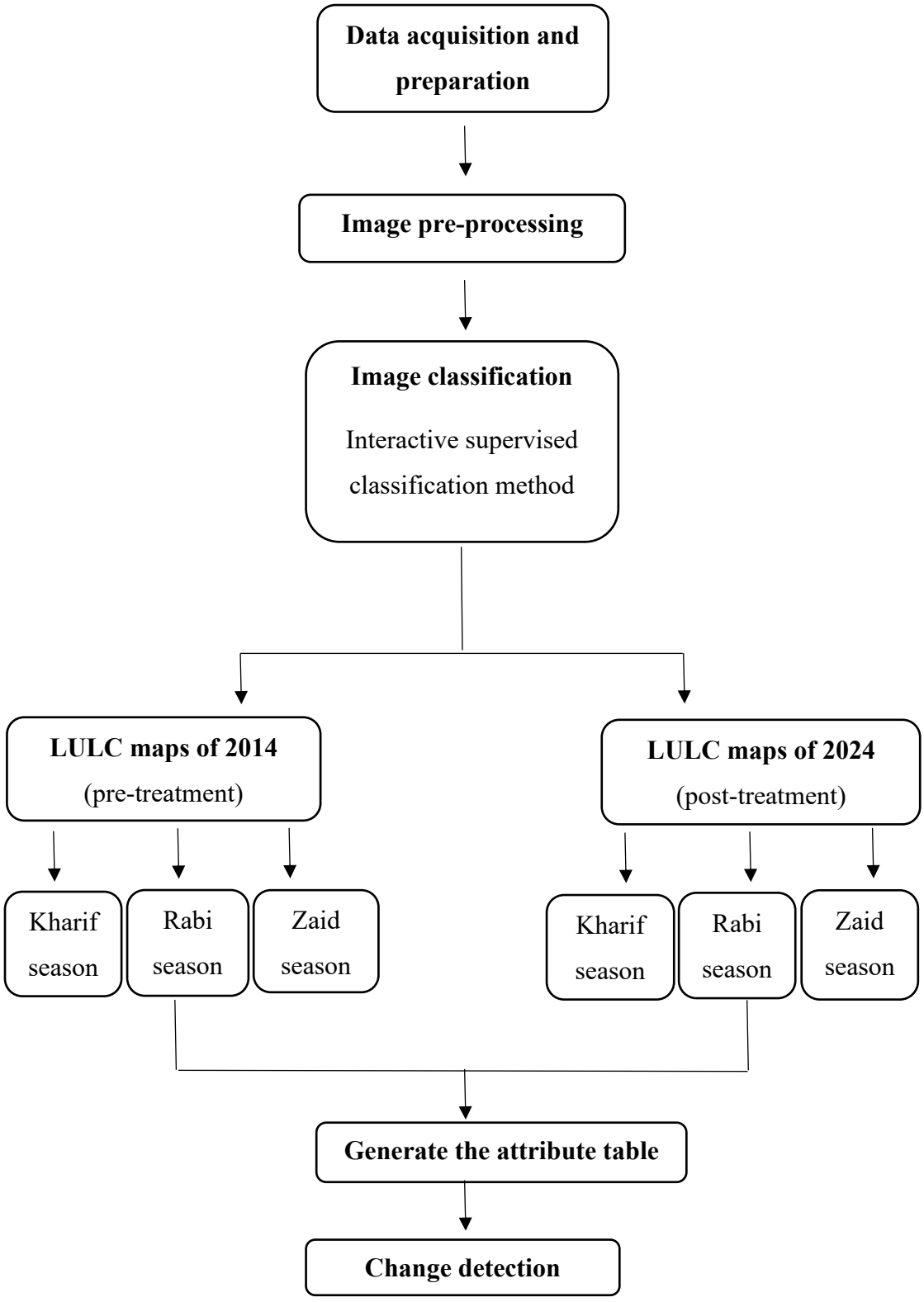


**Fig. 3.10 Land use and land cover (LULC) mapping process**

#### *3.5.1.2 Data acquisition and preparation*

Landsat 8–9 OLI/TIRS satellite imagery was utilized for LULC classification in this study. The data were obtained from the USGS Earth Explorer platform, covering the designated study area. The datasets were downloaded in TIF format and extracted from compressed (zipped) files for further processing. Image selection was based primarily on quality, with a focus on acquiring scenes with minimal cloud cover. As part of the selection criteria, a cloud cover threshold of less than 10% was applied. The final selected images exhibited cloud cover of less than 10%, which was deemed acceptable and did not impact the analysis.

#### *3.5.1.3 Image pre-processing*

Image pre-processing is a crucial step in satellite image interpretation. It involves procedures such as distortion correction and cloud removal, which may be necessary depending on the quality of the imagery. These processes are intended to enhance the visual interpretation and spectral separability of Earth's surface features. Additionally, pre-processing improves the overall quality of input data, ensuring greater accuracy and efficiency in subsequent automated image processing and classification tasks (Seyam *et al*., 2023).

In the satellite images, intensive pre-processing such as geo-referencing and layer stacking were performed to orthorectify the data. Each Landsat image was geo-referenced to the WGS_84 Datum and the UTM Zone 43 North coordinate system. Landsat 8-9 OLI/TIRS imagery includes 11 bands in total. For this study, bands 2 to 7 of both Landsat 8 and Landsat 9 were selected and stacked into a single image using the band composite function in ArcMap 10.8. The resulting composite image was then subset to the study area, optimizing the image processing and analysis by focusing on the region of interest.

#### *3.5.1.4 Image classification*

In satellite image classification, selecting an appropriate method for the study area is critical. In this study, per-pixel supervised classifiers were applied, which classify image pixels based on their similar or identical spectral reflectance properties

(Seyam *et al*., 2023). The well-established supervised classification approach was utilized to group LULC features detected from the satellite imagery.

The classification process consists of three main steps: training sample selection, extraction of signatures, and classification.

A) Training sample selection

The training sample selection process begins with the identification of training sites, which involves identifying specific areas within the satellite imagery that represent each LULC class. These areas are typically digitized directly on the screen to ensure precision and consistency. Main steps for selection of training sample shown in fig.3.11.

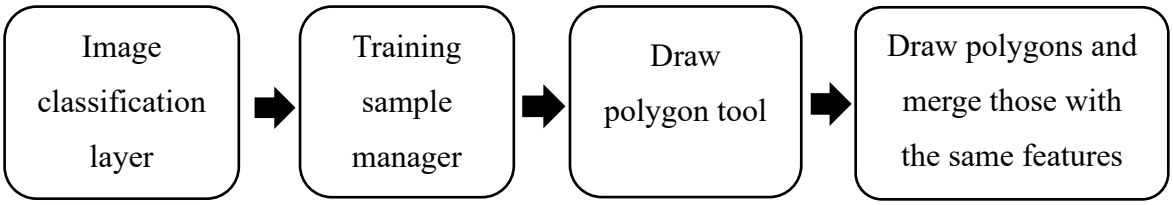


**Fig. 3.11 Steps of training sample selection**

B) Extracting the signature file

After drawing and labelling the training samples, the next step was to create signature files. These files store important details about each land cover type, based on the sample areas marked earlier. The purpose of this step was to prepare a SIG (signal) file for each land use/land cover (LULC) class. These files help the software understand how each type of land cover looks in the satellite image (Seyam *et al*., 2023). Once all the signatures were created, they were saved as ".sig" files either as shape files or feature classes. Training sample collected are shown in Fig.3.12. After drawing and labelling the training samples, the next step was to create signature files. These files store important details about each land cover type, based on the sample areas marked earlier. The purpose of this step was to prepare a SIG (signal) file for each land use/land cover (LULC) class. These files help the software understand how each type of land cover looks in the satellite image (Seyam et al., 2023). Once all the signatures were

created, they were saved as ".sig" files either as shape files or feature classes. Training sample collected are shown in Fig.3.12.

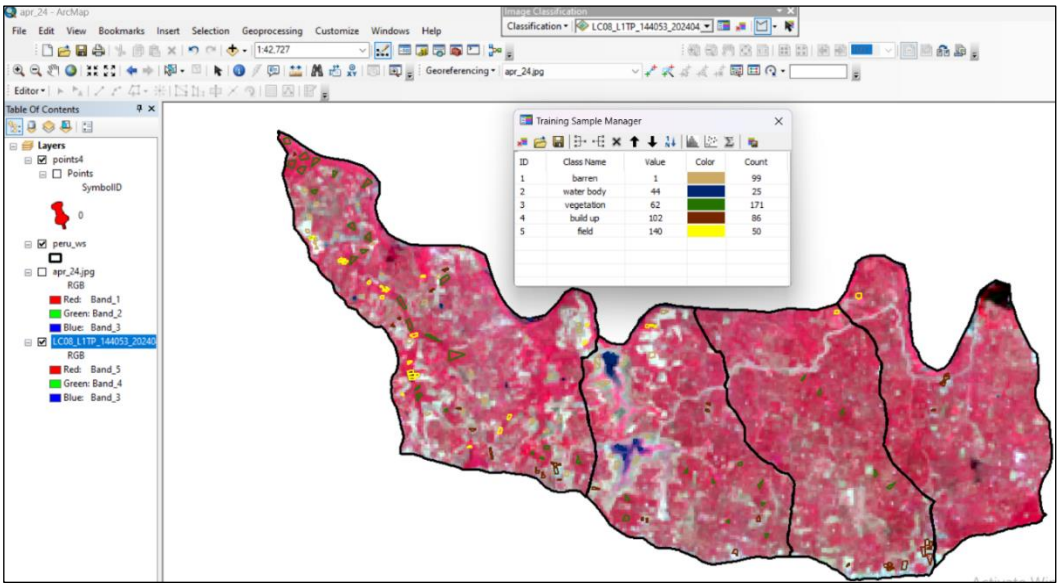


**Fig. 3.12 An Example of a collected training sample**

C) Image classification

The image classification toolbar was used to classify the Landsat satellite images. First, the training samples were checked using the toolbar and the training sample manager to ensure they clearly represented the land cover types in the area and were distinct from one another. Interactive supervised classification method was then applied in ArcMap version 10.8 to identify the different LULC types in the study area.

### *3.5.1.5 LULC change detection*

LULC change detection maps were prepared for the Kharif, Rabi, and Zaid seasons using satellite imagery from 2014 (pre-treatment) and 2024 (post-treatment). To identify areas of land use and land cover change, the post-classification comparison method was used. This involved classifying the satellite images and converting the classified raster outputs into vector layers for easier comparison. Changes were then assessed for each LULC type by comparing the corresponding classes between the two time periods.

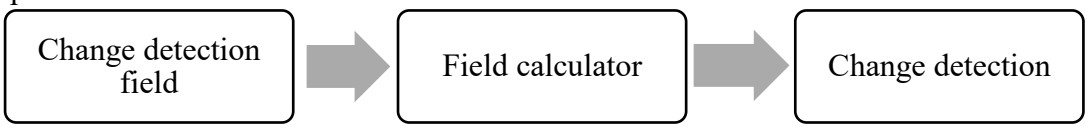


**Fig. 3.13 Steps for LULC change detection**

### 3.5.2 Based on normalized difference vegetation index (NDVI)

#### *3.5.2.1 Data used*

For NDVI classification, Landsat 8–9 (OLI/TIRS) satellite images from the years 2014 and 2024 were used. These images have a spatial resolution of 30 meters and a temporal resolution of 16 days. The satellite data was obtained from the USGS Earth Explorer. Band information is shown in Table 3.4.

**Table 3.4 Landsat 8-9 OLI/TIRS bands**

| Bands | Wavelength (μm) | Resolution (m) |
|---|---|---|
| Band 1 - Coastal aerosol | 0.43-0.45 | 30 |
| Band 2 - Blue | 0.45-0.51 | 30 |
| Band 3 - Green | 0.53-0.59 | 30 |
| Band 4 - Red | 0.64-0.67 | 30 |
| Band 5 - Near Infrared (NIR) | 0.85-0.88 | 30 |
| Band 6 - Shortwave Infrared (SWIR) 1 | 1.57-1.65 | 30 |
| Band 7 - Shortwave Infrared (SWIR) 2 | 2.11-2.29 | 30 |
| Band 8 - Panchromatic | 0.50-0.68 | 15 |
| Band 9 - Cirrus | 1.36-1.38 | 30 |
| Band 10 - Thermal Infrared (TIRS) 1 | 10.6-11.19 | 100 |
| Band 11 - Thermal Infrared (TIRS)2 | 11.50-12.51 | 100 |

#### *3.5.2.2 NDVI classification*

The NDVI map was prepared for the Kharif, Rabi, and Zaid seasons of the years 2014 and 2024 to assess changes in vegetation cover within the study area resulting from the impact of soil and water conservation measures.

NDVI was calculated using Equation. Landsat images with the NIR (Band 5) and Red (Band 4) bands were processed using the Raster Calculator tool in ArcGIS to generate NDVI maps. NDVI change detection analysis was carried out based on vegetation health and vegetation density. NDVI change maps were prepared for all three seasons Kharif, Rabi, and Zaid. To enhance the interpretation of results, the NDVI values were classified into categories as described in Table 3.5 (based on density) and Table 3.6 (based on vegetation health).

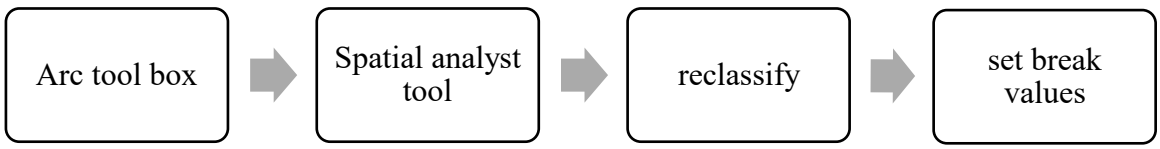


**Fig. 3.14 Steps for NDVI classification**

$$NDVI = \frac{(NIR - RED)}{(NIR + RED)}$$

**Table 3.5 NDVI classification based on vegetation density**

| NDVI value | Classes |
|---|---|
| <0 | Waterbody/ Built up |
| 0-0.2 | Sparse Vegetation |
| 0.2-0.5 | Moderate dense vegetation |
| >0.5 | Dense Vegetation |

**Table 3.6 NDVI classification based on vegetation health**

| NDVI value | Classes |
|---|---|
| <0 | No vegetation |
| 0-0.33 | Unhealthy Vegetation |
| 0.33-0.66 | Moderate vegetation |
| 0.66-1 | healthy Vegetation |

### *3.5.2.3 NDVI change analysis*

After classifying the obtained data, NDVI maps for the pre-treatment year (2014) and post-treatment year (2024) were prepared. To assess changes in vegetation, cover between these two periods, the NDVI difference was calculated using the Raster Calculator in ArcGIS. The expression NDVI Difference = NDVI 2023 − NDVI 2015 was applied, generating a raster in which each pixel value represented the change in NDVI over the study period. Positive values indicated an increase in vegetation, negative values indicated a decrease, and values near zero represented no significant change.

## 3.6 IRRIGATION WATER QUALITY INDEX

The Irrigation Water Quality Index (IWQI) is a comprehensive tool designed to assess the suitability of water for agricultural use. IWQI focuses specifically on parameters that impact soil health and crop productivity. Originating from the work of Horton (1945), who introduced the first WQI based on eight key parameters, the index was later refined by Brown *et al*. (1970) in collaboration with the U.S. National Sanitation Foundation, leading to the development of the National Sanitation

Foundation Water Quality Index (NSFWQI). IWQI incorporates variables such as electrical conductivity, sodium adsorption ratio (SAR), pH, and concentrations of specific ions, enabling a holistic evaluation of the impact of water on irrigation systems and long-term soil sustainability. The procedures for finding IWQI is shown in Fig 3.15.


**Fig. 3.15 Steps for finding IWQI**

### 3.6.1 Water survey

This survey aims to gather information on the water quality and availability in the region, focusing on its suitability for domestic and agricultural purposes. It also seeks to understand the community's awareness and perception of soil and water conservation practices. The collected data will help assess the current state of water resources and suggest potential improvements for sustainable management. The survey was conducted among 50 people from 4 micro watersheds of Perumatty Grama Panchayat.

### 3.6.2 Sample collection

**Table 3.7 Locations of sample collection points**

| SAMPLE | MICROWATERSHED | LONGITUDE | LATITUDE |
|---|---|---|---|
| 1 | Kambalathara- Kalyanappetta | 76°49'15.1" E | 10°38'59.2" N |
| 2 | Kambalathara- Kalyanappetta | 76°49'04.6" E | 10°38'59.6" N |
| 3 | Kambalathara- Kalyanappetta | 76°49'00.9" E | 10°38'51.3" N |
| 4 | Mullanthodu | 76°49'30.4" E | 10°38'34.7" N |
| 5 | Mullanthodu | 76°49'50.3" E | 10°38'32.6" N |
| 6 | Mullanthodu | 76°50'54.9" E | 10°38'11.8" N |
| 7 | Sarkkarpathy | 76°51'05.3" E | 10°38'32.4" N |
| 8 | Sarkkarpathy | 76°50'54.9" E | 10°39'10.2" N |
| 9 | Sarkkarpathy | 76°41'07.4" E | 10°38'51.1" N |
| 10 | Muthuswamy | 76°51'43.6" E | 10°40'15.2" N |
| 11 | Muthuswamy | 76°51'32.0" E | 10°40'15.2" N |
| 12 | Muthuswamy | 76°51'47.5" E | 10°38'59.6" N |
| 13 | Kambalathara- Kalyanappetta | 76°47'58.3" E | 10°39'05.6" N |

In this study, 13 water resources were selected in the study area and samples were collected. Samples were collected in clean, labelled containers and preserved appropriately to avoid contamination or degradation during transport. The details of the locations from where the samples are collected is given in the Table 3.7.

**Plate 3.4 Sample collection**

#### *3.6.2.1 Testing of samples*

The collected water samples were tested in the laboratory for the parameters such as pH, EC, Magnesium, Chloride, Sodium and Calcium. The Laboratory Analysis of Water Quality Parameters were used to compute IWQI. The pH represents the hydrogen ion concentration, critical for determining the acidity or alkalinity of water. Electrical Conductivity (EC) reflects the ion concentration and salinity. Chloride ($Cl^-$) is the major anion that can originate from both natural and anthropogenic sources. Calcium ($Ca^{2+}$) and Magnesium ($Mg^{2+}$) are essential hardness-causing ions in groundwater.

### 3.6.3 Computation of irrigation water quality index (IWQI)

#### *3.6.3.1 Computations of groundwater quality parameters*

The 13 groundwater samples were analysed for six key parameters: pH, Electrical Conductivity (EC), Sodium ($Na^+$), Calcium ($Ca^{2+}$), Magnesium ($Mg^{2+}$), and Chloride ($Cl^-$).

All ion concentrations (except pH) were converted from milligrams per liter (mg/L) to milliequivalents per litre (meq/L) using standard formulas (Ayers & Westcot, 1985):

- $Na^+$ (meq/L) = $Na^+$ (mg/L) ÷ 23
- $Ca^{2+}$ (meq/L) = $Ca^{2+}$ (mg/L) ÷ 20
- $Mg^{2+}$ (meq/L) = $Mg^{2+}$ (mg/L) ÷ 12.15
- $Cl^-$ (meq/L) = $Cl^-$ (mg/L) ÷ 35.45

This standardization enabled comparison across different ion concentrations and compatibility with subsequent index calculations.

#### *3.6.3.2 Sodium hazard evaluations: SAR and sodium percentage (%Na)*

SAR is used to assess the sodium hazard of irrigation water. It was calculated using the formula (Richards, 1954):

$$SAR = \frac{Na^+}{\sqrt{\frac{Ca^{2+} + Mg^{2+}}{2}}}$$

Higher SAR values indicate greater risk of soil dispersion and reduced permeability.

The sodium percentage helps determine the risk of sodium buildup in the soil. It was calculated using (Todd, 1980):

$$\%Na = \frac{Na^+}{Na^+ + Ca^{2+}Mg^{2+}} \times 100$$

Values above acceptable thresholds suggest a greater risk of soil structure degradation.

#### *3.6.3.3 Irrigation water quality index (IWQI) assessment*

i Quality index score ($q_i$) assignment

To normalize the raw water quality data, each parameter (EC, $Na^+$, SAR, $Cl^-$) was converted to a quality index score ($q_i$) on a scale of 0-100 using a class-wise linear interpolation method (Al-Fahdawi *et al*., 2024):

$$q_i = q_{i_{max}} - \frac{\left(x_{ij} - x_{inf}\right) \times \left(q_{i_{max}} - q_{i_{min}}\right)}{x_{sup} - x_{inf}}$$

Where:

- $x_{ij}$ = Observed value
- $x_{inf}, x_{sup}$ = Lower and upper-class limits
- $q_{i_{max}}, q_{i_{min}}$ = Maximum and minimum $q_i$ scores assigned for the class

The classification limits and score ranges were adapted from FAO guidelines (Ayers & Westcot, 1985) and recent literature (Vasistha & Ganguly, 2022).

ii Weightage assignment ($w_i$)

Each parameter was assigned a relative importance score ($S_i$) based on its impact on irrigation water quality. These scores were normalized to ensure their total equaled 1 (Al-Fahdawi *et al*., 2024):

**Table 3.8 Weightage values for different parameters**

| Parameter | $S_i$ | $w_i = \frac{S_i}{\Sigma S_i}$ |
|---|---|---|
| EC | 5 | 0.264 |
| $Na^+$ | 5 | 0.256 |
| SAR | 4 | 0.237 |
| $Cl^-$ | 3 | 0.243 |

These weights reflect each parameter's influence on soil health and crop productivity.

iii Irrigation water quality index (IWQI) calculation

IWQI was calculated using a weighted sum of the qi values for each parameter:

$$IWQI = \Sigma(q_{i_i} \times w_i)$$

Where:

- $q_i$ = Quality Index Score
- $w_i$ = Weightage Assignment

The final IWQI values were categorized as follows (Jhariya *et al*., 2016):

**Table 3.9 Suitability range of IWQI**

| IWQI RANGE | SUITABILITY |
|---|---|
| 85–100 | Highly suitable |
| 70–85 | Moderately suitable |
| 55–70 | Marginally suitable |
| 40–55 | Currently not suitable |
| <40 | Permanently not suitable |

This classification provided a comprehensive index to assess irrigation suitability across the study area.

### 3.6.4 Spatial analysis of IWQI using IDW and ordinary kriging

All calculations including ion conversions, SAR, %Na, $q_i$ values, and IWQI were carried out in Microsoft Excel. Descriptive statistics such as mean, minimum,

maximum, and standard deviation were computed for each parameter to observe variability. Further, analysis such as spatial interpolation or GIS-based mapping was performed in ArcGIS, using IDW or Ordinary Kriging techniques (Al-Fahdawi *et al*., 2024).

#### *3.6.4.1 Inverse distance weighting (IDW)*

Inverse Distance Weighting (IDW) is a deterministic spatial interpolation method commonly used to estimate unknown values at unsampled locations by referencing known values from surrounding points. It is grounded in Tobler's First Law of Geography, which states that "everything is related to everything else, but near things are more related than distant things" (Singh & Verma, 2019). In IDW, weights are assigned inversely proportional to the distance from the prediction location, meaning that nearer points have a greater influence on the estimated value. This technique is frequently applied in environmental and hydrological studies, such as mapping groundwater or irrigation water quality indices (Dewana *et al*., 2022).

The predicted value is calculated as a weighted average using the formula:

$$Z(x_0) = \frac{\sum_{i=1}^{n} \frac{Z(x_i)}{d_i^p}}{\sum_{i=1}^{n} \frac{1}{d_i^p}}$$

Where,

- $Z(x_i) =$ Observed value
- $d_i =$ Distance to the unknown location
- $x_0$ and p $=$ Power parameter

To evaluate the performance of IDW interpolation in representing spatial variation in irrigation water quality, a comparative analysis was carried out using different power parameters: 1, 2, 2.5, 3, 3.5, and 4. The power parameter p in the IDW equation controls the rate at which the influence of a sample point decreases with distance. At lower powers (e.g.,$p = 1$), the influence is more evenly spread across all neighboring points, resulting in a smoother surface. As the power increases, the interpolation gives significantly more weight to nearby points, producing a surface that more closely follows local variations. For instance, $p = 2$ is the most commonly used

value as it reflects the inverse-square law of distance. However, higher values like $p = 3.5\ or\ 4$ increase localization, which may either enhance accuracy or lead to overfitting, depending on the spatial distribution of data points (Dewana *et al*., 2022).

In addition to varying the power parameter, both fixed and variable search radius settings were tested in combination with each power value to assess their influence on interpolation accuracy. This allowed a comprehensive evaluation of how spatial configuration and weighting sensitivity together affect the IDW model's predictive performance.

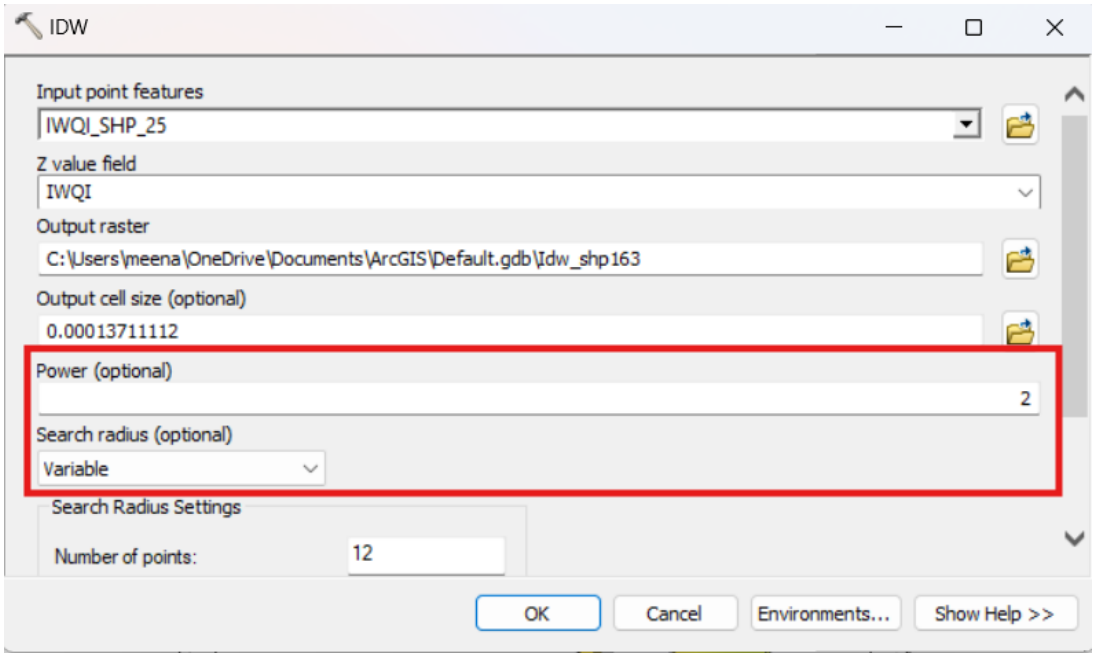


**Fig. 3.16 Dialog box for IDW interpolation**

### *3.6.4.2 Ordinary kriging*

Ordinary kriging is a geostatistical interpolation technique that provides predictions at unsampled locations by considering both the distance and the spatial autocorrelation between known data points. Unlike deterministic methods, Ordinary Kriging uses a statistical model that includes a variogram (or semi variogram) to quantify spatial relationships. The underlying assumption of Ordinary Kriging is that the mean of the variable is constant but unknown across the study area, and it treats the variable of interest as a regionalized random variable (Singh & Verma, 2019). By analysing how variance changes with distance, the variogram informs how weights are optimally assigned to known points, allowing Ordinary Kriging to minimize prediction

error and provide not just an estimate, but also a measure of estimation uncertainty (Dewana *et al*., 2022).

The general Ordinary Kriging estimator is given by:

$$Z(x_0) = \sum_{i=1}^{n} w_i Z(x_i)$$

Where,

- $Z(x_i)$ = Observed value at location
- $x_i, w_i$ = Weight assigned to that point

The weights are determined based on the semi variogram model so that the estimator is unbiased and the prediction variance is minimized. Ordinary Kriging uses semi variogram to model spatial dependence, with commonly used models being spherical, exponential, and Gaussian (Loghmari *et al*., 2018). Because of its ability to account for spatial structure, Ordinary Kriging is especially suitable for environmental studies where understanding and quantifying spatial variability is essential.

In the case of Ordinary Kriging, five semi-variogram models were compared: spherical, circular, exponential, Gaussian, and linear. These models define how spatial correlation between points changes with distance and play a critical role in calculating the weights for interpolation. The spherical model is widely used and assumes that spatial correlation increases with distance up to a certain range, beyond which it levels off. The circular model behaves similarly but with a rounded rise and tends to be more sensitive near the origin. The exponential model assumes a gradual decrease in correlation and never truly reaches a sill, making it suitable for variables with continuous but weak spatial structure. The Gaussian model is ideal for smoothly varying phenomena due to its strong spatial continuity near the origin. Lastly, the linear model assumes a straight-line increase in semi variance with distance, which may oversimplify real-world spatial patterns. By comparing these models, the goal was to identify which best captured the spatial structure of the observed water quality data (Singh & Verma, 2019; Loghmari *et al*., 2018).

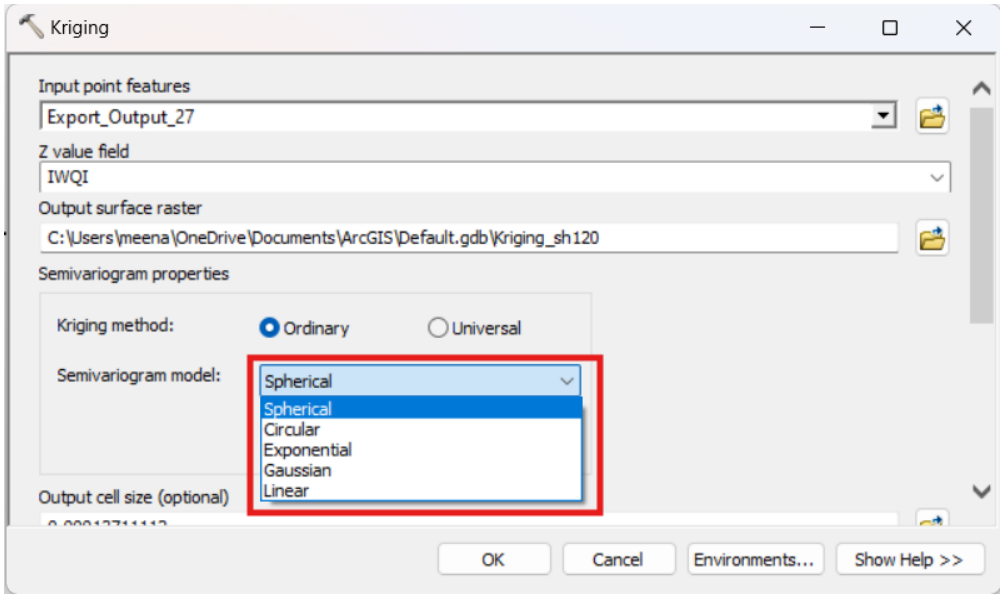


**Fig. 3.17 Dialog box for kriging interpolation**

### 3.6.5 Performance evaluation using statistical performance indicators

#### *3.6.5.1 Validation*

i Split-sample validation approach for spatial interpolation

To evaluate and compare the performance of the spatial interpolation methods, the dataset was systematically divided into two subsets: testing data set and validation data set. Initially, the interpolation was performed using 7 points for interpolation and the remaining 6 points for validation. All IDW power variations and Ordinary Kriging semi-variogram models were applied during this phase, and the predicted values at the validation points were compared with the observed data using statistical error metrics. In the second phase, the same process was repeated with a different configuration, 10 testing data set and 3 validation points to examine how increasing the number of testing data points influenced the model performance. This two-stage setup helped assess the sensitivity of the methods to sample density and validate the consistency and reliability of the spatial predictions across varying data conditions.

ii Leave one out cross validation

To assess the accuracy and robustness of the interpolation methods, Leave-One-Out Cross-Validation (LOOCV) was employed. LOOCV is a widely used validation technique in spatial analysis where each data point is systematically removed one at a time, and its value is predicted using the remaining data. This process is repeated for all

sample points, ensuring that every location serves once as a validation point. The predicted values are then compared with the actual observed values to compute statistical error metrics such as R, $R^2$, Mean Error (ME), Mean Absolute Error (MAE), and Percent Bias (PBIAS). LOOCV is particularly beneficial in geospatial applications with small to moderate sample sizes because it utilizes the entire dataset efficiently without the need to split it into separate training and testing sets (Dewana *et al*., 2022). Although it is computationally intensive, LOOCV provides a comprehensive and unbiased evaluation of interpolation performance, making it a reliable choice for comparing methods like IDW and Ordinary Kriging in spatial water quality studies (Singh & Verma, 2019).

#### *3.6.5.2 Evaluation using statistical performance indicators*

To quantitatively assess the accuracy of different interpolation methods, six statistical error metrics were used: correlation coefficient (R), coefficient of determination ($R^2$), mean error (ME), mean absolute error (MAE), root mean squared error (RMSE), and percent bias (PBIAS). These metrics were calculated by comparing predicted values at validation points with the corresponding observed values. Together, they provide a comprehensive understanding of each method's predictive strength, average error, variability, and directional bias (Dewana *et al*., 2022; Singh & Verma, 2019).

- Correlation Coefficient (R) measures the strength and direction of the linear relationship between observed and predicted values. Values closer to +1 indicate a strong positive linear relationship, implying high predictive accuracy.

$$R = \frac{\sum_{i=1}^{n}(P_i - \bar{P})(O_i - \bar{O})}{\sqrt{\sum(P_i - \bar{P})^2 \ \sum(O_i - \bar{O})^2}}$$

- Coefficient of Determination ($R^2$) quantifies the proportion of variance in observed data explained by the model. It ranges from 0 to 1, with values closer to 1 indicating that the model captures most of the variability in the data.

$$R^2 = \frac{\sum_{i=1}^{n}(P_i - \bar{P})(O_i - \bar{O})}{\sqrt{\sum(P_i - \bar{P})^2 \ \sum(O_i - \bar{O})^2}}$$

- Mean Error (ME) reflects the average bias in the predictions. A value close to 0 suggests that predictions are neither consistently overestimated nor

underestimated. Positive ME indicates underestimation, while negative ME indicates overestimation.

$$ME = \frac{1}{n}\sum_{i=1}^{n}(P_i - O_i)$$

- Mean Absolute Error (MAE) measures the average magnitude of error, ignoring direction. Smaller MAE values indicate that the model's predictions are generally close to the observed values, thus implying better accuracy.

$$MAE = \frac{1}{n}\sum_{i=1}^{n}|P_i - O_i|$$

- Root Mean Squared Error (RMSE) calculates the square root of the average squared differences between predicted and observed values. It gives greater weight to larger errors and is sensitive to outliers. Lower RMSE values imply higher prediction accuracy and a better-performing model (Loghmari *et al*., 2018).

$$RMSE = \frac{1}{n}\sum_{i=1}^{n}(P_i - O_i)^2$$

- Percent Bias (PBIAS) quantifies the average tendency of predictions to be higher or lower than the actual values, expressed as a percentage. A PBIAS of 0% indicates perfect accuracy. Positive values indicate underestimation, and negative values indicate overestimation.

$$PBIAS = \left(\frac{\sum_{i=1}^{n}(P_i - O_i)}{\sum_{i=1}^{n} O_i}\right) \times 100$$

Each of these metrics captures a different aspect of model performance, and their combined analysis helps in selecting the most reliable interpolation method for spatial water quality prediction.

### 3.6.6 Spatial mapping of IWQI

In this study, ArcGIS 10.8 was employed to prepare the maps of each parameter separately and finally the IWQI map. The steps for preparing map are given below:

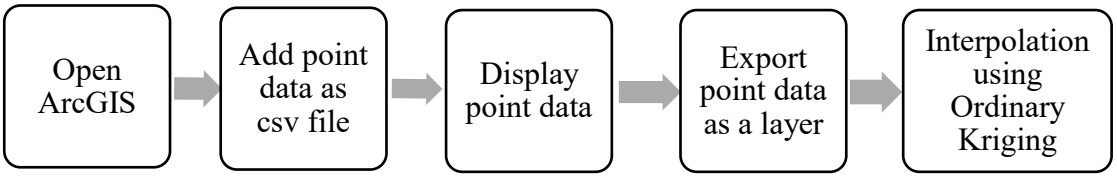


**Fig. 3.18 Steps for map preparation**

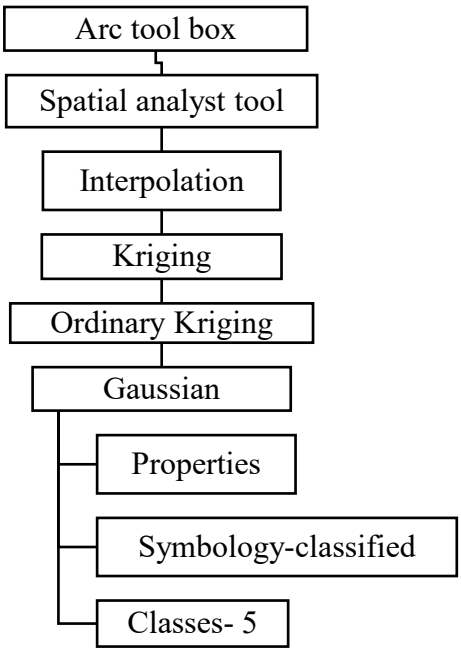


**Fig. 3.19 Steps for interpolation- Ordinary kriging**

1. Chloride ($Cl^-$) map

   The chloride concentration map reveals the spatial distribution of $Cl^-$ ions across groundwater sources. Elevated chloride levels in certain areas indicate potential seawater intrusion or anthropogenic contamination. Mapping $Cl^-$ helps assess risks to irrigation systems and crop health, especially for chloride-sensitive plants.

2. Sodium adsorption ratio (SAR) map

   This map presents the spatial variation in SAR values, an essential indicator of sodium hazard for soil permeability and structure. Higher SAR regions suggest potential soil infiltration issues, affecting long-term irrigation sustainability.

3. Electrical conductivity (EC) map

   The EC map visualizes the distribution of salinity levels in the groundwater. High EC values correspond to greater total dissolved salts, affecting plant water uptake and potentially leading to reduced crop yields in sensitive species.

4. pH map

   The pH distribution map illustrates the acidity or alkalinity of groundwater. Groundwater in this region mostly remains within acceptable pH limits for irrigation; however, localized deviations may impact nutrient solubility and plant health.

5. Magnesium ($Mg^{2+}$) map

   This map shows the spatial variation of magnesium concentrations. While essential for plant growth, excessive magnesium can cause soil structure deterioration and nutrient imbalances. Mapping assists in identifying such hotspots.

6. Sodium ($Na^{+}$) map

   The sodium concentration map identifies zones of potential sodium toxicity in groundwater. Elevated sodium can adversely affect soil permeability and cause physiological disorders in crops, requiring soil amendment strategies.

7. Calcium ($Ca^{2+}$) map

   The calcium distribution map highlights its availability across the study area. Adequate calcium levels support soil structure and mitigate sodium effects. Low calcium zones could exacerbate sodicity problems, demanding careful irrigation planning.

8. IWQI map

   The IWQI map shows how irrigation water quality varies across the study area. Regions with low IWQI values may pose risks to crops and soil over time, highlighting the importance of choosing water sources wisely and planning irrigation carefully.

## 3.7 EFFECT OF LULC ON WQI

LULC significantly influence the WQI of surface water bodies, as variations in land patterns directly affect the quantity and quality of runoff entering it. Urbanization, agricultural expansion, and deforestation contribute to increased loads of sediments, nutrients, and chemical pollutants, often leading to a decline in water quality (Pandey *et al*., 2023). Vegetated areas help maintain better water quality by reducing erosion and acting as natural filters, whereas built-up and barren lands typically accelerate surface runoff and transport contaminants into water bodies (Agapiou, 2020; Abijith and Saravanan, 2022). These land-induced changes are reflected in the WQI, which integrates various physicochemical parameters into a single value to indicate overall water quality status. Thus, assessing LULC dynamics is essential for interpreting spatial and seasonal variations in WQI and for informing sustainable watershed and land management practices (Pandey *et al*., 2023). In this study, since the water samples were collected during the Zaid season, the LULC map corresponding to the Zaid season was taken in ArcGIS 10.8 for conducting zonal statistics analysis. The steps are as follows:

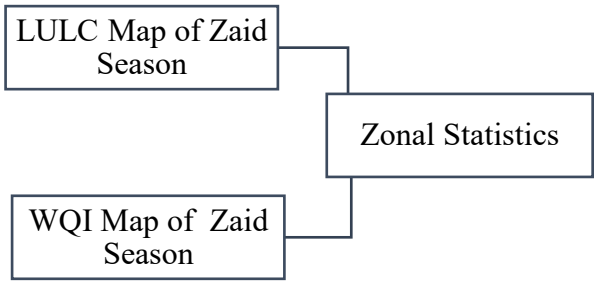


**Fig. 3.20 Zonal statistics**

### 3.7.1 Zonal statistics

Zonal statistics is a spatial analysis technique commonly used in GIS to extract statistical summaries of raster values within predefined vector zones, such as land use classes or watershed boundaries. In LULC and WQI-related studies, zonal statistics helps quantify metrics such as mean, maximum, and standard deviation of water quality parameters (e.g., WQI, NDVI, NDWI) within different land use categories. This enables the assessment of how specific land covers, like urban or agricultural zones, influence surface water quality. For example, urban zones may show higher mean WQI values indicating poorer water quality due to runoff and impervious surfaces, while forested

zones may reflect better water quality conditions. Zonal statistics, therefore, provides a valuable method for spatially correlating land use patterns with environmental indicators and supports targeted water resource management (Zhang *et al*., 2023). By extracting statistical summaries like mean, maximum, and standard deviation of WQI values within each LULC zone, the analysis facilitates clearer interpretation of spatial relationships and supports targeted environmental management decisions.

The steps for Zonal Statistics are given in the following Fig 3.21 and the dialog box for Zonal Statistics as table is given in the Fig. 3.22.

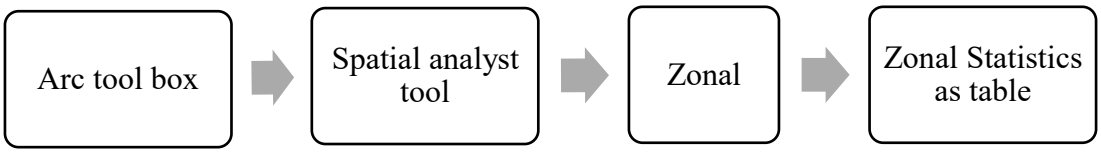


**Fig. 3.21 Steps for zonal statistics as table in ArcGIS**

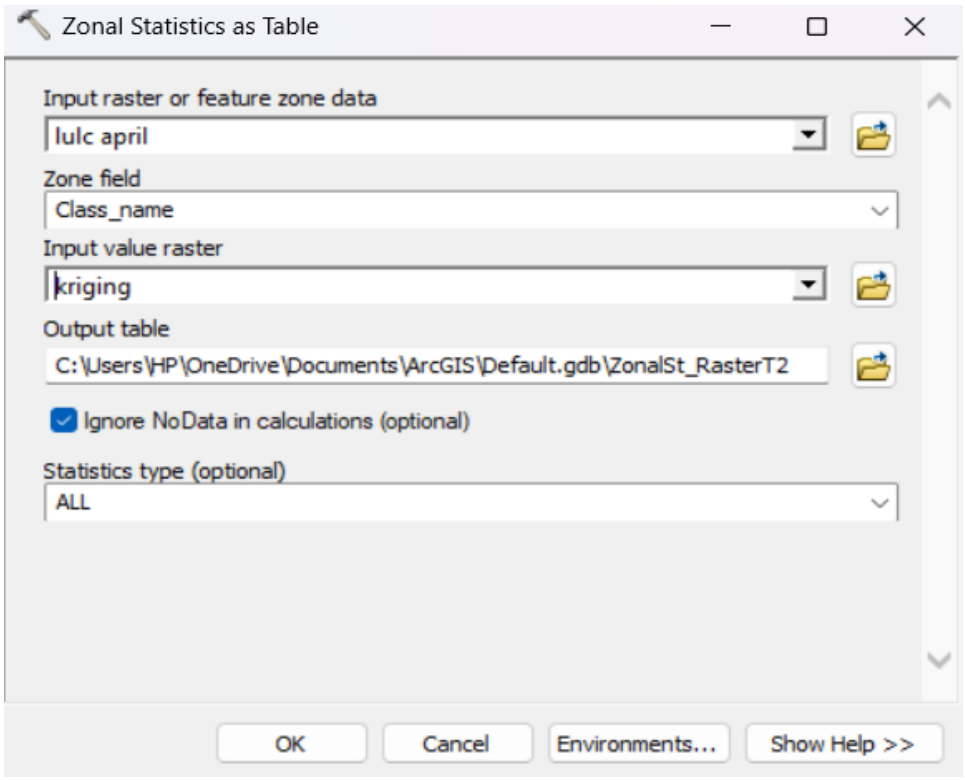


**Fig. 3.22 Dialog box for zonal statistics as table**

# RESULT AND DISCUSSION

# CHAPTER IV

# RESULT AND DISCUSSION

The results and discussion section presents a detailed analysis of the data collected to evaluate the effectiveness of soil and water conservation measures and their impact on land use, vegetation, and water quality in the Perumatty Panchayath. The implementation of conservation structures was examined in relation to geomorphological characteristics of the study area to understand their spatial suitability and effectiveness. Using Remote Sensing and GIS tools, changes in Land Use Land Cover (LULC) and vegetation health were assessed over time through NDVI analysis. The Irrigation Water Quality Index (IWQI) was calculated to determine the usability of water for irrigation, while zonal statistics were used to link water quality and vegetation changes with specific land use categories and the influence of LULC patterns on water quality was analysed to highlight the role of land use practices in shaping groundwater conditions. Together, these analyses provide a comprehensive understanding of the region's environmental dynamics.

## 4.1 IDENTIFICATION OF SOIL AND WATER CONSERVATION MEASURES ADOPTED AND STUDY OF GEOMORPHOLOGICAL PARAMETERS OF STUDY AREA

### 4.1.1 Soil and water conservation measures in the study area

A reconnaissance survey was conducted to identify and assess the status of soil and water conservation measures implemented by the Department of Soil Survey and Soil Conservation in Perumatty Panchayath. Soil and water conservation measures like earthen bunds, farm ponds and Centripetal Terrace were identified and found to be in good condition. Farmers feedback was collected and it was noted that there were significant benefits from these soil and water conservation structure including a remarkable increase in enhanced agricultural productivity and better soil stability. The routine maintenance is necessary to ensure continuous efficiency. Regular monitoring and management are essential to sustain the benefits of these conservation practices and maximize their long-term effectiveness.

The data collected during the survey was processed and analysed in ArcGIS 10.8 to prepare detailed map of spatial distribution of conservation measures in watershed as shown in Fig. 4.1.

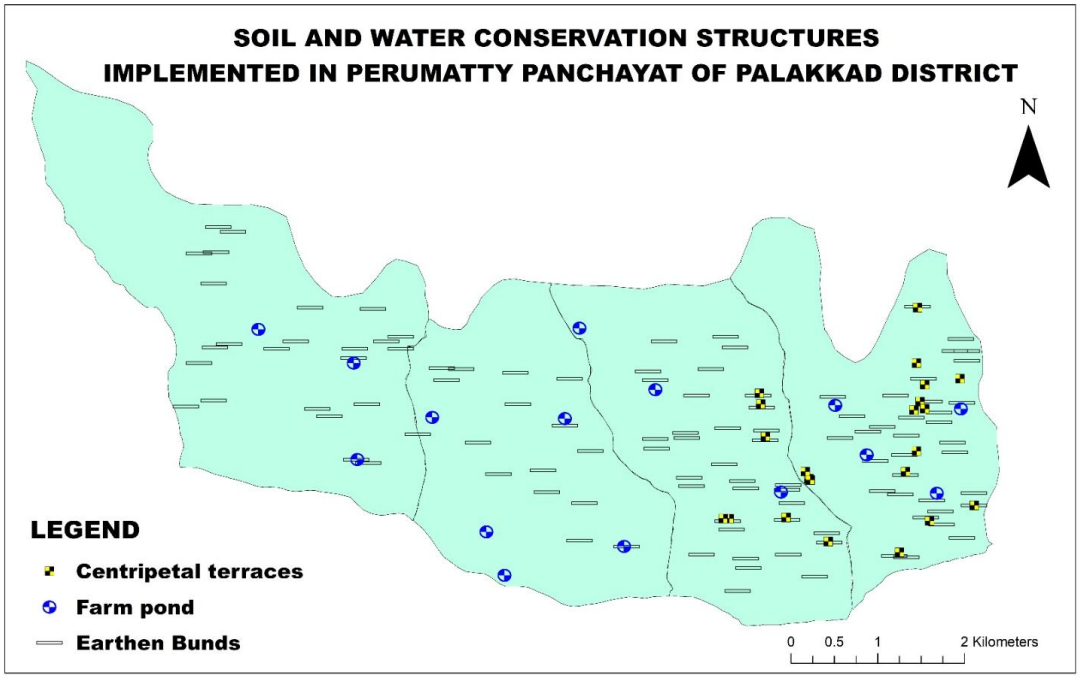


**Fig. 4.1 Soil and water conservation measures implemented in the study area**

### 4.1.2 Geomorphological parameters of watershed

The study area was delineated from SRTM DEM using arc toolbox in ArcGIS 10.8 and it is shown in Fig. 4.2.

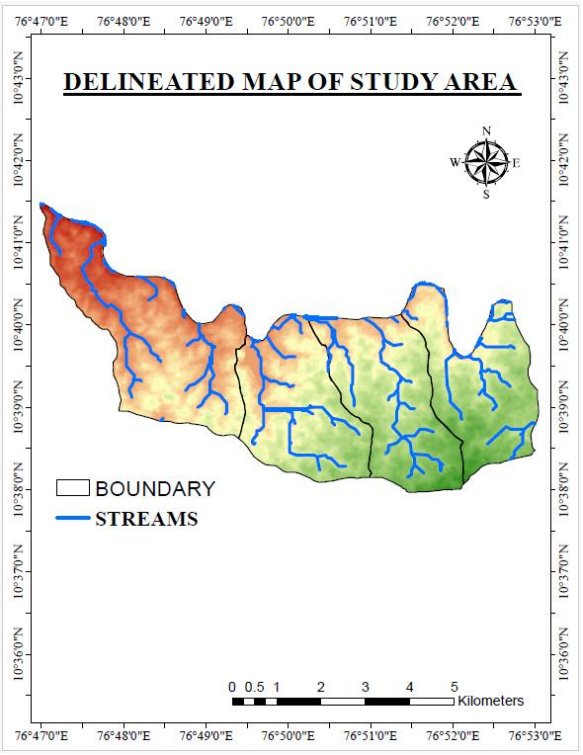


**Fig. 4.2 Delineated map of study area**

#### *4.1.2.1 Morphometric analysis of the study area*

The morphometric analysis of the study area was done in three different aspects such as Linear, Areal and Relief aspects. These aspects were determined based on various parameters discussed below:

Basin parameters:

The total area of the watershed is 33.140 km², indicating the surface over which water collects and flows. It has a perimeter of 45.737 km, defining the outer boundary of the basin. The basin length, measured as the longest flow path from the source to the outlet, is 9.583 km, while the mean basin width, derived from the area-to-length ratio, is 3.458 km. These parameters are fundamental in assessing the basin's shape, runoff behavior, and potential vulnerability to landslides.

**Table 4.1 Basin parameters**

| S.no | Description | Values | Units |
|---|---|---|---|
| | Watershed | Perumatty | |
| | **Basin parameters** | | |
| 1 | Area (A) | 33.140 | $Km^2$ |
| 2 | Perimeter (P) | 45.737 | Km |
| 3 | Basin length ($L_b$) | 9.583 | Km |
| 4 | Mean basin width | 3.458 | Km |

Linear aspects:

The linear aspects of the study area were calculated and are given in Table 4.2 and 4.3. A detailed description is provided below:

1. Stream order (u) and stream number

   Stream ordering is the first step in morphometric analysis. Strahler's method of stream ordering was adopted and it was found that the study area is a third-order drainage basin with a dendritic drainage pattern, as shown in Fig 4.1. The total number of streams in the study area is 54 with 44 numbers of first-order stream, 8 numbers of second-order stream and 2 numbers of third-order stream. The number of streams in each order represent stream number and it is given in Table 4.2. This shows that the total number of streams decreases as the stream order increases. Lower stream orders (below third order) are generally

seasonal, whereas the streams of third order or higher consistently carry a substantial amount of water.

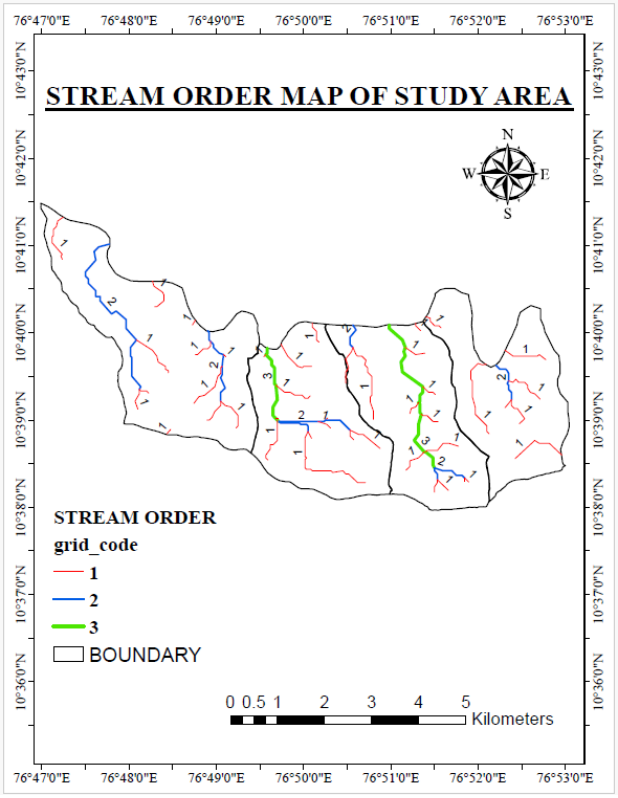


**Fig. 4.3 Stream order map of study area**

2. Bifurcation ratio ($R_b$) and mean bifurcation ratio ($R_{bm}$)

In this Study area, the bifurcation ratio is ranging from 0 to 5.5 as shown in Table 4.2. The mean bifurcation ratio of 4.75 falls within the normal range (3–5) for natural drainage systems (Strahler, 1964) indicated that the watershed is less affected by structural disturbances and that the drainage pattern is not significantly influenced by geological structures (Umrikar, 2017). The overall morphology of the basin was relatively stable and less affected by subsurface geological heterogeneities. The Rho coefficient of 0.032 indicates very poor drainage connectivity and limited stream branching, likely due to a combination of highly resistant lithology, immature drainage network development, or low rainfall and runoff potential. Such a low value suggests that the basin is in an early stage of geomorphic evolution, with minimal stream extension and weak integration between stream orders. This condition may result in slower hydrological response, localized surface runoff, and limited water retention, which are important factors in watershed management and sustainable land-use planning (Nag, 1998).

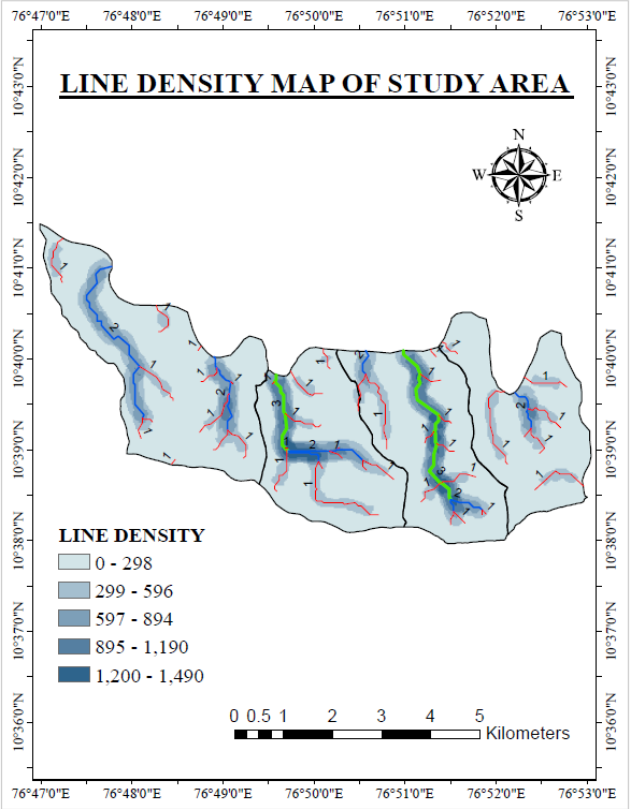


**Fig. 4.4 Line density map of study area**

**Table 4.2 Stream length, Stream length ratio and Bifurcation ratio of the study area**

| Stream order (u) | Stream number ($N_u$) | Stream length ($L_u$) (Km) | Mean stream length ($L_{um}$) (Km) | Stream length ratio ($R_l$) | Bifurcation ratio ($R_b$) |
|---|---|---|---|---|---|
| 1 | 44 | 0.24043 | 0.00546 | 0 | 5.5 |
| 2 | 8 | 0.09698 | 0.012 | 0.05 | 4 |
| 3 | 2 | 0.04931 | 0.02465 | 0.254 | 0 |

3. Drainage density ($D_d$)

The drainage density of 1.603 km/km² falls within the category of low to moderate drainage density, which corresponds to a coarse drainage texture and suggests that the watershed is characterized by highly permeable subsoil, dense vegetation cover, and low relief (Horton, 1945). This indicates a poorly drained basin where surface runoff is limited, and water tends to infiltrate into the ground, resulting in a slower hydrological response. While this can reduce the risk of flash floods, it may increase the potential for soil saturation, gully erosion, or delayed peak flows during prolonged

rainfall events (Ahmed *et al*., 2010). Such characteristics are typical of mature or stable landscapes with a balance between infiltration and surface flow.

**Table 4.3 Linear aspects of the study area**

| Linear Aspects | | | |
|---|---|---|---|
| **S.no** | **Description** | **Values** | **Units** |
| 1 | Total stream length ($L_u$) | 0.386715 | Km |
| 2 | Mean stream length ratio ($R_{slm}$) | 0.014 | |
| 3 | Mean bifurcation ratio ($R_{bm}$) | 3.167 | |
| 4 | Rho coefficient ($\rho$) | 0.004 | |
| 5 | Drainage density ($D_d$) | 1.603 | $Km/Km^2$ |
| 6 | Stream frequency ($F_s$) | 2.142 | $Streams/Km^2$ |
| 7 | Drainage texture ($D_t$) | 1.552 | Streams/Km |
| 8 | Infiltration number ($I_f$) | 3.433 | |
| 9 | Length of overland flow ($L_o$) | 0.312 | Km |
| 10 | Drainage intensity ($D_i$) | 1.337 | Km |

4. Drainage texture ($D_t$)

The drainage texture value of 1.552/km classifies the watershed as having a very coarse drainage texture, which typically indicates low stream frequency and widely spaced drainage lines. This condition reflects a landscape with high infiltration capacity, often due to permeable subsurface lithology, dense vegetation, and gentle topographic gradients (Sreedevi *et al*., 2013). Such areas tend to have reduced surface runoff, resulting in a slower and more regulated hydrological response, which may minimize flash flooding risks but can lead to prolonged soil saturation under persistent rainfall. The coarse drainage texture also suggests stable geomorphic conditions with minimal erosional activity (Smith, 1950).

5. Stream frequency ($F_s$)

A stream frequency of 2.142 per $km^2$ falls within the low stream frequency category, indicating a sparsely developed drainage network. This suggests that the basin has high infiltration capacity, likely due to permeable subsurface materials, dense vegetation, and gentle to moderate relief (Venkatesan, 2014). Such conditions result in reduced surface runoff and a slower hydrological response, which can be beneficial in minimizing the risk of flash flooding. However, it may also indicate limited surface

water availability and a greater reliance on subsurface flow mechanisms for sustaining streamflow during dry periods. The low stream frequency reflects a basin with relatively stable geomorphic conditions and moderate drainage development.

6. Infiltration number ($I_f$)

An infiltration number of 3.433 indicates a moderate to high infiltration capacity of the watershed, which implies that a significant portion of rainfall is likely to percolate into the subsurface, reducing the volume and speed of surface runoff. This suggests that during rainfall events, especially in the monsoon period, the watershed will experience a delayed and moderated hydrological response, helping to minimize the risk of flash flooding and enhancing groundwater recharge. Such values typically reflect the presence of permeable soil, fractured rock strata, and adequate vegetative cover, which promote infiltration and reduce runoff intensity (Bhatt & Ahmed, 2014).

7. Drainage intensity ($D_i$)

A drainage intensity of 1.337 indicates a low intensity of drainage processes within the watershed, which reflects a less dissected terrain with widely spaced stream channels. This suggests that the surface runoff is relatively low, and the basin exhibits greater infiltration potential, leading to slower hydrological response and reduced susceptibility to erosional processes such as gullying and rill formation. Such conditions are typically associated with stable geomorphic settings, gentle slopes, and moderately permeable lithological units, contributing to a more balanced runoff–infiltration relationship (Umirkar, 2017).

8. Length of overland flow ($L_o$)

The length of overland flow of 0.312 km indicates shorter flow paths, which are typically associated with steeper slopes, lower infiltration capacity, and quicker surface runoff. This suggests that rainfall in the watershed is more rapidly converted into surface flow, leading to a faster hydrological response and an increased risk of soil erosion and flash flooding, especially during intense rainfall events. Such conditions are often found in undulating or hilly terrains with impermeable soils or sparse vegetation that limit water infiltration (Sukristiyanti *et al*., 2018).

C) Areal parameters

Areal parameters such as circularity ratio, elongation ratio, form factor, compactness constant, lemniscate ratio, shape factor and compactness of channel maintenance were determined and given in Table 4.4. These parameters focus on size and shape of watershed.

**Table 4.4 Areal aspects of the study area**

| Areal Aspects | | | |
|---|---|---|---|
| **S.no** | **Description** | **Values** | **Units** |
| 1 | Circularity ratio ($R_c$) | 0.199 | |
| 2 | Elongation ratio ($R_e$) | 0.678 | |
| 3 | Form factor ratio ($F_r$) | 0.361 | |
| 4 | Compactness constant ($C_c$) | 2.240 | |
| 5 | Lemniscate's ratio (K) | 0.693 | |
| 6 | Shape factor ($B_s$) | 2.771 | |
| 7 | Constant of channel maintenance (C) | 0.624 | $Km^2/Km$ |

1. Circularity ratio ($R_c$)

Circularity ratio ($R_c$) value close to 1 indicated that the basin shapes are circular, while values between 0.4 to 0.5 are typical for elongated basins with highly permeable and uniform geologic materials (Soni, 2017). The circularity ratio ($R_c$) of 0.199 indicates that the watershed has a highly elongated shape, which suggests that the drainage system is strongly influenced by structural controls, such as faults, joints, or lithological variations (Soni, 2017). Such elongated basins are typically associated with low to moderate relief, high infiltration capacity, and slower concentration time, meaning that runoff takes longer to reach the basin outlet. These characteristics may reduce the risk of sudden peak flows but may also reflect tectonic influence and anisotropic geological conditions (Kuntamalla *et al*., 2018).

2. Elongation ratio ($R_e$)

According to Pareta and Pareta (2011), the shape of a watershed can be classified as highly elongated (Re < 0.5), elongated (Re = 0.5–0.7), less elongated (Re = 0.7–0.8), oval (Re = 0.8–0.9) and circular (Re = 0.9–0.10). Since the study area has Re value of 0.678, the area is elongated in shape.

3. Form factor (Ff)

If form factor is below 0.78, the watershed is elongated. If it is above 0.78, the watershed is circular (Singh *et al*., 2023). This watershed has a form factor of 0.361 signifying an elongated shape which results in low peak flows for longer duration.

4. Compactness constant ($C_c$)

A $C_c$ value of 1.0 represents a perfectly circular catchment, whereas a $C_c$ value greater than 1.0 indicates a significant deviation from a circular basin shape (Singh *et al*., 2023). The compactness constant of 2.24 suggests that this watershed is less compact and more elongated, which typically results in longer flow paths and a slower, more prolonged runoff response.

5. Shape factor ($B_S$) and lemniscate rate (k)

Shape factor or shape index is the reciprocal of form factor (Vincy *et al*., 2012). This study area has a higher shape index of 0.693, indicated an elongated shape which tends to have longer flow paths and a more prolonged runoff response compared to more compact watershed. Lemniscate ratio (k) describes the shape of a watershed and the higher value of k (37.9) for this study area suggests that it is more elongated and less circular (Singh *et al*., 2023).

6. Constant of channel maintenance (C)

The constant of channel maintenance (C) of 0.624/km indicates a lower drainage density, implying that a larger surface area is required to sustain a unit length of stream channel. This value suggests that the watershed has a relatively high infiltration capacity, dense vegetation cover, or permeable sub-surface materials, which reduce surface runoff and erosion. Consequently, the basin falls under the low-to-moderate erodibility category, where the channels are capable of accommodating moderate sediment transport without significant degradation. Such characteristics are typical of semi-stable geomorphic environments with limited vulnerability to surface erosion (Shekar & Mathew, 2023).

D) Relief aspects

The relief aspects focus on topography and elevation surface of the study area and the results are given in Table 4.5.

**Table 4.5 Relief aspects of the study area**

| Relief Aspects | | | |
|---|---|---|---|
| **S.no** | **Description** | **Values** | **Units** |
| 1 | Elevation of basin outlet (h) | 128 | m |
| 2 | Maximum elevation of the basin (H) | 238 | m |
| 3 | Basin relief (R) | 110 | m |
| 4 | Relief ratio ($R_h$) | 0.011 | |
| 5 | Relative relief ($R_r$) | 2.405 | m/Km |
| 6 | Ruggedness number ($H_d$) | 0.176 | |

1. Relief

It triggers stream gradient affecting flood pattern and the amount of sediment that can be transported. The basin relief of 110 meters indicates that the watershed has moderate topographical variation, suggesting a landscape that is neither too steep nor too flat. This level of relief reflects a balanced interaction between surface runoff and erosion potential, which plays a crucial role in influencing the stream gradient, flood behavior, and the volume of sediment transported within the basin. The relief ratio, calculated from the total basin relief and the basin length, is 0.011 (which is < 0.1), suggesting that the watershed exhibits a gentle slope gradient. This implies that the area lies in a region with low to moderate structural control and limited erosional activity, which is typically characteristic of mature drainage basins (Soni, 2017).

2. Aspect

Aspect map represents the direction of the slope as shown in Fig 4.5. The direction of slope is north at 0°, it is east at 90° and so on. It strongly influences water flow across the watershed. The aspect map of the study area shows a varied distribution of slope orientations, with a predominance of northeast, northwest, and southeast-facing slopes. These directions influence sunlight exposure, soil moisture, vegetation growth, and erosion potential. North-facing slopes are cooler and moister, while south-facing slopes, though limited, are warmer and drier. The presence of only a few flat areas suggests the terrain is largely sloping, affecting runoff and drainage. Understanding slope aspect is important for watershed management, as it aids in land use planning, erosion control, and ecological assessment.

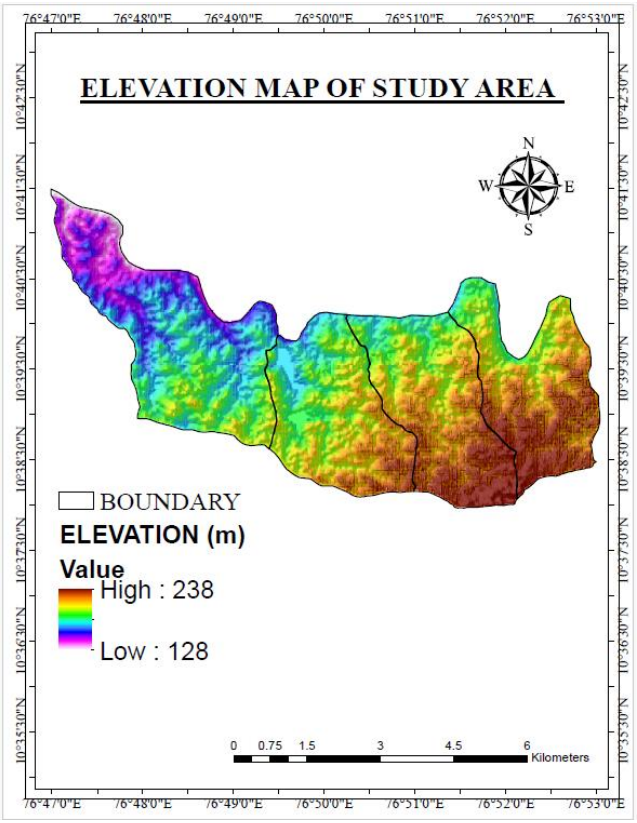


**Fig. 4.5 Elevation map of study area**

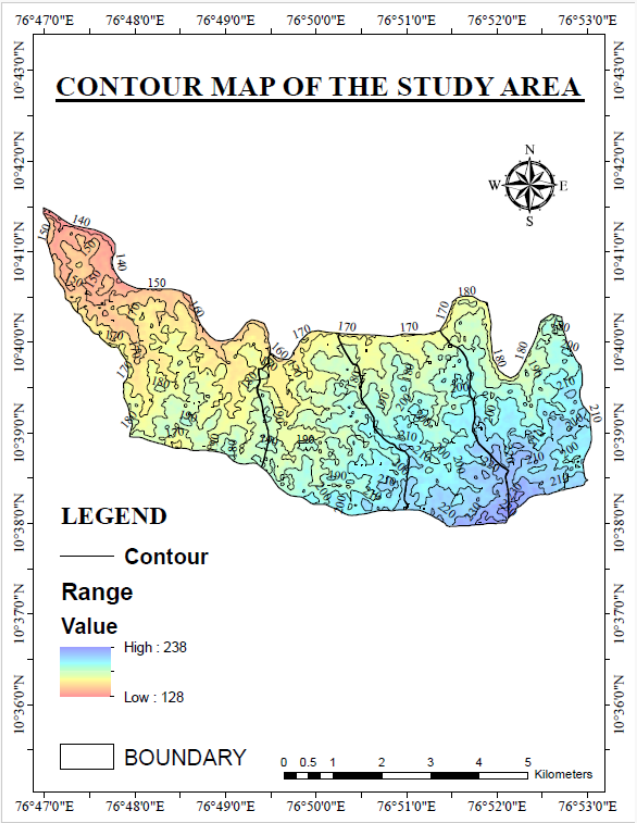


**Fig. 4.6 Contour map of the study area**

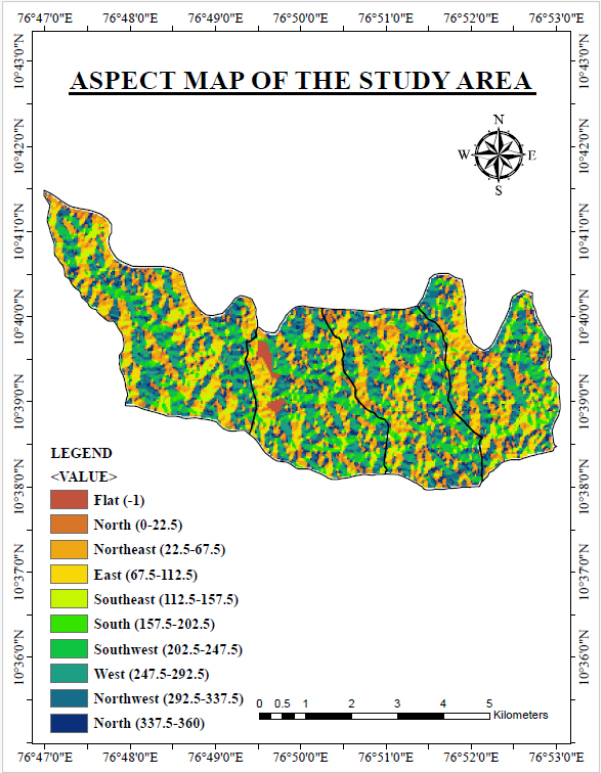


**Fig. 4.7 Aspect map of the study area**

3. Relative relief

The relative relief of 2.405 m/km indicates a very low relief variation within the watershed, suggesting a highly subdued and gently sloping terrain. Such low values reflect minimal elevation differences over horizontal distances, which contribute to slow and controlled surface runoff and enhanced infiltration potential. This implies that the area is less prone to flash flooding and erosion, and is generally associated with mature geomorphic conditions and stable landforms (Rudraiah *et al*., 2008).

4. Ruggedness number

The ruggedness number of 0.176 indicates that the watershed has a very low structural complexity, with gentle terrain and minimal relief variation. This low value suggests that the area is less susceptible to surface erosion, landslides, or intense runoff events. It reflects a landscape where both relief and drainage density are relatively subdued, supporting stable geomorphic conditions and limited erosional activity (Soni, 2017).

5. Slope

The slope of a watershed is one of the important morphometric factors affecting hydrological aspect of a watershed, as it influences the velocity of run-off and concentration time (Sujatha *et al*., 2015). The slope map of the study area reveals that the terrain is predominantly characterized by gentle to moderately gentle slopes, with the majority of the watershed falling within the 0–3.71° (red) and 3.711–6.633° (yellow) slope categories. These areas are typically associated with low to moderate surface runoff, high infiltration potential, and reduced erosion risk, making them suitable for agriculture and other land uses. Moderately steep slopes (6.634–10.45°, shown in light blue) are scattered throughout the area and indicate increased runoff and moderate erosion potential, especially where vegetation is sparse. The steepest slopes (10.46–28.67°, dark blue) are limited in extent but represent zones of higher erosion risk and potential instability, particularly during heavy rainfall.

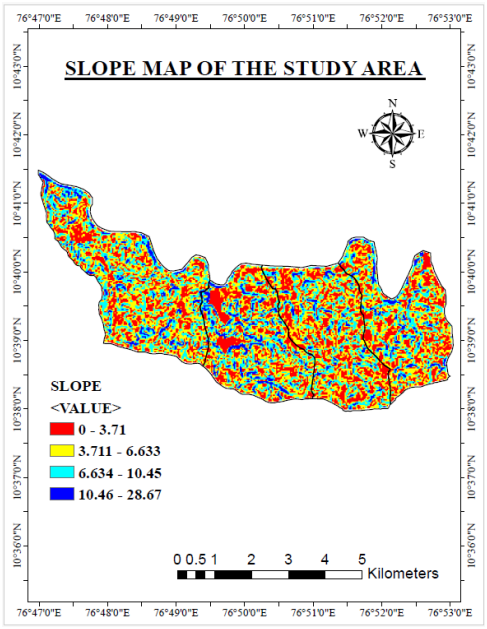


**Fig. 4.8 Slope map of the study area**

## 4.2 ASSESSMENT OF IMPACT OF SOIL AND WATER CONSERVATION MEASURES ON LULC AND NDVI IN THE STUDY AREA USING RS AND GIS

### 4.2.1 Based on LULC change detection

For the assessment of spatial and temporal changes in the study area, Landsat satellite data have been used for pre-treatment (2014) and post-treatment (2024) period.

The satellite images of both periods were classified into five LULC classes for analysing the impact of the soil and water conservation measures watershed treatment activities.

#### *4.2.1.1 Kharif season*

A) LULC pattern of the study area in 2014

The LULC map created from Landsat 8 (OLI/ TIRS) is shown in Fig 4.9. The Land Use Land Cover (LULC) Map for the Kharif Season (Virippu) of 2014 illustrates the spatial distribution of various land cover types in the region. The map identifies five primary categories: vegetation (dark green), fields (yellow), barren land (light brown), built-up areas (dark brown), and water bodies (blue). Vegetation and agricultural fields dominate the area, especially in the eastern and central regions, indicating active cultivation during the monsoon (Kharif) season. Barren land and built-up zones are more scattered but concentrated in certain pockets, while water bodies are mainly located in the southern-central area.

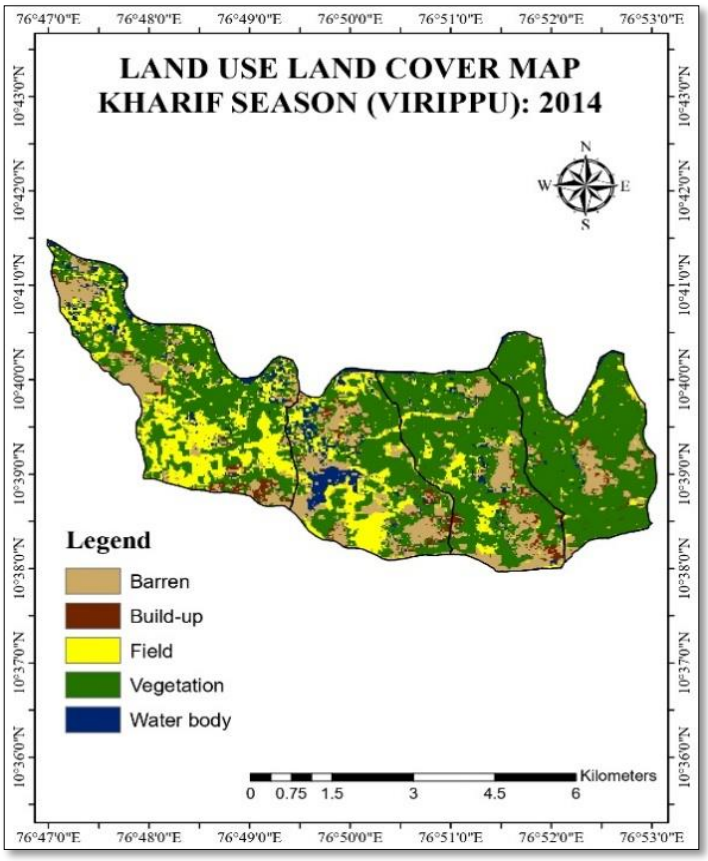


**Fig. 4.9 LULC map of kharif season 2014**

B) LULC pattern of the study area in 2024

This LULC map was derived from Landsat 9 (OLI/ TIRS) and shown in Fig 4.10. The Land Use Land Cover (LULC) Map for the Kharif Season (Virippu) of 2024 presents the distribution of different land cover types across the region. Vegetation (green) remains the dominant cover, particularly in the eastern and central areas, indicating healthy forest or plantation zones. Fields (yellow) are scattered throughout, reflecting active agricultural use, though they appear slightly reduced compared to earlier years. Barren lands (light brown) have increased, especially in the western and southern parts, suggesting possible land degradation or fallow fields. Built-up areas (brown) show noticeable expansion, indicating urban or infrastructural growth. Water bodies (blue) are limited and mainly located in the central-southern region.

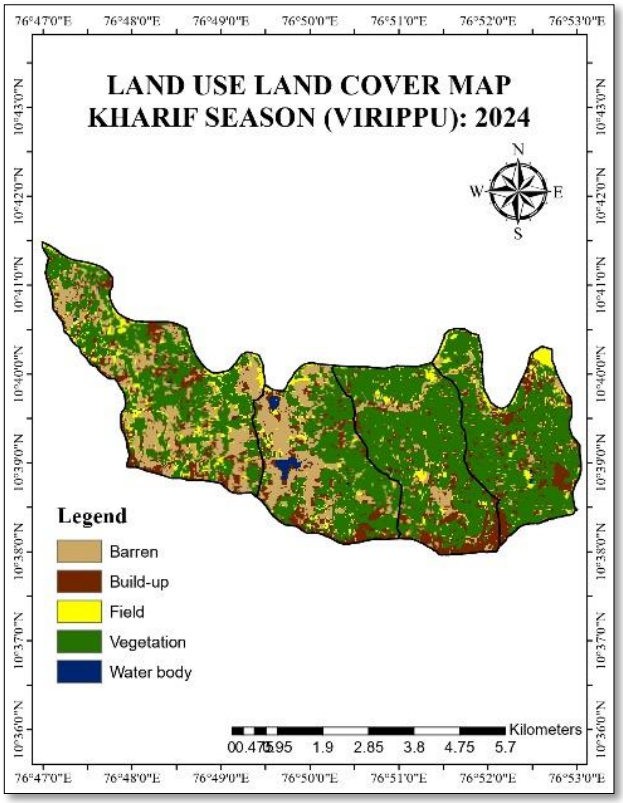


**Fig. 4.10 LULC map of kharif season 2024**

The bar graph shows land cover changes during the Kharif season (Virippu) from 2014 to 2024. Vegetation cover remained stable, showing a slight increase from 18.57 km² in 2014 to 18.62 km² in 2024, indicating minimal change in green cover. However, barren land increased from 5.85 km² to 6.63 km², while field areas significantly declined from 5.75 km² to 2.37 km², suggesting possible land abandonment or conversion. Built-up areas rose sharply from 1.11 km² to 5.22 km²,

highlighting increased urbanization. Meanwhile, water bodies decreased drastically from 1.83 km² to 0.28 km², pointing to potential environmental stress or encroachment. Overall, the data reflects increased human activity with a notable impact on agricultural and water resources.

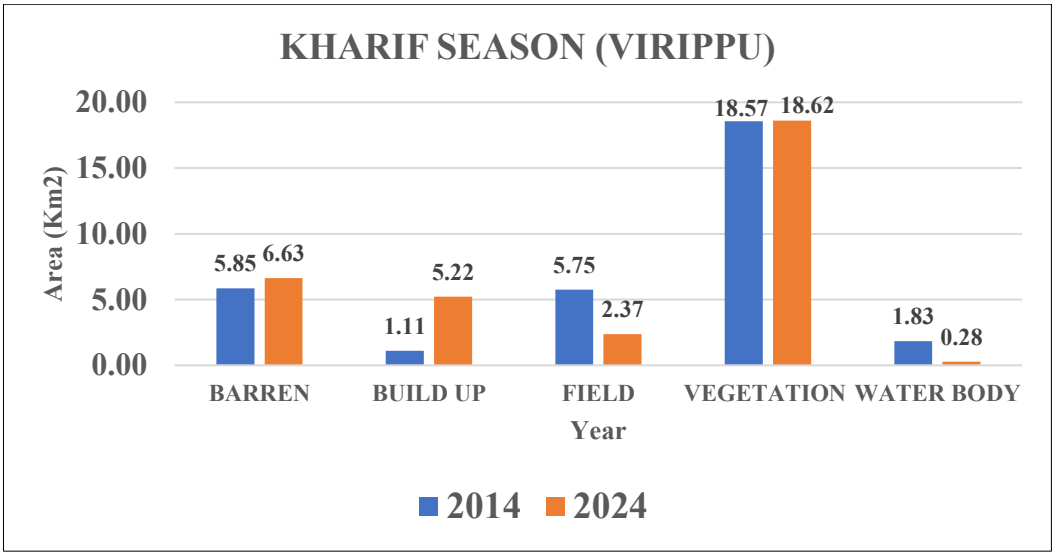


**Fig. 4.11 LULC changes of kharif season**

### *4.2.1.2 Rabi season*

A) LULC pattern of the study area in 2014

The Land Use Land Cover (LULC) Map for the Rabi Season (Mundakan) of 2014 illustrates the distribution of land cover types during the dry winter cropping season as shown in Fig. 4.12. Vegetation (green) dominates the eastern and southern regions, indicating significant forest or perennial cover. Agricultural fields (yellow) are widespread, especially in the central and northwestern parts, reflecting active cultivation during the Rabi season. Water bodies (blue) are prominently visible in the central-southern area, suggesting sufficient water availability for irrigation. Barren lands (light brown) and built-up areas (dark brown) appear scattered but more concentrated in the western and southern boundaries.

B) LULC pattern of the study area in 2024

The Land Use Land Cover (LULC) Map for the Rabi Season (Mundakan) of 2024 shows the spatial distribution of land cover during the dry agricultural season as shown in Fig. 4.13. Vegetation (green) continues to dominate the landscape, particularly in the eastern, southern, and central regions, indicating strong forest or perennial crop

cover. Fields (yellow) remain prominent but appear more fragmented compared to 2014, suggesting shifts in cultivation patterns or reduction in active farmland. Notably, water bodies (blue) have expanded, especially in the central and southeastern zones, which may reflect improved water storage or seasonal water accumulation. Built-up areas (brown) have slightly increased, pointing to gradual urban or infrastructural development, while barren lands (light brown) are scattered but limited.

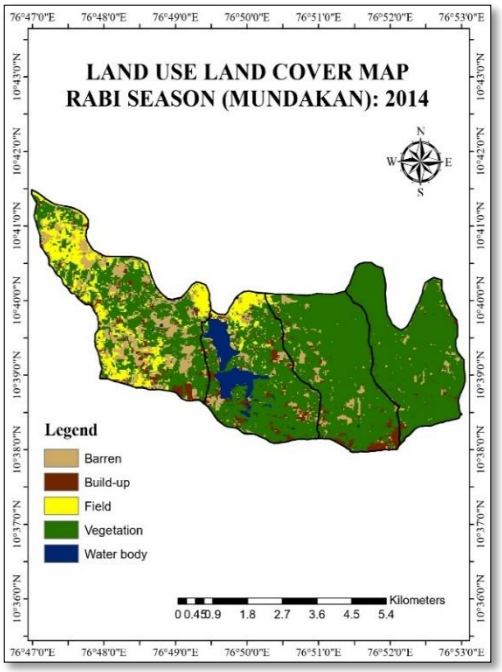


**Fig. 4.12 LULC map of rabi season 2014**

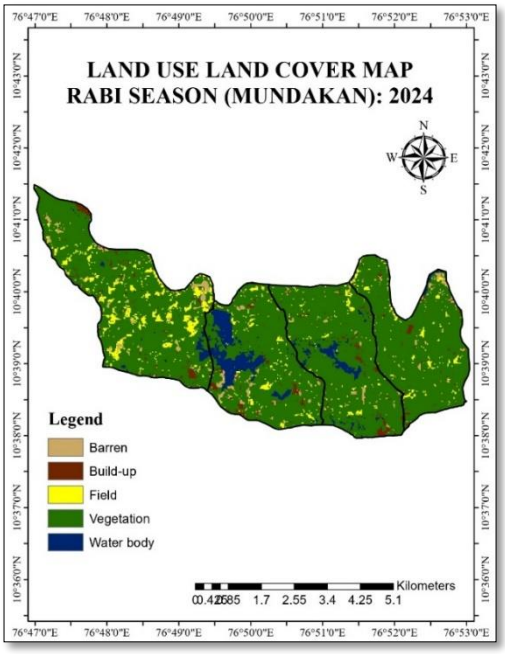


**Fig. 4.13 LULC map of rabi season 2024**

The bar graph illustrates land cover changes during the Rabi season (Mundakan) from 2014 to 2024. The most notable shift is in vegetation, which increased significantly from 22.69 km² in 2014 to 28.03 km² in 2024, indicating improved vegetative cover. Conversely, barren land decreased sharply from 4.19 km² to 1.02 km², and field area declined from 3.19 km² to 1.71 km², suggesting possible land use conversion or fallowing. Build-up areas also reduced from 1.87 km² to 0.73 km², and water bodies saw a slight increase from 1.20 km² to 1.62 km². Overall, the data suggests a positive trend in vegetation expansion, possibly due to better land management or favourable climatic conditions.

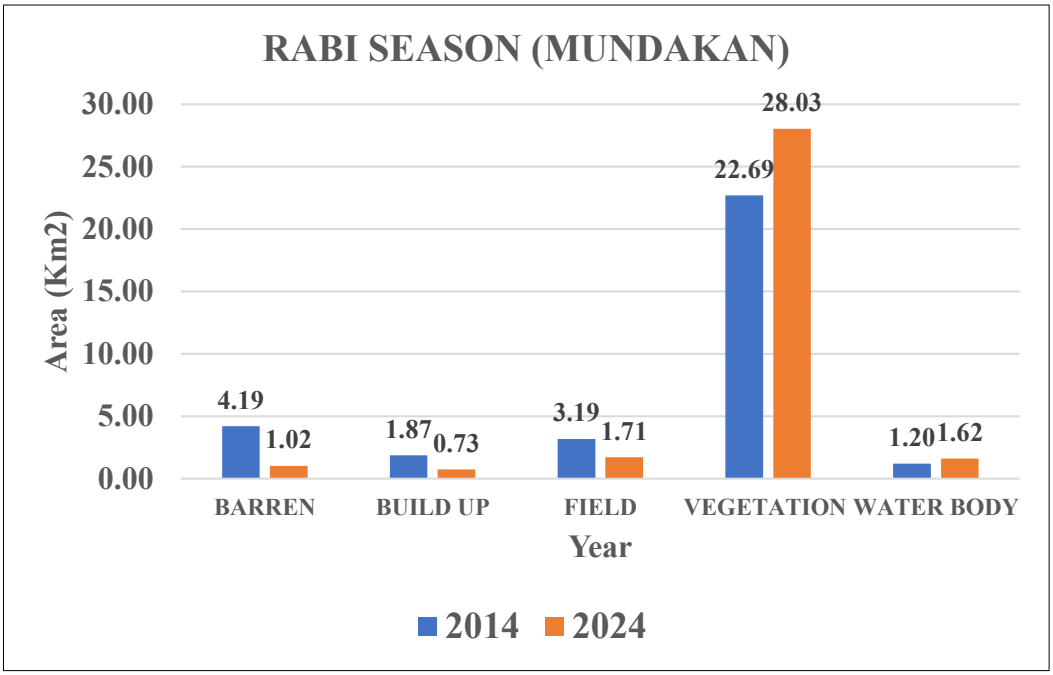


**Fig. 4.14 LULC changes of rabi season**

***4.2.1.3 Zaid season***

A) LULC pattern of the study area in 2014

The Land Use Land Cover (LULC) Map for the Zaid Season (Puncha) of 2014 provides a detailed snapshot of land utilization patterns during the off-season cropping period as shown in Fig. 4.15. The map reveals that field areas (yellow) dominate the western and central regions, indicating intensive agricultural activity. Vegetation (green) is also prominent, particularly in the eastern and southeastern zones, reflecting either natural vegetation or fallow cropland. Barren land (light brown) is widespread across the region, especially in patches adjacent to field zones, possibly representing uncultivated or degraded lands. Built-up areas (brown) are sparsely distributed,

suggesting limited urban development at that time. Water bodies (blue) are scattered, primarily in central locations, providing crucial water resources for irrigation and seasonal farming. Overall, the map shows a predominantly agricultural landscape with moderate vegetation and minimal urban sprawl.

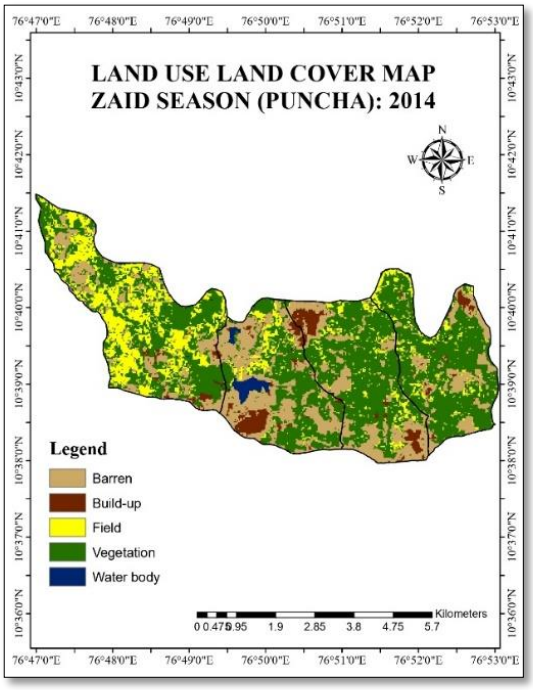


**Fig. 4.15 LULC map of zaid season 2014**

B) LULC pattern of the study area in 2024

The Land Use Land Cover (LULC) map of Puncha for the Zaid season (2024) illustrates the spatial distribution of various land categories, including vegetation, agricultural fields, barren land, built-up areas, and water bodies as shown in Fig. 4.16. The map shows that vegetation and agricultural fields dominate the region, indicating active cultivation and good green cover during the Zaid season. Water bodies are centrally located, supporting irrigation, while built-up areas are scattered along the periphery. Barren land appears in small patches, mostly in the northwestern and central zones. Overall, the map reflects a predominantly rural landscape with significant agricultural activity and adequate water resources.

The bar graph illustrates land cover changes during the Zaid season (Puncha) from 2014 to 2024 as shown in Fig. 4.17. The most notable change is the significant decrease in barren land, from 8.74 km² in 2014 to 3.28 km² in 2024, indicating land reclamation or improvement. Field areas increased substantially from 5.51 km² to 9.77 km², suggesting expansion in agricultural activities. Vegetation cover showed a slight

increase from 16.89 km² to 17.28 km², while built-up areas rose marginally from 1.51 km² to 1.63 km², pointing to modest urban growth. Water bodies more than doubled, increasing from 0.47 km² to 1.15 km², reflecting possible water resource development or seasonal water retention. Overall, the data suggests a positive trend in land use efficiency and vegetation health.

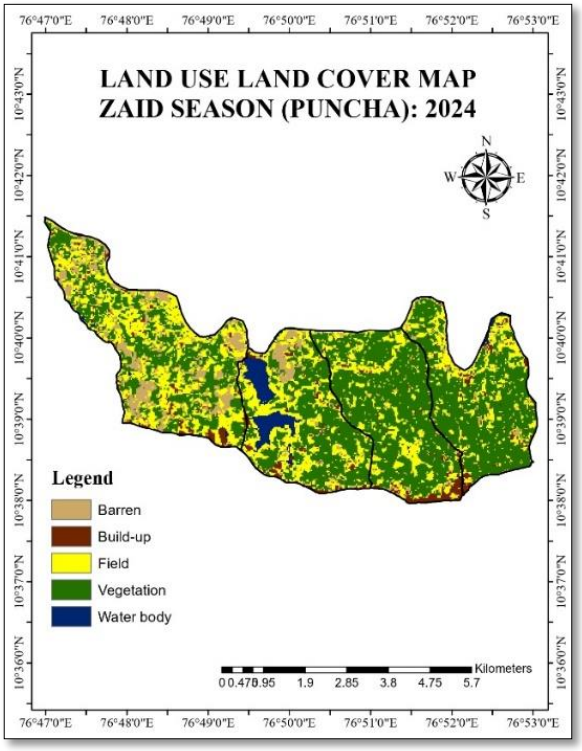


**Fig. 4.16 LULC map of zaid season 2024**

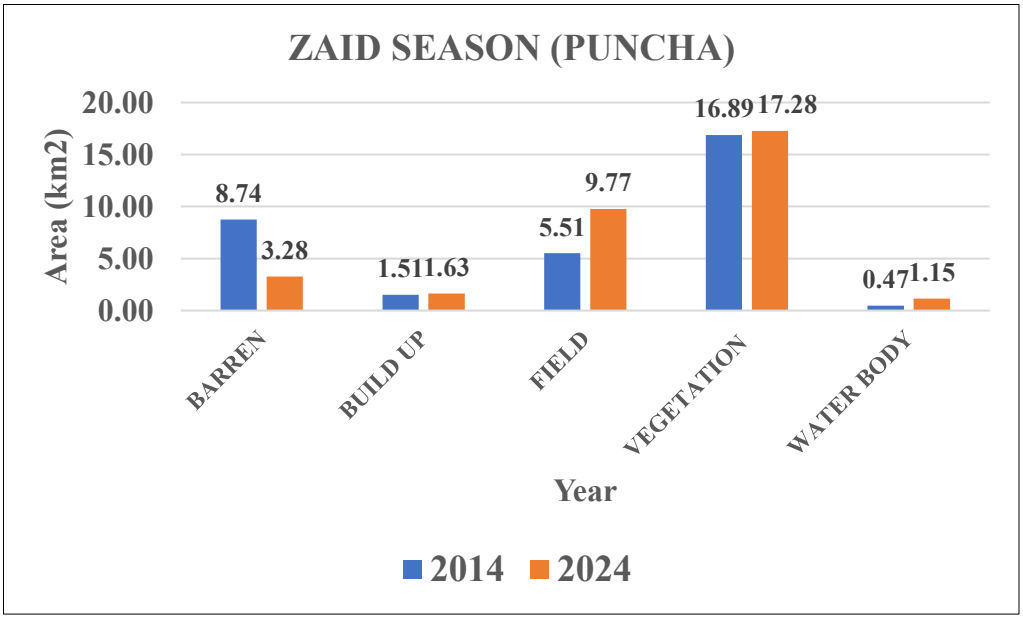


**Fig. 4.17 LULC changes of zaid season**

#### *4.2.1.4 LULC changes during 2014 to 2024: kharif season*

The LULC Change Detection Map for the Kharif Season (Virippu) from 2014 to 2024 highlights the dynamic transformations in land use and land cover over a decade as shown in Fig. 4.18. A significant portion of the region shows vegetation remaining stable, especially in the eastern and central zones, while notable transitions from fields and vegetation to barren land indicate increasing land degradation. Urban expansion is evident through the conversion of vegetation, barren, and field areas into built-up land, particularly in southern and western areas. Some positive changes are also observed, such as barren to vegetation and field conversions, suggesting land reclamation or afforestation efforts. Changes in water bodies are relatively minor but localized.

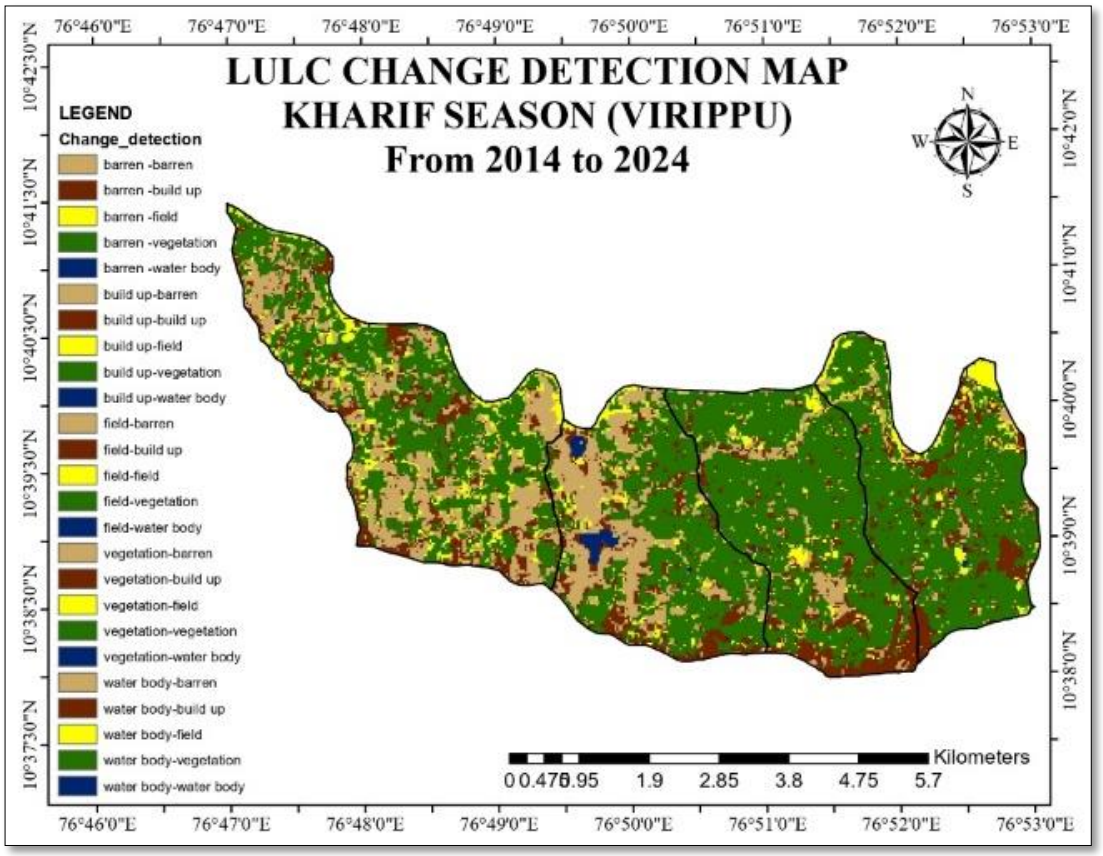


**Fig. 4.18 LULC change detection map of kharif season**

The change analysis for the Kharif season (Virippu) reveals significant land use transitions, with the most stable category being vegetation to vegetation, covering 13.74 km². Notable conversions include field to barren (2.55 km²), vegetation to build-up (2.03 km²), and barren to field (2.24 km²), indicating both degradation and agricultural expansion. Transitions such as vegetation to field (1.23 km²), field to vegetation (1.67 km²), and barren to build-up (1.59 km²) also highlight dynamic land changes as shown

in Fig. 4.19. Minimal changes occurred in water body conversions, all below 0.45 km², suggesting relative stability in water bodies compared to other land classes.

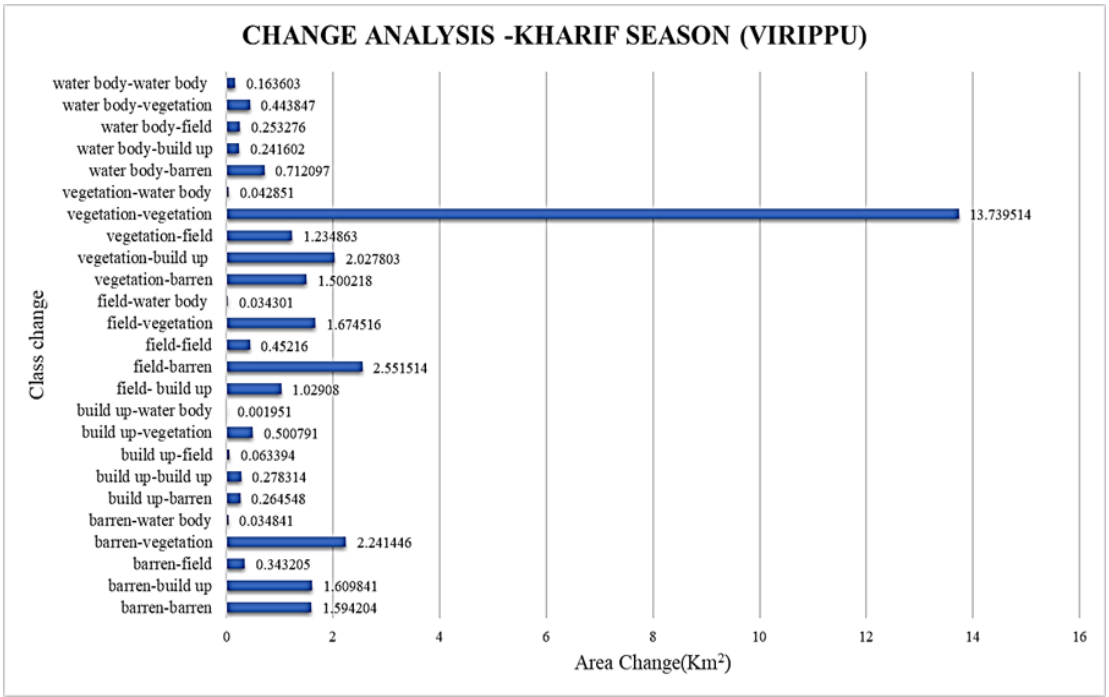


**Fig. 4.19 LULC change analysis of kharif season**

### *4.2.1.5 LULC changes during 2014 to 2024: rabi season*

This LULC Change Detection Map for the Rabi Season (Mundakan) from 2014 to 2024 illustrates the spatial transformation of land use and cover over the decade as shown in Fig. 4.20. The dominant transitions observed are from field to vegetation, barren to vegetation, and field to waterbody, indicating a shift toward more natural or semi-natural land covers. The expansion of water bodies in central and southeastern regions is especially notable, possibly reflecting increased water retention or management practices. Minor but visible increases in built-up areas are seen primarily in the western and southern zones, suggesting localized urban growth. Additionally, patches of vegetation converted to field or build-up indicate slight land conversion pressures. Overall, the map highlights a trend of ecological recovery in some areas alongside moderate anthropogenic development.

The change analysis for the Rabi season (Mundakan) shows that the most significant stability is within the vegetation class, with 20.38 km² of land remaining as vegetation. Major conversions include barren to vegetation (3.22 km²), field to vegetation (2.53 km²), and build-up to vegetation (1.43 km²), indicating substantial

greening or reforestation. Conversely, there are smaller transitions such as vegetation to field (0.90 km²) and vegetation to barren (0.39 km²), showing minor degradation. Water body areas remained relatively stable (0.75 km²), with limited transitions to vegetation (0.39 km²) and field (0.03 km²), suggesting consistent hydrological features as shown in Fig. 4.21.

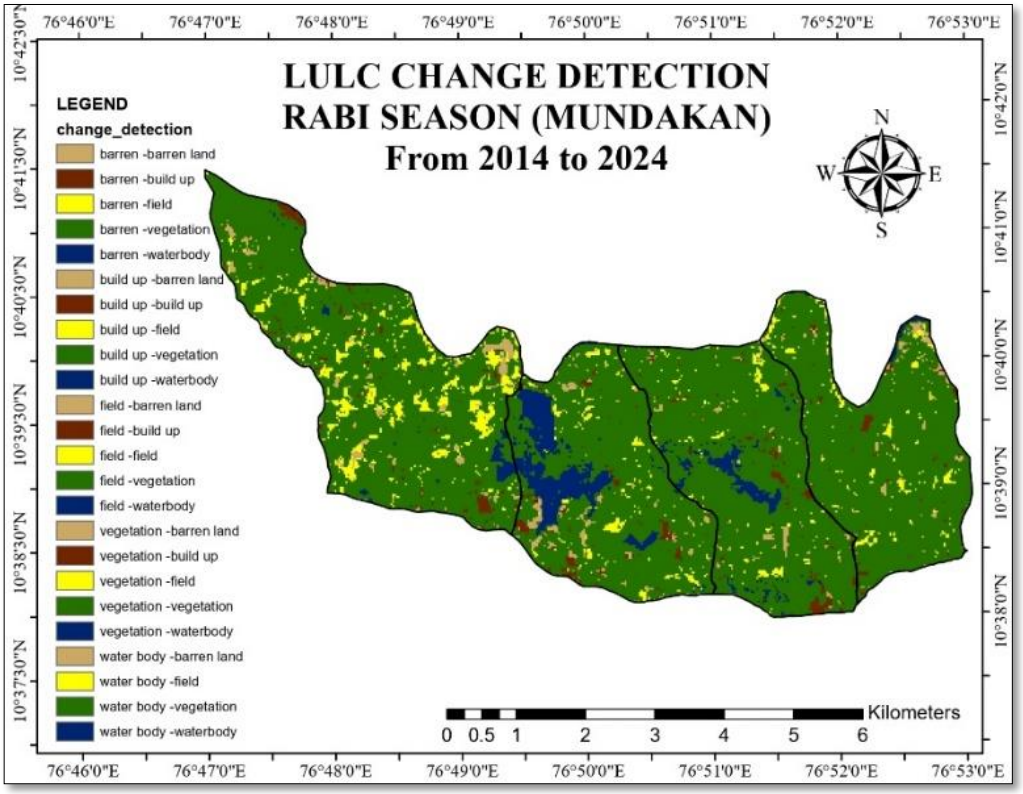


**Fig. 4.20 LULC change detection map of rabi season**

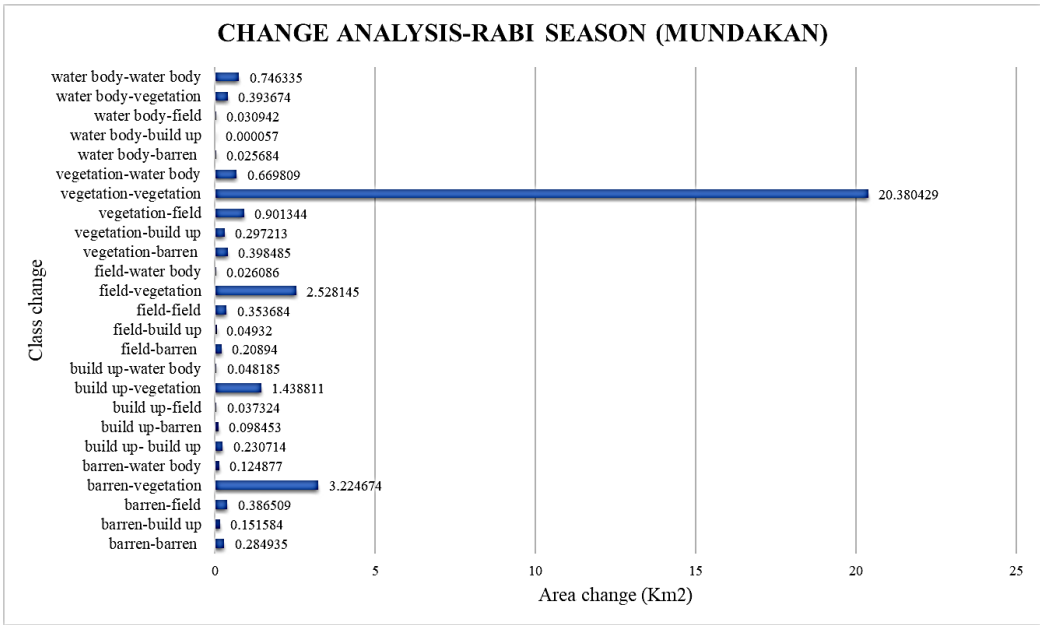


**Fig. 4.21 LULC change analysis of rabi season**

#### *4.2.1.6 LULC changes during 2014 to 2024: zaid season*

LULC change detection map for Puncha during the Zaid season from 2014 to 2024 reveals significant land cover transitions, primarily the conversion of vegetation to agricultural fields, indicating increased seasonal cultivation as shown in Fig. 4.22. Some areas show regeneration from barren land to vegetation, while others reflect urbanization or land degradation with the expansion of built-up and barren areas. Notable changes around central water bodies suggest fluctuations due to irrigation or seasonal effects. Overall, the region exhibits dynamic land use patterns, driven by agricultural practices, environmental changes, and human activities.

The change analysis for the Zaid season (Puncha) reveals that the vegetation class has shown the highest stability, with 11.46 km² of land remaining as vegetation. Significant land cover conversions include barren land to field (3.44 km²), field to vegetation (3.79 km²), and barren land to vegetation (2.97 km²), suggesting improvements in agricultural and vegetative cover. Field to field (2.26 km²) and barren to barren (0.81 km²) also indicate class persistence. Notable but smaller transitions include build-up to field (0.54 km²), build-up to vegetation (0.57 km²), and field to barren (1.24 km²), indicating dynamic land use patterns during this season.

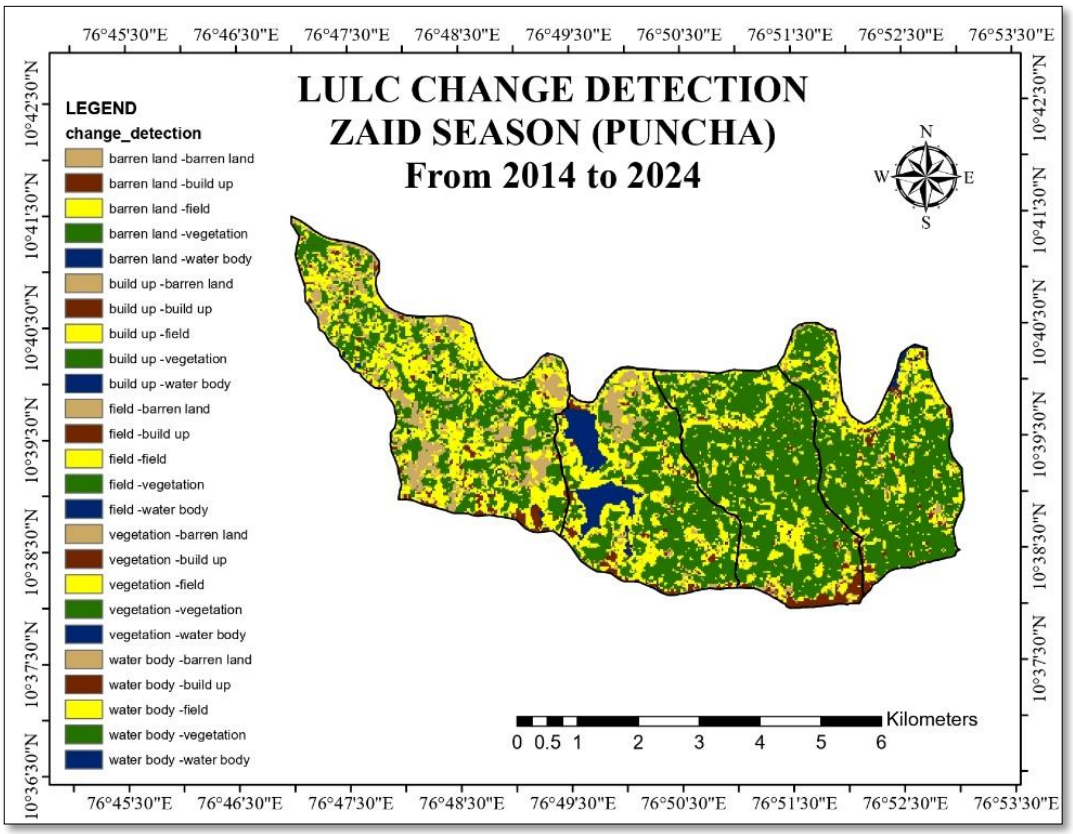


**Fig. 4.22 LULC change detection map of zaid season**

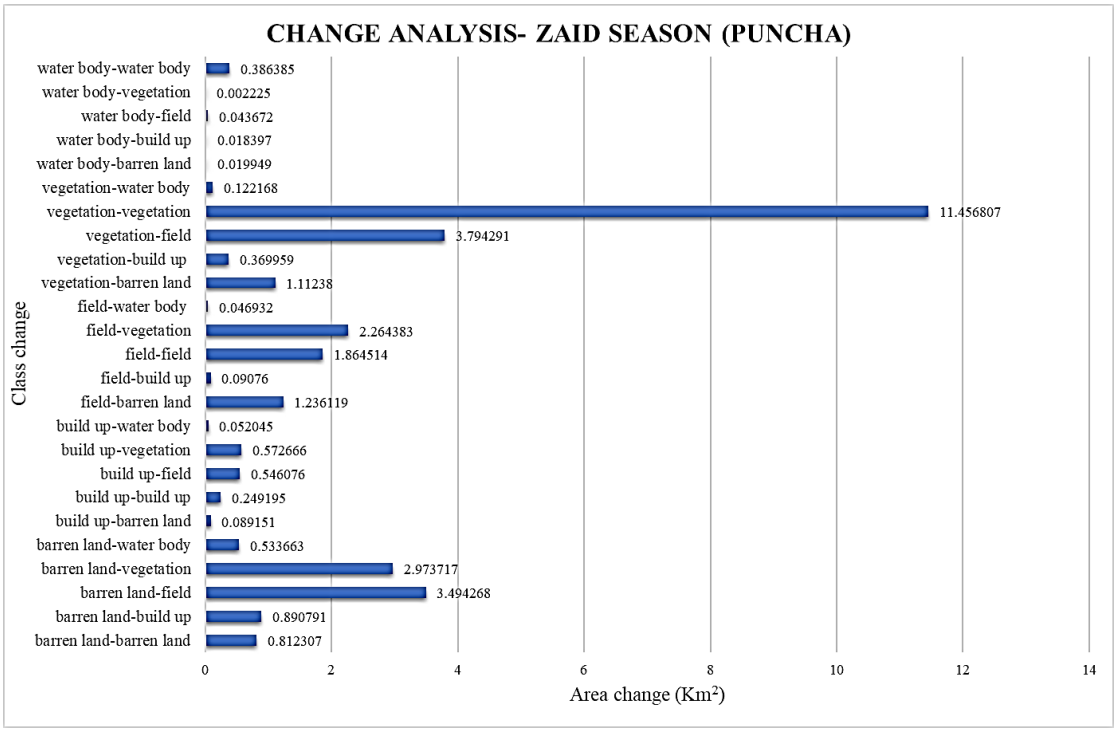


**Fig. 4.23 LULC change analysis of zaid season**

### 4.2.2 NDVI changes analysis

The NDVI map was prepared for the year 2014 and 2024 to assess the changes in vegetation cover within the study area resulting from the impact of soil and water conservation measures.

#### *4.2.2.1 Kharif season*

The Kharif (Virippu) season NDVI map of 2014 presents a widespread presence of healthy vegetation, as indicated by significant green patches concentrated in the central and southern parts of the region as shown in Fig. 4.24. The NDVI values show a relatively higher range, reflecting vigorous crop growth and dense foliage typical of the monsoon season. The predominance of yellow to green tones suggests favorable agro-climatic conditions, such as ample rainfall and high soil moisture, supporting strong biomass production. This map indicates that 2014 was a productive Kharif season with active agricultural activity and healthy vegetation cover.

In the 2024 Kharif (Virippu) season NDVI map, the spatial distribution of vegetation appears more homogeneous, with a dominance of orange and light-yellow hues as shown in Fig. 4.25. Compared to 2014, there is a noticeable reduction in the extent and intensity of green patches, indicating a decline in vegetation health. The

NDVI values range slightly lower, pointing to moderate vegetation vigor across most of the region. This could be indicative of altered cropping patterns, reduced rainfall, or increased pressure on land and resources. The overall shift suggests a marginal deterioration in monsoon season vegetation over the decade.

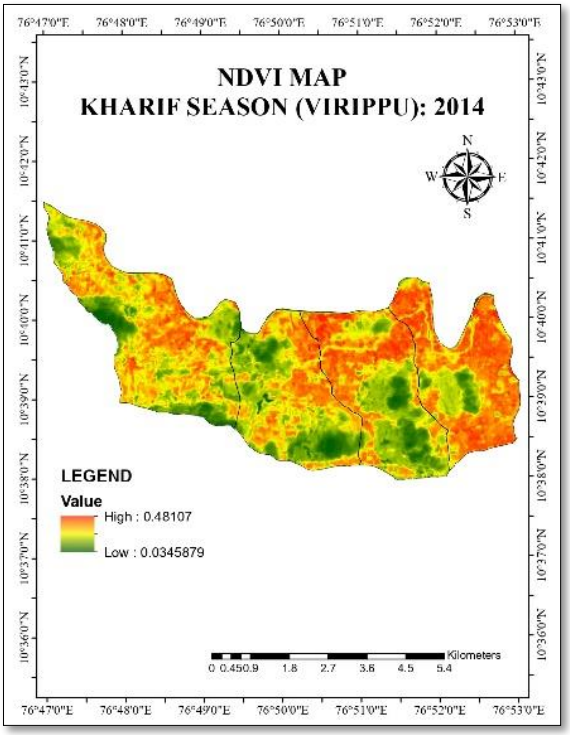


**Fig. 4.24 NDVI map of kharif season 2014**

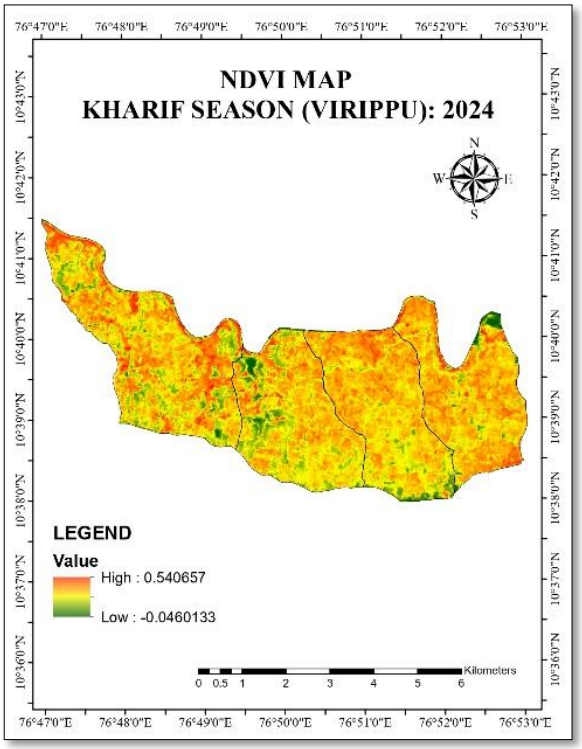


**Fig. 4.25 NDVI map of kharif season 2024**

### *4.2.2.2 Rabi season*

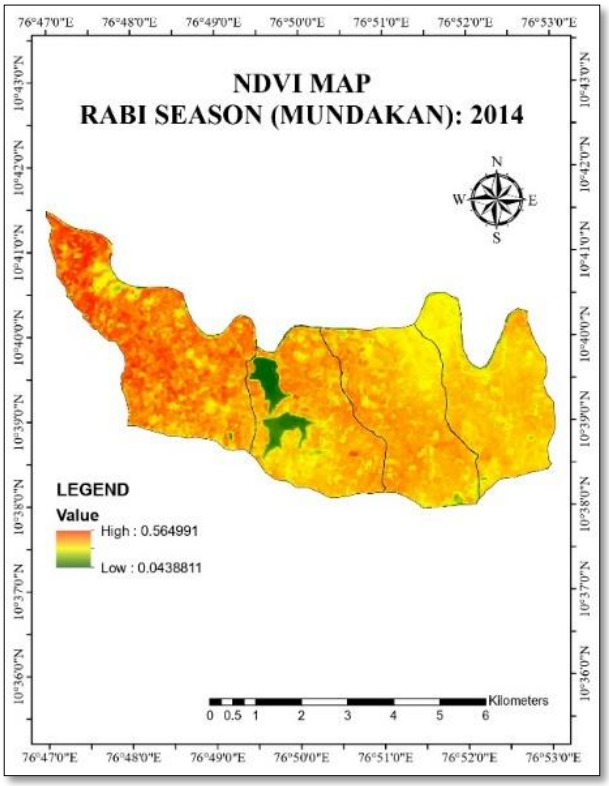


**Fig. 4.26 NDVI map of rabi season 2014**

The NDVI map for the Rabi (Mundakan) season of 2014 shows better vegetation cover compared to 2024, with several distinct green areas mainly in the central regions. The map exhibits a mix of yellow, orange, and green shades, indicating varied vegetation health across the landscape. Higher NDVI values in some patches suggest robust crop growth or effective irrigation support during this season. The broader spread of vegetated areas implies that agricultural activity may have been more intensive or better supported by environmental factors in 2014, leading to improved vegetation dynamics during the Rabi season.

The NDVI map for the Rabi (Mundakan) season of 2024 illustrates predominantly moderate to low vegetation density across the region. The color distribution is mostly in the orange to light yellow spectrum, indicating limited vegetative vigor during this dry season. A few small green patches appear in the central and southern parts, representing localized areas of healthier vegetation or irrigated crops. The overall NDVI values are modest, which could be attributed to factors such as water scarcity, less favorable climatic conditions, or reduced cropping intensity

during this season. This trend reflects a relatively stressed agricultural landscape in the Rabi season of 2024.

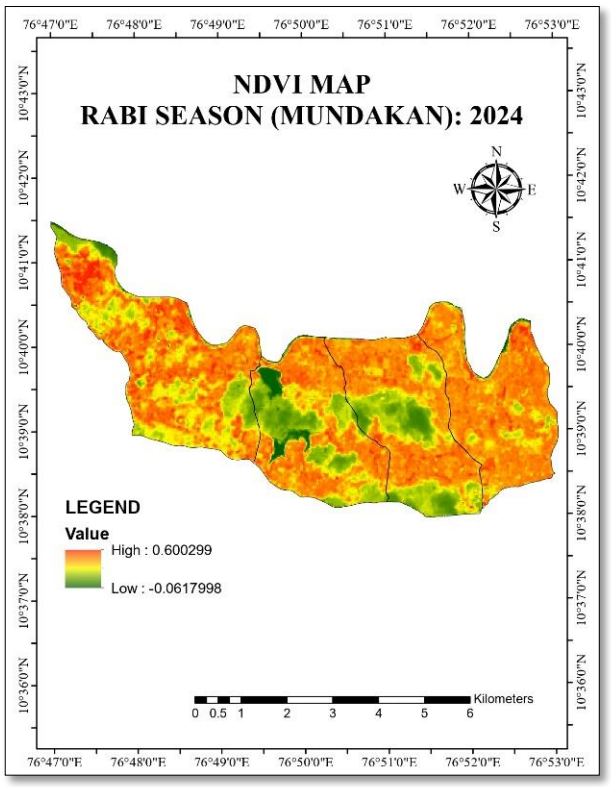


**Fig. 4.27 NDVI map of rabi season 2024**

### *4.2.2.3 Zaid season*

The NDVI map for the Zaid season of 2014 reveals a moderate to high level of vegetation variability across the region as shown in Fig. 4.28. The NDVI values range from -0.0063 to 0.5059, indicating areas with both sparse and dense vegetation cover. A mix of orange and green shades dominates the landscape, suggesting heterogeneous vegetation health. The presence of several green patches, especially in the central and southwestern regions, indicates zones of higher biomass and active vegetation growth, possibly due to better water availability or crop management.

The NDVI map for 2024 shows a relatively uniform distribution of vegetation with less green intensity compared to 2014 as sown in Fig. 4.29. NDVI values range from -0.0028 to 0.4485, slightly lower in maximum value, suggesting a general decline in vegetation vigour. The map is predominantly covered with orange and light-yellow shades, indicating a prevalence of moderate vegetation cover. Only a few isolated green

zones, particularly in the southwest, suggest healthier vegetation. This could reflect changes in land use, water availability, or cropping intensity over the decade.

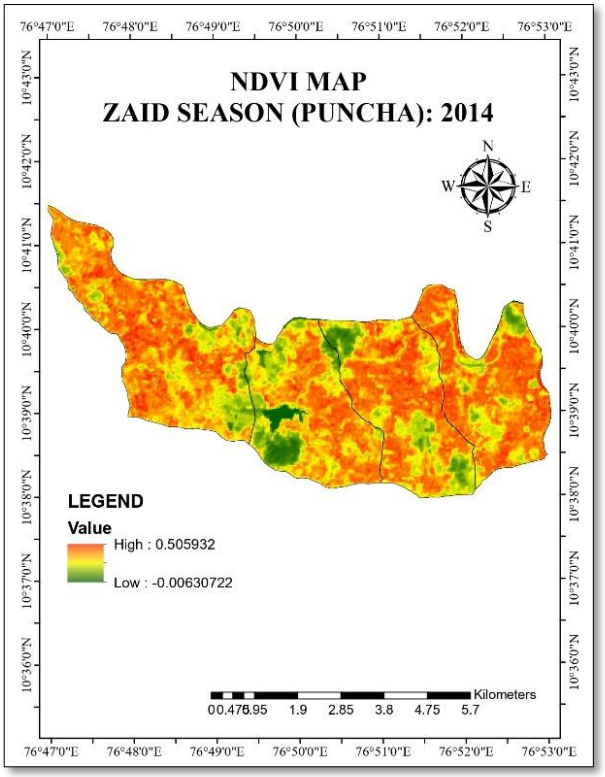


**Fig. 4.28 NDVI map of zaid season 2014**

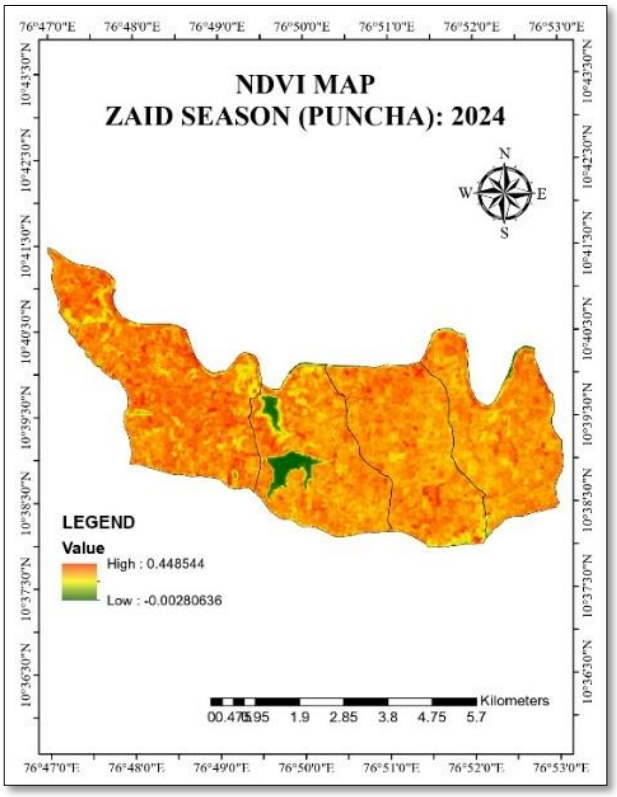


**Fig. 4.29 NDVI map of zaid season 2024**

The NDVI mean value comparison between 2014 and 2024 reveals a noticeable decline in vegetation health across all three agricultural seasons. During the Kharif season, the NDVI mean dropped from 0.2578 in 2014 to 0.2473 in 2024. In the Rabi season, the mean decreased more significantly, from 0.3044 in 2014 to 0.2692 in 2024, indicating a considerable reduction in vegetation density. Similarly, the Zaid season recorded a drop from 0.2498 in 2014 to 0.2229 in 2024. Overall, this trend reflects a gradual deterioration in vegetation health and coverage over the decade, possibly due to land use changes, climatic variability, or anthropogenic activities.

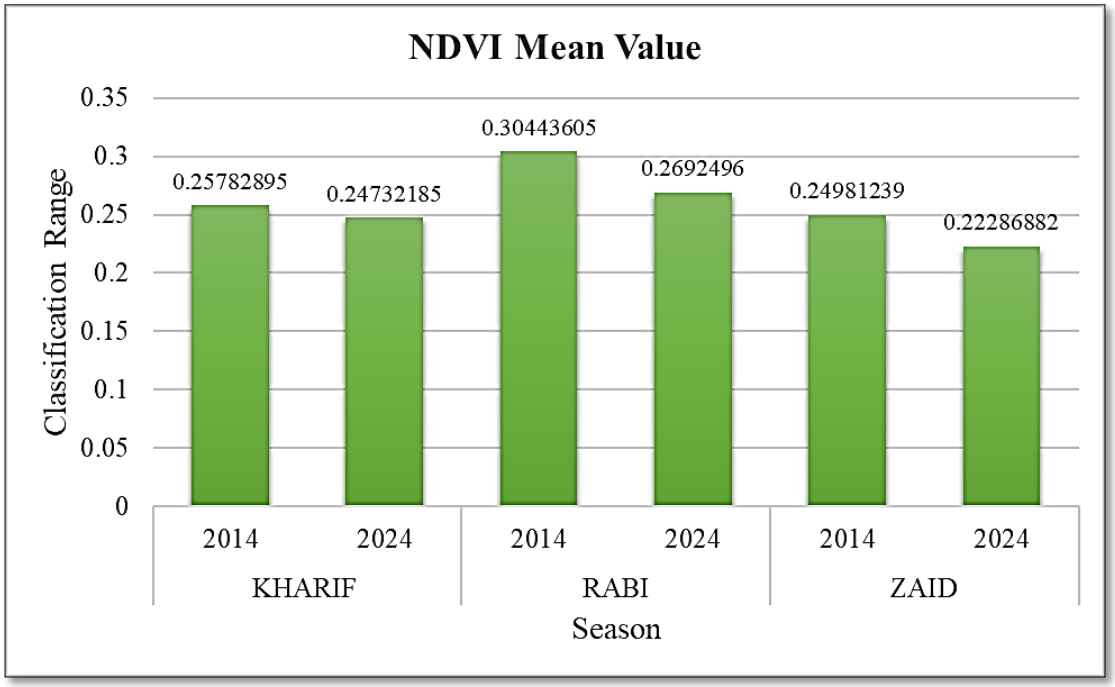


**Fig. 4.30 NDVI mean value**

### 4.2.3 NDVI changes analysis based on density

The NDVI change analysis over the years indicates a general decline in vegetation density and health across all seasons. While the 2014 maps show more green patches reflecting higher NDVI values and healthier vegetation, the 2024 maps exhibit a dominance of yellow to orange tones, suggesting reduced biomass and crop vigour. This shift implies possible impacts of climatic variability, reduced water availability, or changes in land use and cropping intensity. Overall, the analysis highlights a gradual deterioration in vegetation cover and productivity over the decade.

### *4.2.3.1 Kharif season*

The NDVI Change Map for the Kharif season (Virippu) from 2014 to 2024 reveals significant spatial variations in vegetation density across the Puncha region as shown in Fig. 4.31. The map categorizes the area into four classes: Dense Vegetation (dark green), Moderate Vegetation (light green), Sparse Vegetation (orange), and Water Body/Barren (red). While dense and moderate vegetation dominate much of the region, especially in the eastern and northern parts, noticeable patches of sparse vegetation and barren land are evident in the central and southern zones. This suggests a decline in vegetation health or cover in some areas over the decade, likely due to factors such as land use change, deforestation, or climatic stress. Overall, the map indicates a mixed trend of vegetation dynamics, with both conservation and degradation patterns coexisting**.**

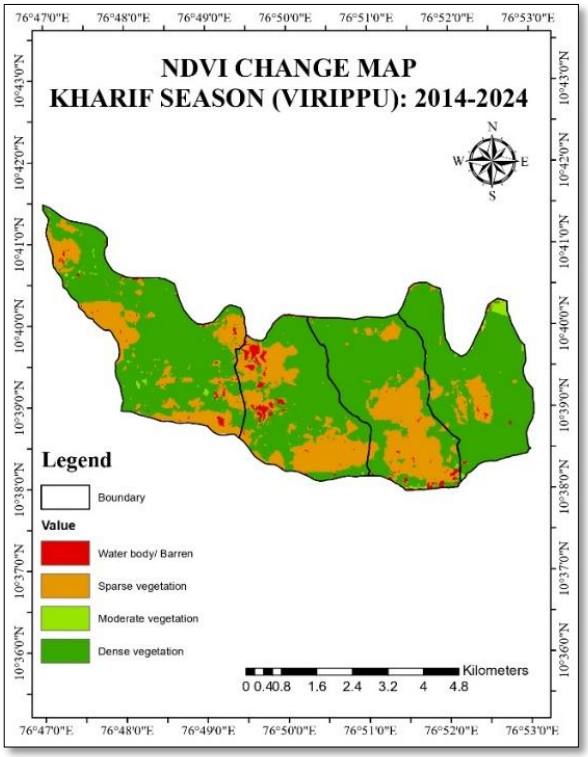


**Fig. 4.31 NDVI change map of kharif season based on density**

The NDVI (Normalized Difference Vegetation Index) change analysis for the Kharif season (Virippu) indicates that the majority of the area, approximately 71.007%, experienced no significant change in vegetation cover as shown in Fig. 4.32. However, 27.905% of the area showed a positive change in NDVI, reflecting an improvement in vegetation health or density. A small portion, 1.087%, experienced a negative change,

suggesting a decline in vegetative cover during this season. Overall, the analysis reflects a largely stable or improving vegetative condition across the region.

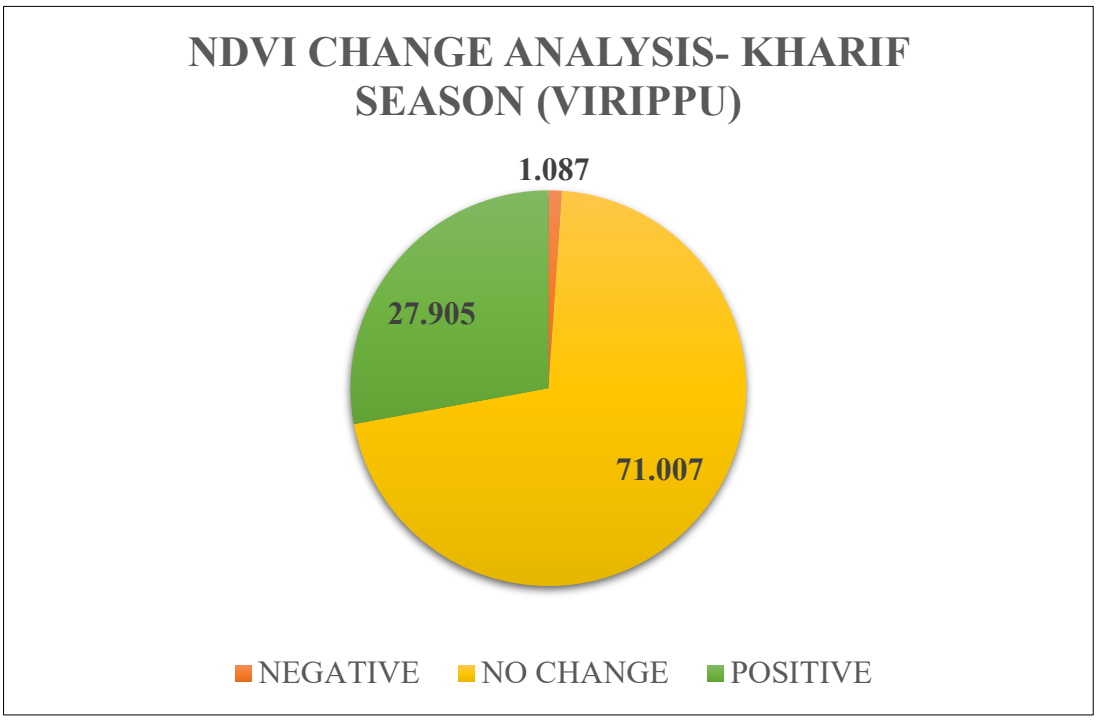


**Fig. 4.32 NDVI change analysis of kharif season based on density**

### *4.2.3.2 Rabi Season*

The NDVI Change Map for the Rabi season (Mundakan) from 2014 to 2024 illustrates varying vegetation density trends across the Puncha region as shown in Fig. 4.33. The landscape is primarily dominated by moderate vegetation (light green), with some areas of dense vegetation (dark green), indicating reasonably healthy crop and vegetation cover. However, significant patches of sparse vegetation (orange) and water body or barren land (red), especially in central and southern regions, suggest localized degradation or reduced vegetation productivity. These changes may result from land use shifts, irrigation issues, or climatic factors affecting Rabi crop cycles. Overall, while vegetation health is moderately sustained, areas with sparse or no vegetation highlight the need for targeted agricultural and environmental interventions.

The NDVI change analysis for the Rabi season (Mundakan) reveals that a significant portion of the area, around 84.065%, showed no change in vegetation cover. Approximately 13.441% of the area experienced a negative change, indicating a decline in vegetation health or density as shown in Fig. 4.34. Only 2.495% of the area showed a positive change, suggesting a slight improvement in vegetation during the season.

Overall, the data suggests that vegetation remained largely stable, with limited regions of improvement and some areas experiencing degradation.

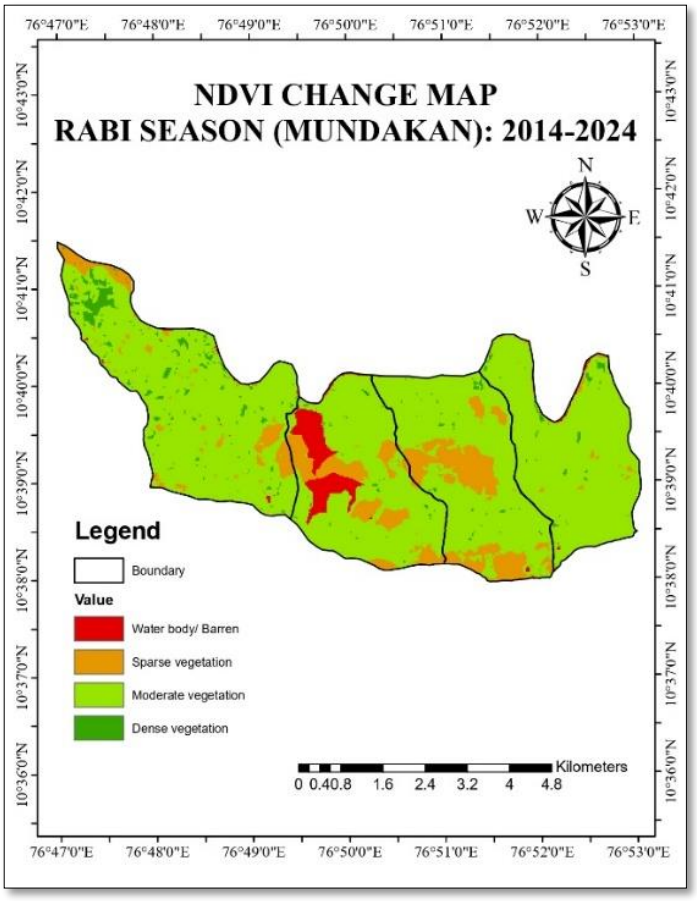


**Fig. 4.33 NDVI change map of rabi season based on density**

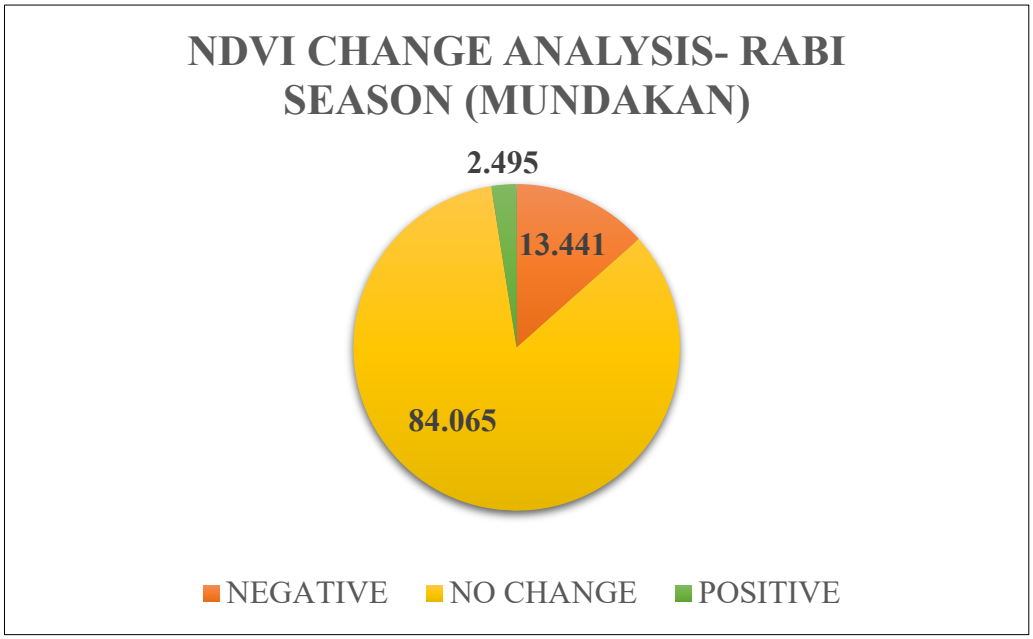


**Fig. 4.34 NDVI change analysis of rabi season based on density**

### *4.2.3.3 Zaid Season*

The NDVI Change Map for the Zaid season (Puncha) from 2014 to 2024 shows the spatial variation in vegetation density across the region as shown in Fig. 4.35. The majority of the area is covered by moderate vegetation (light green), indicating average vegetation health during the off-season cropping period. Dense vegetation (dark green) is limited, reflecting reduced agricultural activity typical of the Zaid season. However, noticeable patches of sparse vegetation (orange) and waterbody/barren land (red), particularly in central and southern zones, highlight areas of concern where vegetation has significantly declined or is absent. These patterns suggest seasonal stress, fallow land, or possible water scarcity, emphasizing the need for improved land and water management practices during the Zaid season.

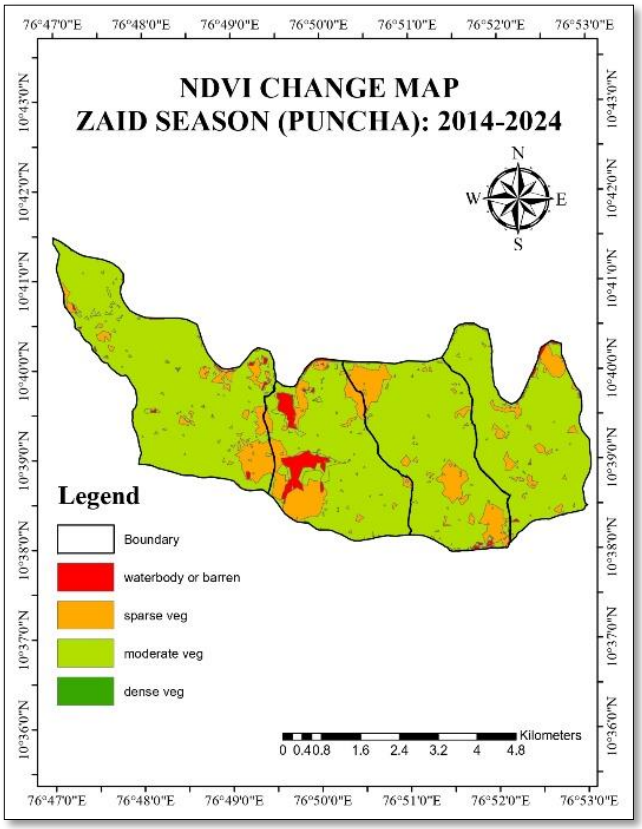


**Fig. 4.35 NDVI change map of zaid season based on density**

The NDVI change analysis for the Zaid season (Puncha) shows that 85.641% of the area experienced no change in vegetation cover, indicating stability in vegetation during this season as shown in Fig. 4.36. About 12.743% of the area showed a positive change, suggesting improved vegetation health or density. Meanwhile, only 1.616% of the area experienced a negative change, indicating a minor decline in vegetation.

Overall, the season was marked by vegetation stability with a small portion of improvement and minimal degradation.

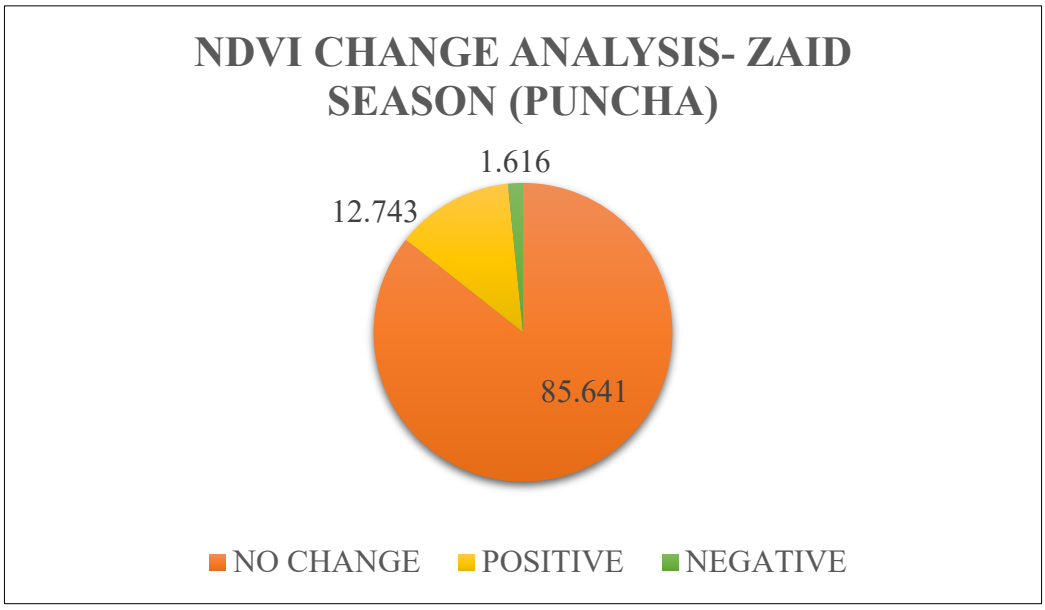


**Fig. 4.36 NDVI change analysis of zaid season based on density**

### 4.2.4 NDVI changes analysis based on vegetative health

#### *4.2.4.1 Kharif season*

This NDVI Change map for the Kharif season illustrates vegetation health across the Puncha region. The map classifies areas into three categories based on NDVI (Normalized Difference Vegetation Index): Moderate Healthy Vegetation (green), Unhealthy Vegetation (yellow), and No Vegetation (red). A significant portion of the region shows moderate healthy vegetation, indicating relatively good plant cover and productivity as shown in Fig. 4.37. However, widespread patches of unhealthy vegetation suggest areas experiencing stress, possibly due to reduced rainfall, soil degradation, or human activities. Scattered red zones denote completely barren or built-up areas with no vegetation. Overall, the map highlights a mixed vegetation health status, calling for targeted management interventions in stressed areas.

The NDVI change analysis for the Kharif season (Virippu) indicates that a majority of the area, about 62.479%, experienced no significant change in vegetation health between the observed periods as shown in Fig. 4.38. However, a substantial 31.926% of the area showed a positive change, reflecting an improvement in vegetation cover or health. Conversely, a smaller portion, 5.596%, underwent a negative change,

suggesting degradation or loss of vegetation. Overall, this suggests a relatively stable vegetation trend during the Kharif season, with a notable proportion of improvement.

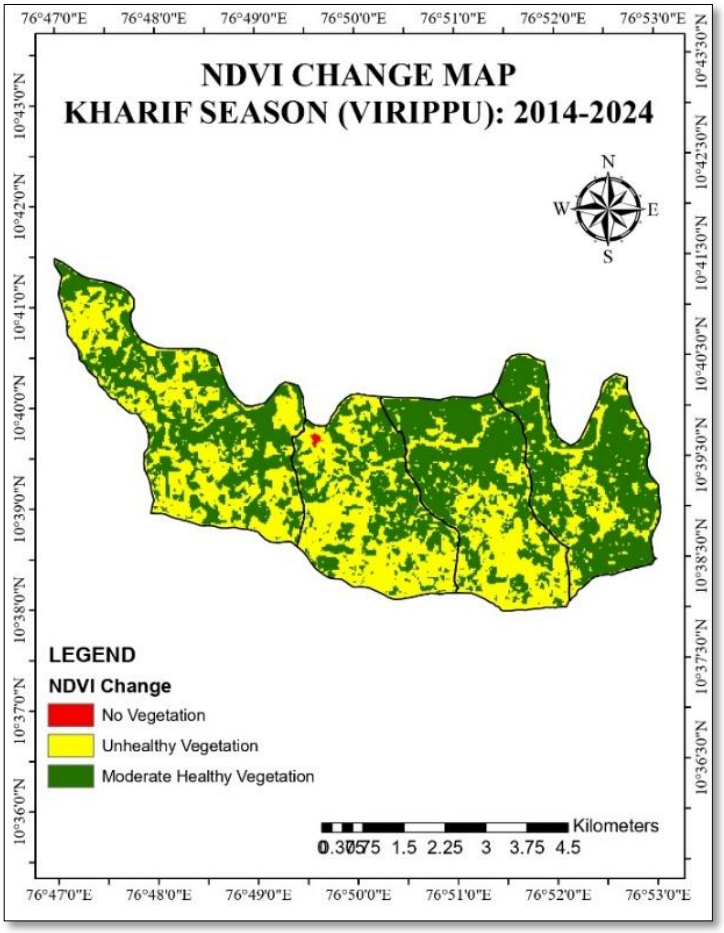


**Fig. 4.37 NDVI change map of kharif season based on vegetative health**

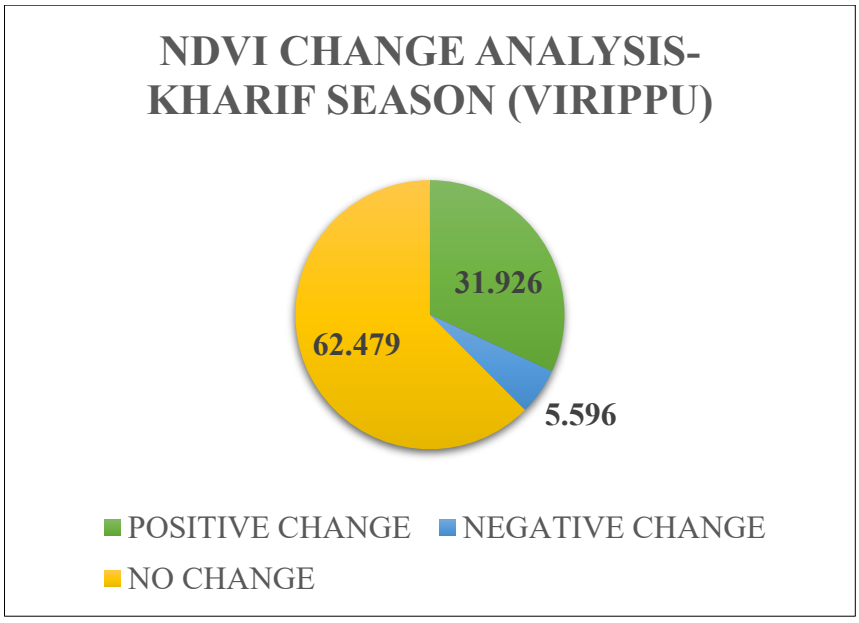


**Fig. 4.38 NDVI change analysis of kharif season based on vegetative health**

### *4.2.4.2 Rabi season*

The NDVI Change Map for the Rabi season (Mundakan) from 2014 to 2024 illustrates vegetation health trends over the decade. The majority of the area is covered by moderate healthy vegetation (green), indicating stable and relatively healthy crop cover during the Rabi season. However, there is a noticeable spread of unhealthy vegetation (yellow), particularly in the central and southeastern regions, suggesting declining vegetation vigor, possibly due to soil degradation, reduced irrigation, or changing agricultural practices. Small pockets of no vegetation (red) are also visible, highlighting barren lands or non-cultivated areas. This spatial pattern reflects a moderate decline in vegetation health over time, underlining the importance of adopting sustainable farming methods to improve Rabi season productivity.

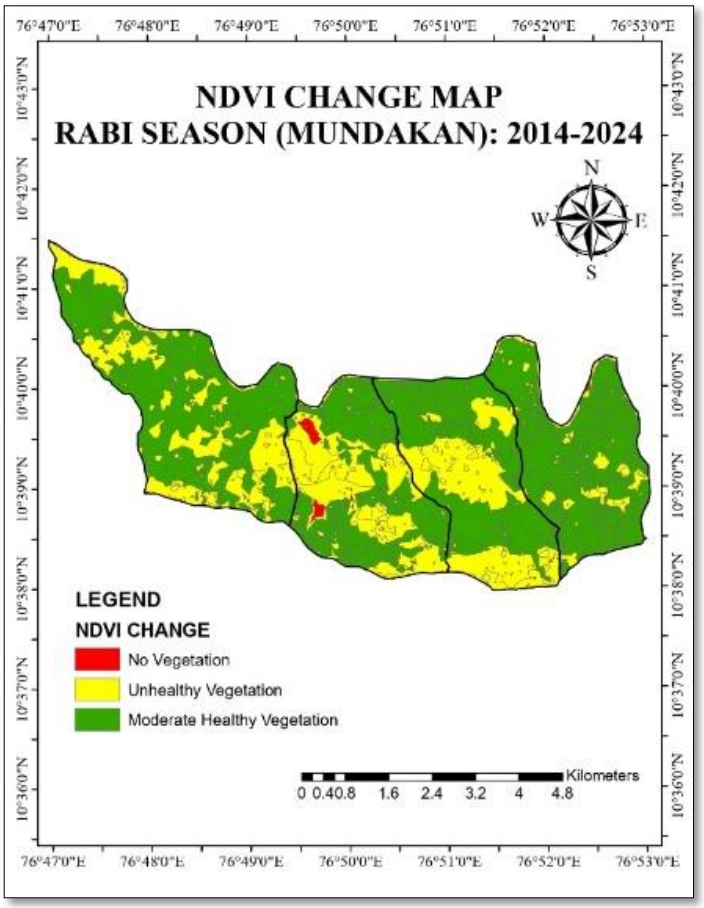


**Fig. 4.39 NDVI change map of rabi season based on vegetative health**

The NDVI change analysis for the Rabi season (Mundakan) reveals that 58.979% of the area experienced no significant change in vegetation health. A considerable 23.983% of the area underwent a negative change, indicating a decline in

vegetation condition during the season. Meanwhile, 17.038% of the area showed a positive change, reflecting some improvement in vegetation health. This pattern suggests that although the majority of the land remained stable, there was a notable proportion experiencing vegetation stress or degradation during the Rabi season.

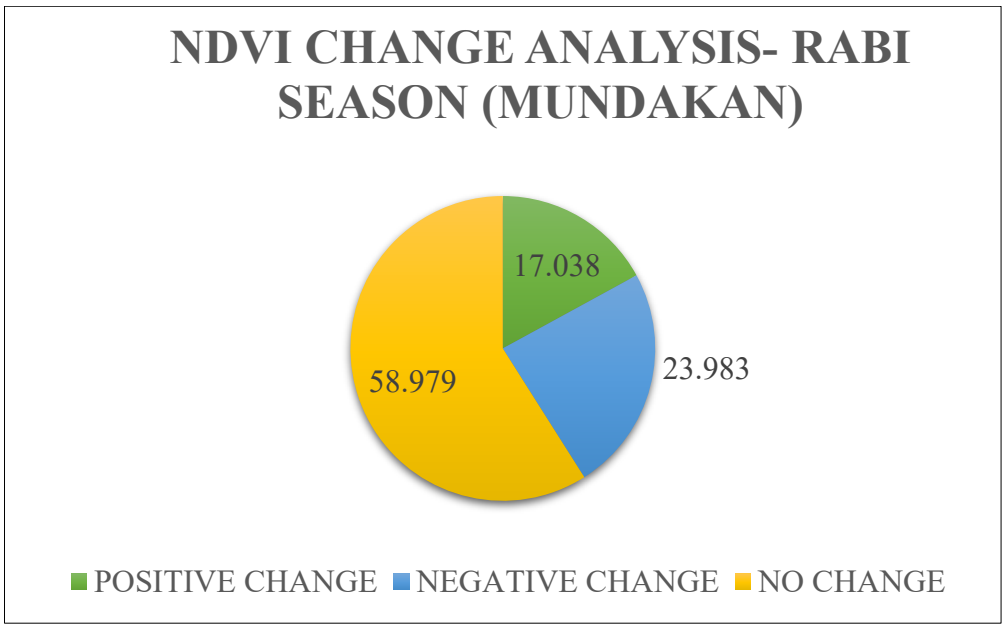


**Fig. 4.40 NDVI change analysis of rabi season based on vegetative health**

### *4.2.4.3 Zaid season*

The NDVI Change Map for the Zaid season (Puncha) from 2014 to 2024 highlights significant variations in vegetation health across the region. A substantial portion of the area is covered by unhealthy vegetation (yellow), particularly in the central and western parts, indicating a decline in plant vigor likely due to limited water availability or suboptimal cultivation practices during the dry Zaid season. Moderate healthy vegetation (green) is seen mainly in the eastern and southeastern zones, suggesting more favorable growing conditions there. Scattered patches of no vegetation (red) further point to barren lands or fallow areas. Overall, the map reflects a concerning trend of reduced vegetation health during the Zaid season, emphasizing the need for improved water management and adaptive agricultural strategies.

The NDVI change analysis for the Zaid season (Puncha) reveals that 53.616% of the area experienced no significant change in vegetation density or health between the years analyzed. However, a substantial 39.903% of the region showed a negative change in NDVI values, indicating a decline in vegetation cover or crop vigor. Only

6.481% of the area exhibited a positive change, reflecting improved vegetation health. This suggests a concerning trend of vegetation degradation during the Zaid season, possibly due to environmental stress, water scarcity, or shifts in land use practices.

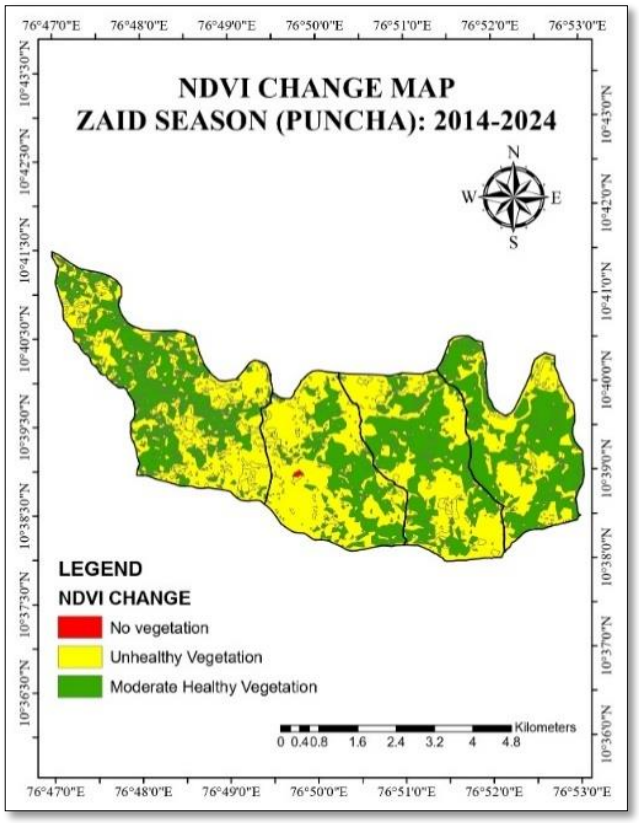


**Fig. 4.41 NDVI change map of zaid season based on vegetative health**

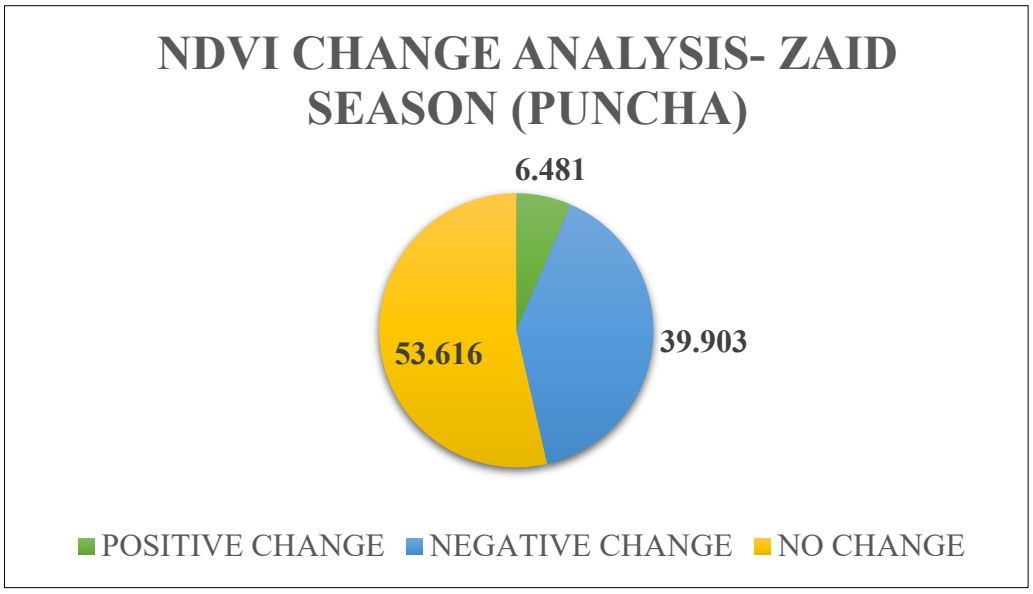


**Fig. 4.42 NDVI change analysis of zaid season based on vegetative health**

4.3 IRRIGATION WATER QUALITY INDEX

### 4.3.1 Water survey

The result of survey conducted from 50 people of 4 micro watersheds of Perumatty Grama Panchayath is given in the Table 4.6.

**Table 4.6 Summary of the survey conducted**

| QUESTIONS | PERCENTAGE | |
|---|---|---|
| Primary source of drinking water? | | |
| Well | 61.70 | |
| Canal | 10.64 | |
| Kokkarni | 38.30 | |
| Bore well | 21.28 | |
| Pond | 14.89 | |
| Others | 14.89 | |
| Do you use this water for irrigation, or other purposes? | | |
| Yes | 80.85 | |
| No | 19.15 | |
| If no, then what is the source for irrigation? | | |
| Supply water | 4.26 | |
| Dam | 10.64 | |
| Same source | 34.04 | |
| QUESTIONS | YES | NO |
| Have you noticed any changes in water availability over the years? | 95.7 | 4.3 |
| Do you notice any changes in the taste, color, or smell of water? | 53.2 | 46.8 |
| Have there been any health issues related to water in your household or neighbourhood? | 2.1 | 97.9 |
| Have you conducted any water quality tests? | 17.0 | 83.0 |
| Have you installed any treatment system for drinking water? | 36.2 | 63.8 |
| Do you think the quality of irrigation water has changed over time? | 76.6 | 23.4 |
| Have you observed any impact of water quality on crop growth or yield? | 80.9 | 19.1 |
| Do you face any issues like soil salinity or poor crop performance due to water quality? | 72.3 | 27.7 |
| Do those crops require good water quality? | 93.6 | 6.4 |
| Have you made any changes in your irrigation practices to cope with water quality issues? | 72.3 | 27.7 |
| Are you aware of any soil and water conservation measures in your area? | 78.7 | 21.3 |
| Have you noticed changes in vegetation, land productivity, or water levels due to these structures? | 78.7 | 21.3 |

### 4.3.2 Collection of water samples

The 13 sample collection points are located in the study area map using ArcGIS as given in the Fig. 4.43.

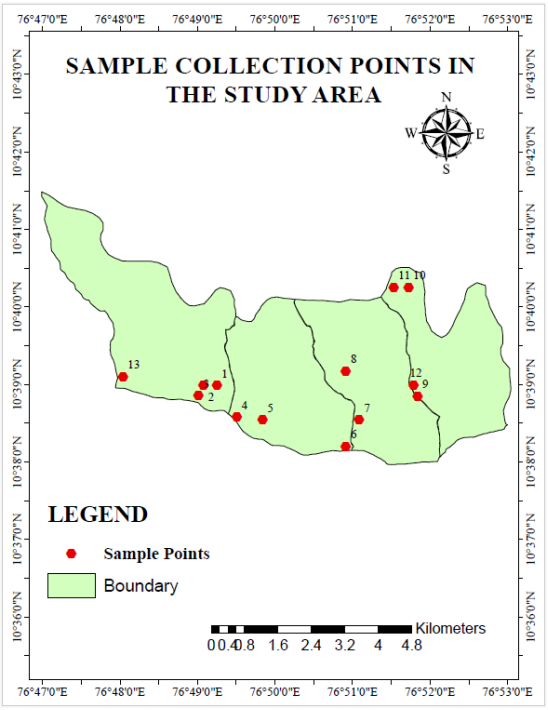


**Fig. 4.43 Sample collection points**

### 4.3.3 Testing and laboratory analysis of samples

The results of the testing and laboratory analysis of the water samples are given in the Fig. 4.44.

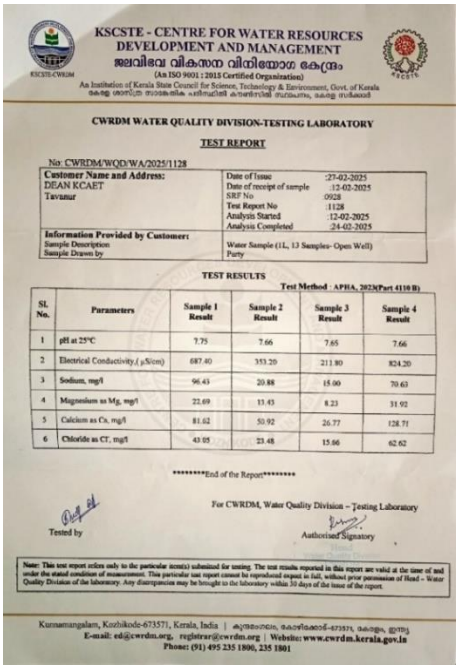

KSCSTE - CENTRE FOR WATER RESOURCES DEVELOPMENT AND MANAGEMENT
ജലവിഭവ വികസന വിനിയോഗ കേന്ദ്രം
(An ISO 9001 : 2015 Certified Organization)
An Institution of Kerala State Council for Science, Technology & Environment, Govt. of Kerala

CWRDM WATER QUALITY DIVISION-TESTING LABORATORY

TEST REPORT

No: CWRDM/WQD/WA/2025/1128

| | |
|---|---|
| **Customer Name and Address:** DEAN KCAET Tavanur | Date of Issue :27-02-2025<br>Date of receipt of sample :12-02-2025<br>SRF No :0928<br>Test Report No :1128<br>Analysis Started :12-02-2025<br>Analysis Completed :24-02-2025 |
| **Information Provided by Customer:**<br>Sample Description<br>Sample Drawn by | Water Sample (1L, 13 Samples- Open Well)<br>Party |

TEST RESULTS

Test Method : APHA, 2023(Part 4110 B)

| Sl. No. | Parameters | Sample 1 Result | Sample 2 Result | Sample 3 Result | Sample 4 Result |
|---|---|---|---|---|---|
| 1 | pH at 25°C | 7.75 | 7.66 | 7.65 | 7.66 |
| 2 | Electrical Conductivity,(µS/cm) | 687.40 | 353.20 | 211.80 | 824.20 |
| 3 | Sodium, mg/l | 96.43 | 20.88 | 15.00 | 70.63 |
| 4 | Magnesium as Mg, mg/l | 22.69 | 13.43 | 8.23 | 31.92 |
| 5 | Calcium as Ca, mg/l | 81.62 | 50.92 | 26.77 | 128.71 |
| 6 | Chloride as Cl, mg/l | 43.05 | 23.48 | 15.66 | 62.62 |

********End of the Report********

Tested by

For CWRDM, Water Quality Division – Testing Laboratory

Authorised Signatory

Note: This test report refers only to the particular item(s) submitted for testing. The test results reported in this report are valid at the time of and under the stated condition of measurement. This particular test report cannot be reproduced (copied) in full, without prior permission of Head - Water Quality Division of the laboratory. Any discrepancies may be brought to the laboratory within 30 days of the issue of the report.

Kunnamangalam, Kozhikode-673571, Kerala, India | കുന്നമംഗലം, കോഴിക്കോട്-673571, കേരളം, ഇന്ത്യ
E-mail: ed@cwrdm.org, registrar@cwrdm.org | Website: www.cwrdm.kerala.gov.in
Phone: (91) 495 235 1800, 235 1801

**Fig. 4.44 CWRDM test report**

**Table 4.7 Summary of test report**

| Sl. No. | Parameters | Sample 1 | Sample 2 | Sample 3 | Sample 4 | Sample 5 | Sample 6 |
|---|---|---|---|---|---|---|---|
| 1 | pH at 25°C | 7.75 | 7.66 | 7.15 | 7.56 | 7.2 | 7.31 |
| 2 | Electrical Conductivity (µS/cm) | 169 | 156 | 218.5 | 202 | 839 | 893 |
| 3 | Sodium (mg/l) | 7.57 | 7.56 | 12.16 | 10.76 | 90.63 | 90.15 |
| 4 | Magnesium as Mg (mg/l) | 2.06 | 2.03 | 2.66 | 2.53 | 19.54 | 17.92 |
| 5 | Calcium as Ca (mg/l) | 12.75 | 12.65 | 18.75 | 17.91 | 127.01 | 130.75 |
| 6 | Chloride as $Cl^-$ (mg/l) | 36.95 | 36.65 | 62.5 | 61.4 | 31.11 | 117.42 |

| Sl. No. | Parameters | Sample 7 | Sample 8 | Sample 9 | Sample 10 | Sample 11 | Sample 12 | Sample 13 |
|---|---|---|---|---|---|---|---|---|
| 1 | pH at 25°C | 7.56 | 7.8 | 7.7 | 8.16 | 7.56 | 7.75 | 8.1 |
| 2 | Electrical Conductivity (µS/cm) | 1093.6 | 840.8 | 318 | 177 | 192 | 356 | 412 |
| 3 | Sodium (mg/l) | 135.9 | 79.32 | 21.06 | 20.6 | 26.81 | 35.66 | 41.78 |
| 4 | Magnesium as Mg (mg/l) | 37.49 | 17.72 | 5.66 | 5.56 | 6.12 | 8.04 | 8.96 |
| 5 | Calcium as Ca (mg/l) | 139.9 | 124.68 | 30.16 | 29.75 | 31.8 | 41.75 | 45.65 |
| 6 | Chloride as $Cl^-$ (mg/l) | 113.51 | 62.42 | 70.45 | 19.57 | 19.57 | 40.65 | 41.05 |

### 4.3.4 Computation of irrigation water quality index (IWQI)

#### *4.3.4.1 Computation of groundwater quality parameters*

Thirteen groundwater samples collected from the study area were analyzed to assess their suitability for irrigation purposes. The selected parameters, Electrical Conductivity (EC), Sodium ($Na^+$), Calcium ($Ca^{2+}$), Magnesium ($Mg^{2+}$), and Chloride ($Cl^-$) play vital roles in determining the usability of water for agricultural applications (Ayers & Westcot, 1985). All ion concentrations, except pH, were converted from mg/L to meq/L using standard conversion factors to enable compatibility with index-based calculations and ensure uniformity in comparative analysis.

In this study, pH was not included in the calculation of the Irrigation Water Quality Index (IWQI), despite being a commonly measured parameter in water quality assessments. The pH values observed across all sampling locations were fairly uniform,

ranging from 7.15 to 8.16, which indicates neutral to slightly alkaline conditions that are generally considered acceptable for irrigation. Moreover, previous studies, such as Ibrahim *et al*. (2023), have demonstrated that while pH is routinely monitored, it is not always incorporated into the IWQI itself. This is because pH typically contributes less to irrigation suitability compared to parameters like electrical conductivity (EC), sodium adsorption ratio (SAR), sodium, and chloride, which have more direct impacts on soil structure and crop health.

#### *4.3.4.2 Sodium hazard evaluation: SAR and sodium percentage (%Na)*

Sodium Adsorption Ratio (SAR), which quantifies the potential risk of soil permeability reduction due to excess sodium, ranged from 0.59 (Sample 11) to 2.43 (Sample 1) as given in Table 4.8. These values are well below the critical threshold of 10 (Richards, 1954), suggesting that none of the samples pose a significant sodium hazard to soil structure.

The Sodium Percentage (%Na), which reflects the relative sodium concentration compared to calcium and magnesium, ranged from 12.39 % to 41.34 %. While Sample 1 exhibited the highest %Na, it still remained within the acceptable limits for irrigation (Todd, 1980). However, elevated %Na values in certain samples indicate the potential for long-term sodicity issues, especially in poorly drained soils or under continuous use.

#### *4.3.4.3 Irrigation water quality index (IWQI) assessment*

To holistically evaluate irrigation suitability, the Irrigation Water Quality Index (IWQI) was computed using a weighted aggregation of quality scores ($q_i$) for four key parameters: EC, $Na^+$, SAR, and $Cl^-$. Each parameter's score was derived through class-wise linear interpolation based on classification limits adapted from FAO standards and recent literature (Ayers & Westcot, 1985; Al-Fahdawi *et al*., 2024). The assigned weightings (EC: 0.264, $Na^+$: 0.256, SAR: 0.237, $Cl^-$: 0.243) reflect their relative importance to irrigation quality (Al-Fahdawi *et al*., 2024).

The computed IWQI values ranged from 90.18 to 97.86, with all 13 samples falling into the "Highly suitable for irrigation" category (IWQI > 85), as per the classification system proposed by Jhariya *et al*. (2016). These findings suggest uniformly high irrigation water quality across the study area.

A sample calculation for Sample 1 is provided to demonstrate the step-by-step process, from raw data transformation to final IWQI computation and the summary is given in Table 4.8.

Sample 1:

| | | |
|---|---|---|
| pH (at 25° C) | = | 7.75 |
| EC (µS/cm) | = | 687.4 |
| Sodium (mg/l) | = | 4.192 |
| Magnesium (mg/l) | = | 1.867 |
| Calcium (mg/l) | = | 4.081 |

The equations mentioned in section 3.6.3 was used to find quality index score for EC, Sodium, SAR and Chloride as follows and then IWQI was calculated;

EC:

$$q_{i_{max}} = 100$$

$$q_{i_{min}} = 75$$

$$x_{ij} = 687.4$$

$$x_{inf} = 250$$

$$x_{sup} = 750$$

$$q_i = q_{i_{max}} - \frac{(x_{ij} - x_{inf}) \times (q_{i_{max}} - q_{i_{min}})}{x_{sup} - x_{inf}}$$

$$q_i = 100 - \frac{(687.4-250)\times(100-75)}{750-250} = 86.878$$

Sodium:

$$q_{i_{max}} = 85$$

$$q_{i_{min}} = 60$$

$$x_{ij} = 4.193$$

$$x_{inf} = 3$$

$$x_{sup} = 6$$

$$q_i = q_{i_{max}} - \frac{(x_{ij} - x_{inf}) \times (q_{i_{max}} - q_{i_{min}})}{x_{sup} - x_{inf}}$$

$$q_i = 100 - \frac{(4.193-3)\times(85-60)}{6-3} = 90.062$$

SAR:

$$q_{i_{max}} = 100$$

$$q_{i_{min}} = 85$$

$$x_{ij} = 2.431$$

$$x_{inf} = 0$$

$$x_{sup} = 10$$

$$q_i = q_{i_{max}} - \frac{(x_{ij} - x_{inf}) \times (q_{i_{max}} - q_{i_{min}})}{x_{sup} - x_{inf}}$$

$$q_i = 100 - \frac{(2.431-0)\times(100-85)}{10-0} = 96.353$$

Chloride:

$$q_{i_{max}} = 100$$

$$q_{i_{min}} = 85$$

$$x_{ij} = 1.214$$

$$x_{inf} = 0$$

$$x_{sup} = 1.5$$

$$q_i = q_{i_{max}} - \frac{(x_{ij} - x_{inf}) \times (q_{i_{max}} - q_{i_{min}})}{x_{sup} - x_{inf}}$$

$$q_i = 100 - \frac{(1.214-0)\times(100-85)}{1.5-0} = 87.856$$

IWQI;

$$IWQI = \Sigma(q_{i_i} \times w_i)$$

$$= (0.264 \times 86.878) + (0.256 \times 90.062) + (0.243 \times 87.856) + (0.237 \times 96.353) = 90.176$$

**Table 4.8 Summary of sample data and it's inference after computation**

| SAMPLE No | SAR | %Na | IWQI | INFERENCE |
|---|---|---|---|---|
| 1 | 2.4310616 | 41.342747 | 90.17636 | Highly suitable for irrigation |
| 2 | 0.6718788 | 19.912065 | 96.1723 | Highly suitable for irrigation |
| 3 | 0.6496023 | 24.443932 | 97.86083 | Highly suitable for irrigation |
| 4 | 1.4426086 | 25.308954 | 97.60396 | Highly suitable for irrigation |
| 5 | 1.1978357 | 20.81263 | 92.96699 | Highly suitable for irrigation |
| 6 | 1.0871125 | 20.263432 | 94.10976 | Highly suitable for irrigation |
| 7 | 0.7353401 | 12.387538 | 93.45461 | Highly suitable for irrigation |
| 8 | 1.1042492 | 20.274959 | 94.66069 | Highly suitable for irrigation |
| 9 | 1.3549143 | 24.737775 | 93.36652 | Highly suitable for irrigation |
| 10 | 0.6071142 | 24.446722 | 97.71366 | Highly suitable for irrigation |
| 11 | 0.5924358 | 13.43352 | 94.28781 | Highly suitable for irrigation |
| 12 | 0.8745402 | 16.181337 | 92.0674 | Highly suitable for irrigation |
| 13 | 1.395937 | 34.911331 | 92.92321 | Highly suitable for irrigation |

#### *4.3.4.4 Implications for irrigation management*

The results clearly indicate that the groundwater across all four micro-watersheds is highly suitable for irrigation. The consistently high IWQI values (all > 90) imply that the water is free from salinity or sodicity risks and can be safely used for crop cultivation under standard agronomic practices (Ayers & Westcot, 1985; Jhariya *et al*., 2016).

Although the SAR and %Na values for a few samples (e.g., Samples 1 and 13) are comparatively higher, they still remain within acceptable limits. It is therefore advisable to implement routine monitoring in such locations to detect early signs of degradation. In areas with marginal soil drainage, ameliorative practices such as gypsum application, use of salt-tolerant crops, and ensuring adequate leaching can help maintain long-term productivity (Richards, 1954; Al-Fahdawi *et al*., 2024).

### 4.3.5 Spatial analysis of IWQI using IDW and ordinary kriging

To visualize the spatial variation in irrigation water quality across the study area, Inverse Distance Weighting (IDW) and Ordinary Kriging interpolation methods were employed using ArcGIS. IDW was applied with varying power parameters ranging from 1 to 4, while Ordinary Kriging was performed using five different semi variogram

models: spherical, circular, exponential, Gaussian, and linear. The resulting spatial distribution maps, shown below, illustrate the interpolated irrigation water quality index (IWQI) values based on 13 observed sample points.

From the IDW maps, it is evident that the influence of sample points becomes more localized as the power parameter increases. At lower powers (e.g., p = 1 and 2), the interpolation surfaces are smoother and more generalized, reflecting broader regional trends. As the power increases to 3.5 or 4, the maps exhibit sharper gradients and localized variations, especially near the sampling points, indicating more weight being given to nearby data. This can potentially highlight small-scale variability but may also lead to overfitting if sample density is low.

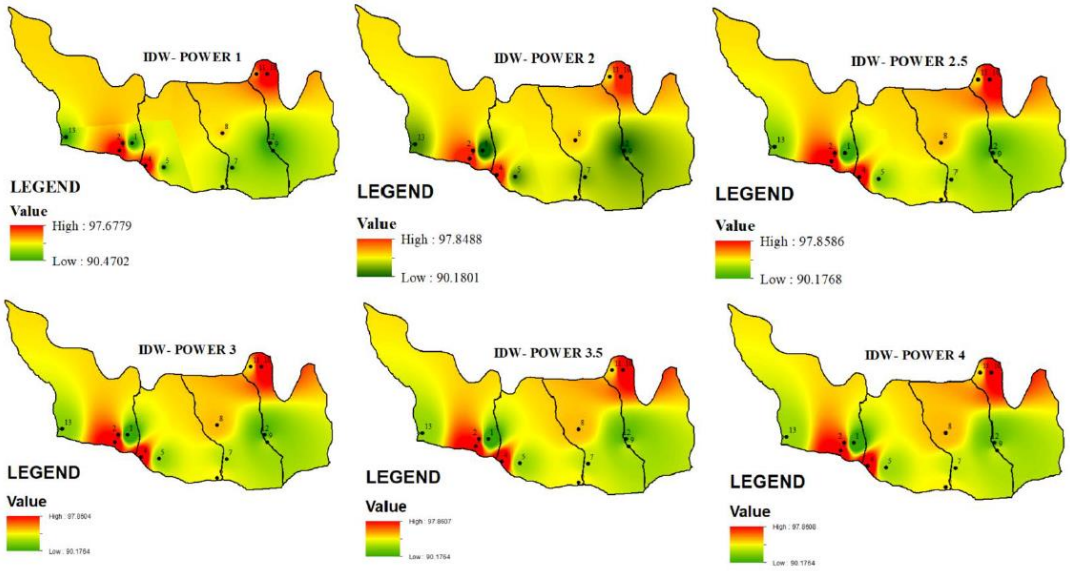


**Fig. 4.45 Different maps generated under different powers**

The Ordinary Kriging maps, on the other hand, display distinct spatial patterns depending on the semi variogram model used. The spherical and Gaussian models produce relatively smooth transitions, suggesting a consistent spatial structure. The exponential model shows localized high and low-value zones, capturing subtle variations in spatial correlation. The linear model, by contrast, shows abrupt changes and patchy distributions, which may oversimplify the spatial relationship. Overall, the exponential and Gaussian models appear more effective in capturing localized variability, while spherical and circular models provide a balanced interpolation with broader coverage.

These maps support the evaluation of spatial patterns in water quality and can guide targeted management interventions in areas exhibiting lower IWQI values.

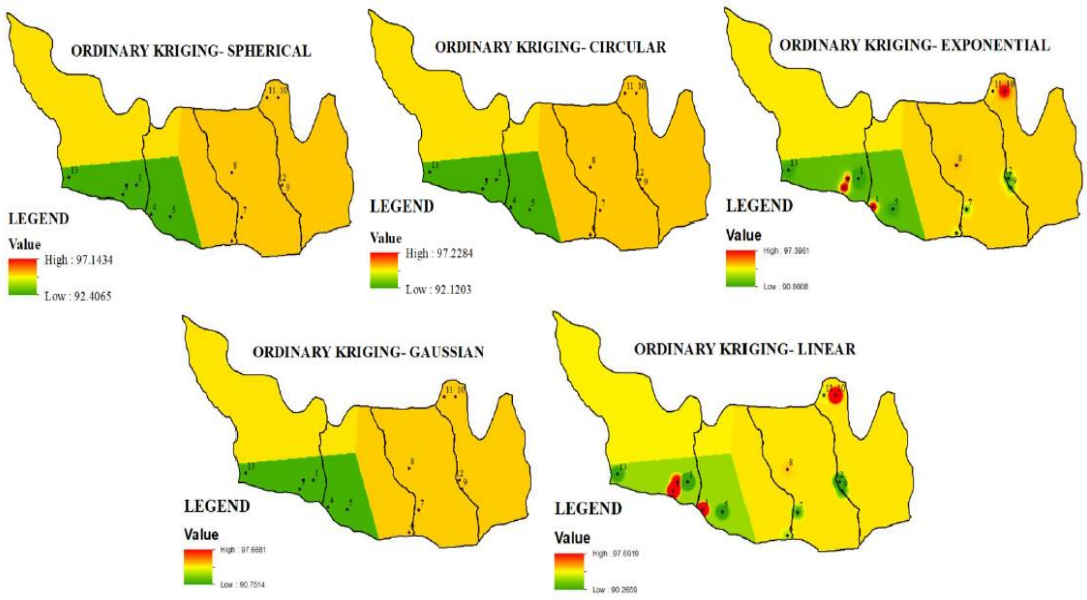


**Fig. 4.46 Different maps generated under different semi-variograms**

### 4.3.6 Performance evaluation using statistical performance indicators

#### *4.3.6.1 Validation*

To evaluate the accuracy of the spatial interpolation methods, validation was performed using three approaches: Leave-One-Out Cross-Validation (LOOCV), split-sample validation with 10 training data set and 3 validation data set, and 7 training data set and 6 validation data set. In each case, the observed values derived from field measurements and calculations were compared with the predicted values obtained from GIS-based interpolation. This comparison allowed for an objective assessment of how well the IDW and Ordinary Kriging methods replicated the actual spatial distribution of irrigation water quality. The predictive performance was quantified using various error metrics such as Correlation Coefficient (R), Coefficient of Determination ($R^2$), Mean Error (ME), Mean Absolute Error (MAE), and Percent Bias (PBIAS), as detailed in the following section.

#### *4.3.6.2 Evaluation*

i. Split-sample validation approach for spatial interpolation

To evaluate the spatial interpolation performance, IDW and Ordinary Kriging methods were applied after splitting the sample into 6 validation data set and 7 training data set and 3 validation data set and 10 training data set.

- 6 validation data sets and 7 testing data sets

In this phase of the study, interpolation accuracy was evaluated using 6 validation data sets and 7 training data sets, allowing for a more robust assessment of model performance across different spatial configurations. Different statistical performance indicators were evaluated as shown in the Table 4.9.

**Table 4.9 Statistical metrics for 6 validation data sets and 7 testing data sets**

| | 1 | 2 | 2.5 | 3 | 3.5 | 4 | Spher-ical | Circ-ular | Expon-ential | Gaus-sian | Lin-ear |
|---|---|---|---|---|---|---|---|---|---|---|---|
| **R** | -0.34 | -0.43 | -0.45 | -0.47 | -0.49 | -0.51 | -0.24 | -0.29 | 0.00 | 0.00 | -0.37 |
| **R2** | 0.12 | 0.19 | 0.20 | 0.22 | 0.24 | 0.26 | 0.06 | 0.09 | 0.00 | 0.00 | 0.14 |
| **RMSE** | 2.98 | 3.67 | 3.91 | 4.09 | 4.29 | 4.40 | 2.96 | 3.12 | 2.59 | 2.59 | 3.24 |
| **MAE** | 2.46 | 3.17 | 3.38 | 3.53 | 3.68 | 3.77 | 2.42 | 2.57 | 1.99 | 1.99 | 2.73 |
| **ME** | -1.72 | -1.89 | -1.94 | -1.98 | -2.08 | -2.08 | -1.80 | -1.88 | -1.57 | -1.57 | -1.83 |
| **PBIAS** | 1.80 | 1.98 | 2.04 | 2.07 | 2.18 | 2.18 | 1.89 | 1.97 | 1.64 | 1.64 | 1.92 |

In the case of IDW interpolation, it was observed that increasing the power from 1 to 4 led to progressively higher RMSE and MAE values. The lowest RMSE (2.98) and MAE (2.46) were recorded for power = 1, while power = 4 produced the highest RMSE (4.40) and MAE (3.77), indicating reduced prediction accuracy with higher powers. Thus, IDW with power = 1 showed the best balance of predictive performance among the IDW variations.

For Ordinary Kriging, the Gaussian and Exponential semi variogram models yielded the lowest RMSE (2.60) and MAE (1.99), with relatively better ME and PBIAS values compared to others. Interestingly, the correlation coefficients (R) were effectively zero for both models, and $R^2$ was also zero, indicating that these models did not capture linear trends well, despite the lower error metrics. This could be attributed to the smooth transitions typical of exponential and Gaussian models, which may reduce prediction error in sparsely sampled areas. However, the Spherical model, while

having slightly higher RMSE and MAE, yielded better R (-0.244) and $R^2$ (0.0596) than Exponential and Gaussian, hinting at a better fit to the spatial structure. The Linear model showed the highest $R^2$ (0.1365) among Ordinary Kriging models but also resulted in the highest RMSE (3.24) and MAE (2.73), making it less favourable overall.

When comparing IDW and Ordinary Kriging, the Exponential and Gaussian models outperformed IDW in terms of lower error metrics, suggesting better interpolation accuracy. However, IDW with power = 1 remained competitive, particularly in terms of simplicity and performance consistency. The spatial maps further illustrate these findings, IDW maps exhibit sharp gradients near sampling points (especially at higher powers), while Ordinary Kriging maps, particularly with Gaussian and Exponential models, display smoother and more generalized spatial patterns.

In conclusion, for this setup with 6 validation data sets and 7 testing data sets, Ordinary Kriging using the Gaussian or Exponential semi variogram model provided the most accurate predictions, followed closely by IDW with power = 1. Therefore, these models are recommended for generating spatial water quality maps under similar sampling conditions.

- 3 validation data sets and 10 testing data sets

With three validation data set and ten testing data set, the performance of the IDW and Ordinary Kriging interpolation methods was evaluated to determine their predictive accuracy in spatial water quality mapping.

**Table 4.10 Statistical metrics for 3 validation data sets and 10 testing data sets**

| | 1 | 2 | 2.5 | 3 | 3.5 | 4 | Spher-ical | Circ-ular | Expon-ential | Gaus-sian | Lin-ear |
|---|---|---|---|---|---|---|---|---|---|---|---|
| **R** | 0.51 | 0.32 | 0.60 | 0.27 | 0.37 | 0.39 | - | - | 0.05 | -0.19 | - |
| **R2** | 0.26 | 0.11 | 0.36 | 0.08 | 0.14 | 0.15 | - | - | 0.00 | 0.04 | - |
| **RMSE** | 1.16 | 1.00 | 1.06 | 0.97 | 1.01 | 1.03 | 1.20 | 1.20 | 1.20 | 1.20 | 1.20 |
| **MAE** | 0.47 | 0.37 | 0.43 | 0.32 | 0.39 | 0.41 | 0.50 | 0.50 | 0.49 | 0.50 | 0.50 |
| **ME** | -0.39 | -0.29 | -0.35 | -0.24 | -0.30 | -0.31 | -0.41 | -0.41 | -0.41 | -0.41 | -0.41 |
| **PBIAS** | 1.78 | 1.31 | 1.57 | 1.06 | 1.37 | 1.42 | 1.86 | 1.86 | 1.86 | 1.86 | 1.86 |

For the IDW method, the power values tested ranged from 1 to 4. Among these, IDW with power 3 demonstrated the most favorable overall performance. It achieved the lowest RMSE of 0.968 and MAE of 0.322, which indicates that the predictions were

closest to the observed values with minimal average error. Additionally, this configuration resulted in the lowest PBIAS (1.062), meaning the prediction bias was relatively small, reflecting comparatively better model efficiency.

While IDW with power 2.5 gave the highest R value of 0.603 and $R^2$ of 0.364, these improvements in correlation did not translate into better error performance compared to power 3. The RMSE and MAE were slightly higher, and the bias was more pronounced. On the other hand, power values of 1, 2, 3.5, and 4 showed either higher error magnitudes or stronger biases, making them less optimal for this dataset.

In the case of Ordinary Kriging, across all these models, the results were nearly identical and notably poor. The RMSE was consistently high at approximately 1.202, and the MAE remained close to 0.495, which signifies that the predictions deviated more from the actual values than in the IDW cases. Moreover, the PBIAS was around 1.856, showing a significant overestimation in the predicted values. All models also recorded very low or negative R and $R^2$ values, with the best R (0.047) observed for the Exponential model, which is statistically insignificant.

In conclusion, when using three validation data set and ten testing data set, IDW with power 3 clearly outperformed all other methods and configurations. It provided a better balance between correlation and error statistics and showed less prediction bias. Conversely, all Ordinary Kriging models failed to deliver acceptable results, likely due to insufficient spatial variability representation with the limited dataset. Therefore, for scenarios involving a small number of validation points, IDW with a carefully chosen power setting, particularly power 3 in this case, is recommended over Ordinary Kriging.

ii. Leave-one-out cross-validation (LOOCV)

To evaluate the accuracy and robustness of spatial interpolation techniques used for mapping irrigation water quality, Leave-one-out cross-validation (LOOCV) was conducted. This method systematically excludes each sample point one at a time, predicts its value using the remaining dataset, and compares the prediction against the observed value. Statistical performance indicators were computed to assess and compare the performance of Inverse Distance Weighting (IDW) and Ordinary Kriging.

**Table 4.11 Statistical metrics for LOOCV**

| | 1 | 2 | 2.5 | 3 | 3.5 | 4 | Spher-ical | Circ-ular | Expon-ential | Gaus-sian | Lin-ear |
|---|---|---|---|---|---|---|---|---|---|---|---|
| **R** | -0.30 | -0.15 | -0.11 | -0.09 | -0.08 | -0.07 | -0.79 | -0.78 | -0.76 | -0.78 | -0.56 |
| **R2** | 0.09 | 0.02 | 0.01 | 0.01 | 0.01 | 0.01 | 0.62 | 0.61 | 0.58 | 0.61 | 0.32 |
| **RMSE** | 2.61 | 2.87 | 2.96 | 3.01 | 3.04 | 3.06 | 2.65 | 2.66 | 2.63 | 2.63 | 2.58 |
| **MAE** | 1.98 | 2.32 | 2.45 | 2.52 | 2.56 | 2.58 | 2.09 | 2.10 | 2.07 | 2.08 | 1.99 |
| **ME** | 0.18 | 0.36 | 0.45 | 0.50 | 0.52 | 0.55 | 0.10 | 0.11 | 0.12 | 0.08 | 0.18 |
| **PBIAS** | -0.19 | -0.38 | -0.47 | -0.53 | -0.55 | -0.58 | -0.11 | -0.11 | -0.13 | -0.09 | -0.19 |

IDW interpolation was at different power values ranging from 1 to 4. As the power increased, the interpolation became increasingly influenced by nearby points, but the overall predictive performance deteriorated. Despite having the best results among the IDW powers, the low R and $R^2$ values indicate weak correlation and low predictive reliability, consistent with findings by Dewana *et al*. (2022) and Singh & Verma (2019), who emphasized the limitations of IDW in heterogeneous landscapes. With increasing powers (2 to 4), a consistent degradation in performance was observed, with $R^2$ decreasing to 0.00546 at Power 4 and RMSE increasing to 3.0619. PBIAS also worsened, indicating increasing deviation from observed values.

Ordinary Kriging, a geostatistical interpolation method, was tested using five different semi variogram models: spherical, circular, exponential, Gaussian, and linear. Among these, the gaussian semi variogram exhibited the best performance. This indicates a strong correlation between predicted and observed values and suggests that Ordinary Kriging with a gaussian semi variogram captures spatial variability better than IDW. The exponential and spherical models also showed relatively high $R^2$ values (0.57678 and 0.620 respectively) and comparable error metrics, further demonstrating Ordinary Kriging's reliability in spatial prediction.

Notably, even the worst-performing Ordinary Kriging model (linear semi variogram) outperformed the best IDW power (Power = 1) in terms of $R^2$ and PBIAS, suggesting Ordinary Kriging's overall superiority in modelling complex spatial patterns of groundwater quality.

The comparison clearly highlights that Ordinary Kriging outperforms IDW in all major validation metrics. While IDW is computationally simpler, its performance especially at higher powers deteriorates significantly. Ordinary Kriging, though more computationally intensive, delivers more reliable and accurate predictions, making it

the preferred choice for interpolating groundwater quality parameters in small-scale watersheds with variable conditions, aligning with previous studies (Al-Fahdawi *et al*., 2024; Vasistha & Ganguly, 2022).

The results highlighted the better performance of the Ordinary Kriging method, particularly with the Gaussian semi-variogram model. Among all interpolation techniques evaluated, Ordinary Kriging with the Gaussian model consistently yielded the lowest error metrics (RMSE, MAE) and exhibited minimal bias (PBIAS), demonstrating its strong ability to capture spatial dependence in the dataset. This method's effectiveness in the LOOCV scenario, where each point is validated individually using the remaining data, underscores its reliability for irrigation water quality mapping when adequate sampling is available. These findings support the selection of Ordinary Kriging with a Gaussian semi-variogram as the most suitable interpolation approach for achieving high-accuracy spatial predictions in well-sampled conditions (Li & Heap, 2008).

### 4.3.7 Spatial mapping of IWQI

The following are the maps generated by interpolating the 13 sample points using the Ordinary Kriging Gaussian semi-variogram model.

1. Chloride ($Cl^-$) map

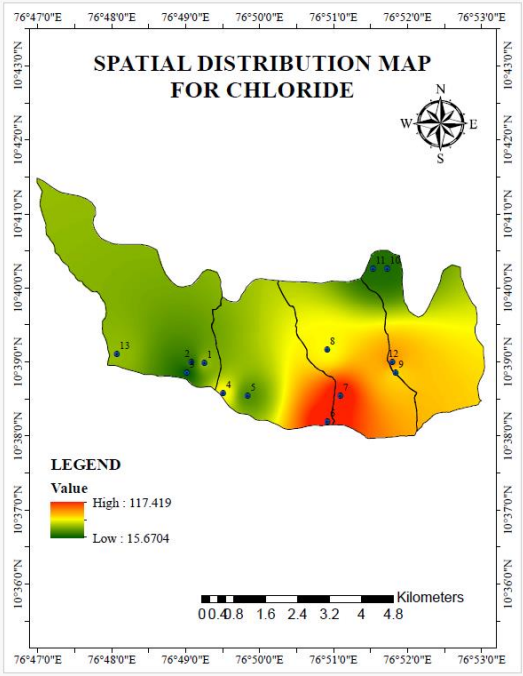


**Fig. 4.47 Spatial distribution map for chloride**

2. Sodium adsorption ratio (SAR) map

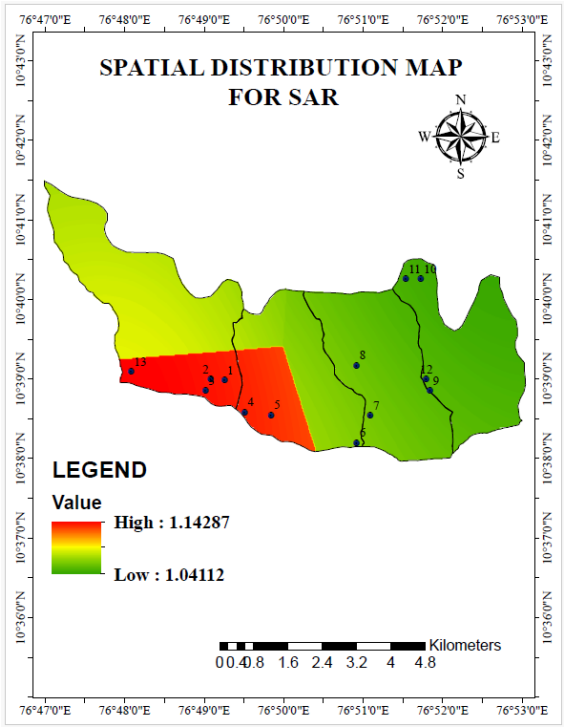


**Fig. 4.48 Spatial distribution map for SAR**

3. Electrical conductivity (EC) map

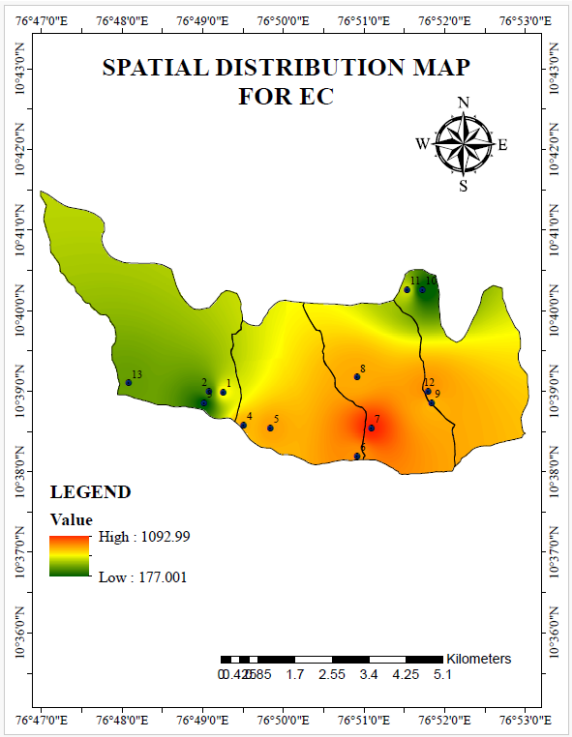


**Fig. 4.49 Spatial distribution map for EC**

4. pH map

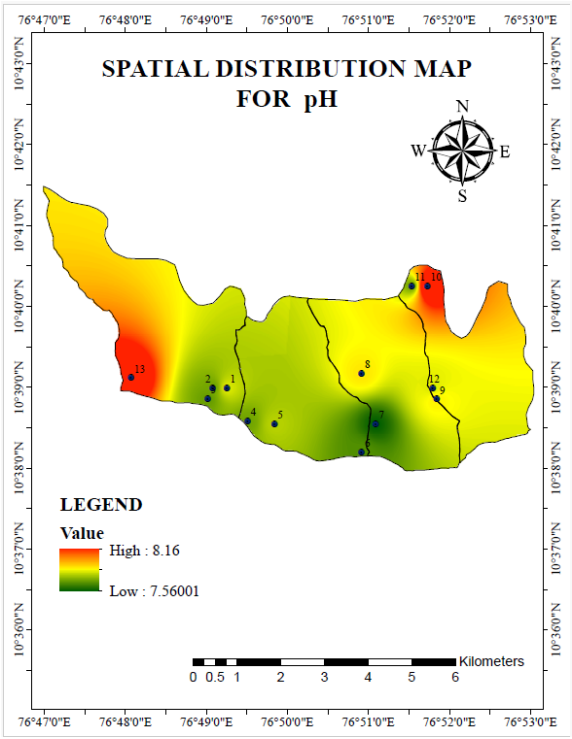


**Fig. 4.50 Spatial distribution map for pH**

5. Magnesium ($Mg^{2+}$) map

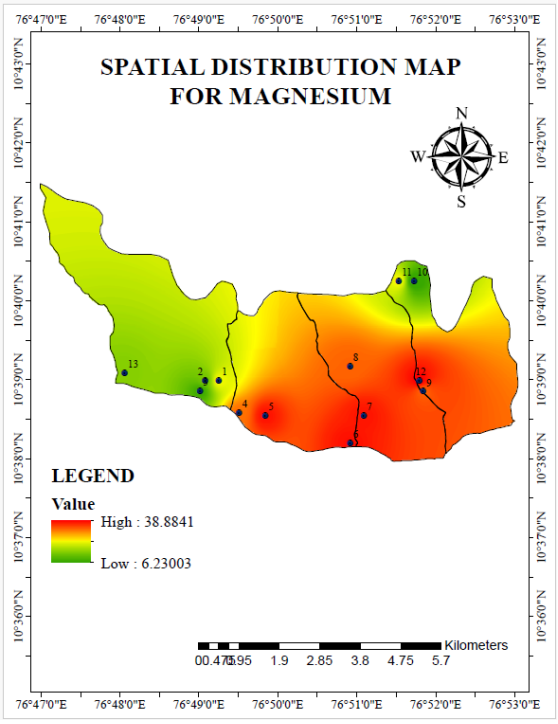


**Fig. 4.51 Spatial distribution map for magnesium**

6. Sodium ($Na^+$) map

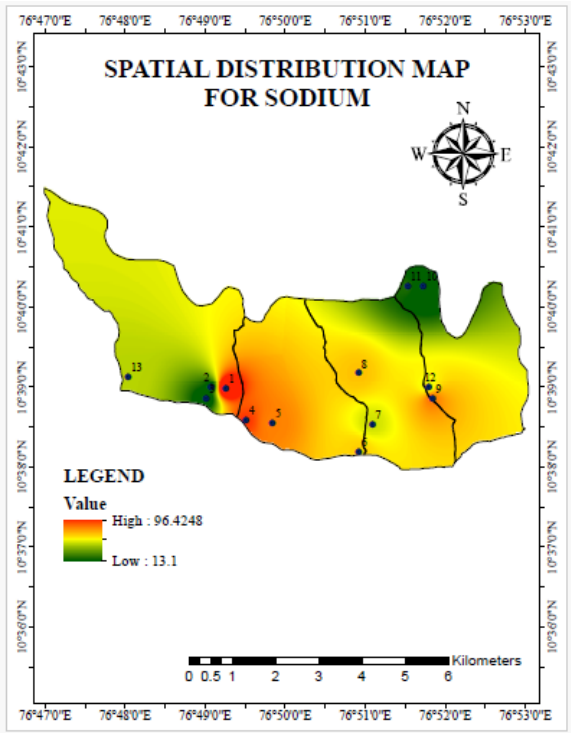


**Fig. 4.52 Spatial distribution map for sodium**

7. Calcium ($Ca^{2+}$) map

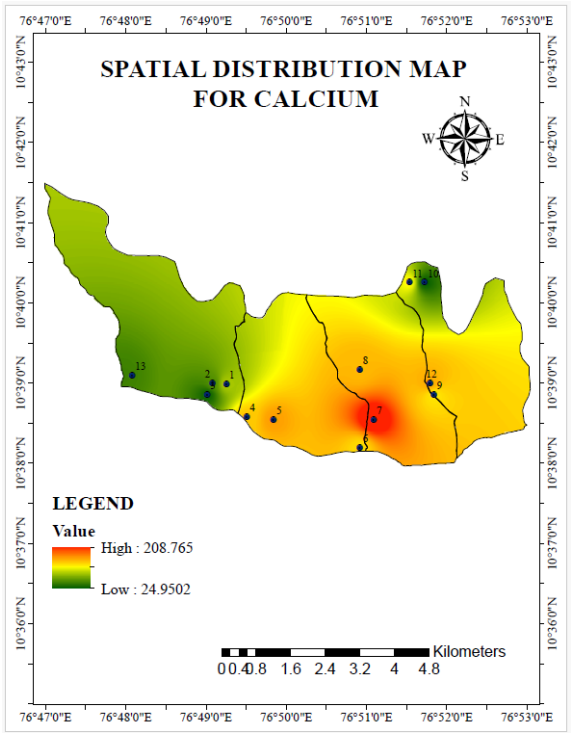


**Fig. 4.53 Spatial distribution map for calcium**

8. IWQI map

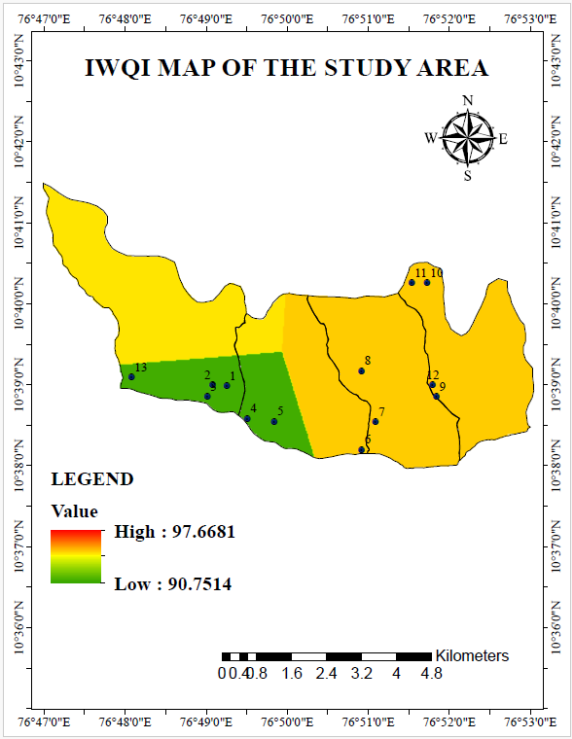


**Fig. 4.54 Spatial distribution map for IWQI**

4.4 EFFECT OF LULC ON WQI

The result of the Zonal Statistics done in the ArcGIS is given in the Table 4.12.

**Table 4.12 Summary of zonal statistics**

| CLASS NAME | COUNT | AREA | MIN | MAX | RANGE | MEAN | STD | SUM |
|---|---|---|---|---|---|---|---|---|
| **Barren** | 12035 | 7936630 | 94.07 | 94.54 | 0.47 | 94.30 | 0.17 | 1136206.79 |
| **Build -up** | 3264 | 2152485 | 94.25 | 94.49 | 0.24 | 94.37 | 0.14 | 308293.89 |
| **Field** | 4352 | 2869980 | 93.86 | 94.79 | 0.93 | 94.33 | 0.15 | 411121.41 |
| **Vegetation** | 28924 | 19074290 | 94.56 | 95.57 | 1.01 | 95.07 | 0.11 | 2733133.26 |
| **Waterbody** | 1470 | 969409.7 | 93.04 | 94.54 | 1.50 | 93.79 | 0.18 | 138797.39 |

The zonal statistics derived from GIS analysis provide a clear understanding of how different land use/land cover (LULC) classes influence water quality in the study area. The analysis was based on water quality index (WQI) or a comparable parameter extracted across five primary land cover types: barren land, built-up areas, agricultural fields, vegetation, and waterbodies. Each class was assessed for statistical attributes such as mean, minimum, maximum, standard deviation, and spatial extent, helping to identify patterns in water quality variation across the landscape.

Among all LULC types, vegetation covers the largest area (approximately 19 million square meters) and demonstrates the highest mean WQI value of 95.07, along with the lowest standard deviation (0.11). This suggests that water quality is not only highest but also most stable in vegetated zones. Dense vegetation plays a critical ecological role by stabilizing soil, reducing surface runoff, and naturally filtering pollutants before they reach water bodies. As a result, these areas contribute significantly to maintaining consistently high-water quality across the landscape.

In contrast, barren lands show a mean WQI of 94.30, slightly lower than that of vegetated areas, and a higher standard deviation of 0.17. Although the range is modest (0.47), it indicates greater variability in water quality. This is likely due to erosion and the unregulated movement of sediments and debris into nearby water systems from exposed and sparsely vegetated surfaces, which can intermittently degrade water quality depending on weather and land conditions.

Agricultural fields (labelled as "Field") display a mean WQI of 94.33, which is slightly higher than barren land but lower than vegetation. However, fields have a range of 0.93, one of the widest among all classes, indicating considerable variability. This fluctuation can be attributed to diverse agricultural practices, such as the timing and intensity of fertilizer and pesticide use, irrigation methods, and cropping patterns. Depending on how they are managed, fields can act both as sources of nutrient enrichment and as points of pollution.

Build-up or urban areas have a mean WQI of 94.37 and a moderate standard deviation (0.15) with a small range (0.24), suggesting relatively consistent but slightly diminished water quality. Urban zones contribute to water degradation mainly through surface runoff that carries oils, heavy metals, detergents, and other non-point source pollutants into nearby streams and lakes. Although urban infrastructure may help in regulating water flow, impervious surfaces increase the volume and speed of runoff, reducing the natural filtration processes and slightly lowering water quality.

Waterbodies, though covering a smaller area (~969,410 square meters), exhibit a mean WQI of 93.79, the lowest among all classes, and the highest range (1.50), indicating significant variability. This is expected, as waterbodies act as receptors of all upstream activities and integrate the cumulative effects of various adjacent land uses. While they may not directly contribute to pollution, their water quality reflects inputs

from all surrounding environments, including agricultural runoff, urban discharge, and erosion from barren land.

Overall, the analysis reveals a clear trend: vegetated areas maintain the best and most stable water quality, while barren, agricultural, and urban zones introduce varying degrees of degradation. Waterbodies serve as indicators of overall watershed health, showing both the direct and indirect impacts of land management. These findings highlight the importance of protecting and expanding vegetative cover while implementing sustainable urban and agricultural practices to safeguard water resources for the future.

# SUMMARY AND CONCLUSION

# CHAPTER V

# SUMMARY AND CONCLUSION

The present study was conducted in Perumatty Grama Panchayat of Palakkad district, Kerala, a semi-arid region experiencing serious groundwater depletion and land degradation. With a geographical area of 60.91 km², this panchayat forms part of the Chitturpuzha sub-basin within the Bharathapuzha river basin and has been classified as overexploited in terms of groundwater usage. Excessive dependence on borewells for irrigation and domestic use, combined with changing cropping patterns and erratic rainfall, has made the area highly vulnerable to water scarcity. In this context, the study focused on assessing the effectiveness of soil and water conservation (SWC) structures implemented as part of watershed development programs, utilizing remote sensing, GIS tools, and field validation techniques.

Data for the study were collected from multiple sources. The Department of Soil Survey and Soil Conservation (DSSSC), Palakkad, provided reports on existing conservation interventions, while topographic maps from the Survey of India and a 30-meter resolution SRTM DEM were used for terrain analysis and watershed delineation. Landsat 8 and 9 OLI/TIRS satellite imagery for the years 2014 and 2024 was used to analyse changes in land use/land cover (LULC) and to compute the Normalized Difference Vegetation Index (NDVI). ArcGIS 10.8 served as the core platform for watershed delineation, LULC classification, morphometric analysis, and spatial interpolation of water quality indices. Google Earth Pro was used for ground-truthing, and Microsoft Excel facilitated statistical and graphical analysis of water quality and morphometric parameters.

Three primary soil and water conservation measures were identified in the study area, viz. earthen bunds, farm ponds, and centripetal terraces. Earthen bunds were constructed to slow down surface runoff and enhance water infiltration. These are particularly beneficial for marginal farmers due to their low cost and ability to increase soil moisture. Farm ponds function as rainwater harvesting systems, capturing surface runoff and providing a supplemental irrigation source during dry periods. Centripetal terraces were implemented to control erosion and promote deeper percolation by redirecting runoff toward the centre of agricultural plots. Each of these structures plays

a crucial role in water retention, soil conservation, and enhancing local groundwater recharge.

A key aspect of the study was the morphometric analysis of four micro watersheds; Kambalathara- Kalyanappetta, Sarkkarpathy, Mullanthod, and Muthuswamy. The SRTM DEM was processed using ArcGIS to delineate the catchments and derive various linear, areal, and relief parameters. The watershed was classified as a third-order basin with a dendritic drainage pattern, having homogeneous lithological conditions. The basin has a total area of 33.14 km² and a perimeter of 45.737 km. Basin length was calculated to be 9.583 km with a mean width of 3.458 km, reflecting its elongated shape. Linear parameters such as total stream length (0.386 km), drainage density (1.603 km/km²), and stream frequency (2.142 streams/km²) suggested a moderately dissected terrain with a balanced hydrological response. The mean bifurcation ratio was found to be 3.167, within the expected natural range, implying minimal geological disturbances (Strahler, 1964). The infiltration number (3.433) and drainage intensity (1.337) further indicated moderate infiltration potential and low runoff, while the length of overland flow (0.312 km) pointed to moderate slope gradients and potential for recharge.

Areal and relief aspects reinforced these interpretations. A circularity ratio of 0.199 and an elongation ratio of 0.678 indicated an elongated basin shape, promoting longer runoff concentration time and reducing flash flood risk. The compactness constant (2.240) and shape factor (2.771) confirmed the non-circular morphology of the basin, associated with delayed peak flows. The basin relief was found to be 110 m, and a relief ratio of 0.011 denoted low to moderate slope gradients. A ruggedness number of 0.176 indicated structural stability and reduced susceptibility to erosion and landslides. The aspect map showed a mix of northeast, northwest, and southeast facing slopes, affecting soil moisture distribution and vegetation growth. These morphometric insights were essential to understand how conservation measures aligned with the topographical and hydrological characteristics of the region.

Field surveys, supported by remote sensing and GIS analysis, revealed that the conservation structures were well maintained and had positively influenced local agricultural practices. Interviews with farmers indicated that the availability of water had improved, and there was a visible enhancement in crop yield and soil condition.

Spatial mapping in ArcGIS further confirmed the widespread distribution of conservation structures across the micro watersheds. These findings aligned well with previous studies suggesting that simple interventions such as bunding and terracing can substantially improve water retention and reduce soil erosion (Araya *et al*., 2015; Rockström *et al*., 2003).

The study also examined changes in LULC patterns over a ten-year period using classified Landsat images for 2014 and 2024. During the Kharif season, vegetation cover remained stable, with a marginal increase from 18.57 km² to 18.62 km². However, significant declines were observed in field area, which reduced from 5.75 km² to 2.37 km², possibly due to shifting land use or abandonment. Built-up areas increased from 1.11 km² to 5.22 km², reflecting urban expansion. Alarmingly, water bodies shrank from 1.83 km² to just 0.28 km², pointing to water stress. In contrast, during the Rabi season, vegetation cover increased considerably from 22.69 km² to 28.03 km², and barren land decreased from 4.19 km² to 1.02 km². These trends suggest that conservation measures were more effective during the Rabi season, likely due to improved water retention and delayed runoff.

NDVI analysis was used to quantify vegetation health across seasons. The spatial patterns of NDVI revealed improvements in vegetative potential in regions where conservation structures were densely implemented. These observations support the conclusion that soil and water conservation practices significantly contributed to enhancing vegetation cover, particularly during the dry season when water availability is critical. The NDVI results thus validated the effectiveness of bunds, farm ponds, and terracing in sustaining plant growth by improving soil moisture conditions.

The study further evaluated irrigation water suitability using the Irrigation Water Quality Index (IWQI). Water samples were tested for parameters such as pH, electrical conductivity (EC), sodium, calcium, magnesium, and chloride. IWQI values were calculated by assigning weights to each parameter and aggregating them using established methods. Most locations were classified as suitable to moderately suitable for irrigation. Spatial interpolation of IWQI using both IDW and Kriging methods showed that Kriging with the Gaussian semi variogram provided the most accurate predictions based on higher $R^2$ and lower error metrics values. Validation techniques, including leave-one-out cross-validation (LOOCV), confirmed these results. The

spatial distribution maps clearly indicated that zones with conservation structures had comparatively better IWQI values, affirming the positive impact of watershed interventions on groundwater quality.

Overall, the integration of field surveys, morphometric analysis, NDVI assessment, and IWQI mapping provided a holistic understanding of the environmental dynamics within Perumatty Panchayat. The findings clearly demonstrate that soil and water conservation measures have led to improvements in vegetation health, soil moisture, and irrigation water quality. The elongated geomorphic nature of the basin has complemented the effectiveness of conservation efforts by allowing sufficient time for infiltration and reducing peak runoff. The application of geospatial technologies, particularly GIS and remote sensing, proved indispensable in capturing the spatial and temporal variations in land cover, vegetation, and water quality. These tools not only enhanced the precision of analysis but also enabled the visualization of complex interactions between terrain, vegetation, and hydrology.

In conclusion, this study affirms that strategic implementation of soil and water conservation measures, when aligned with the geomorphological characteristics of a watershed, can significantly enhance land productivity and water sustainability. The positive feedback from farmers, improved vegetation cover during the Rabi season, and improved IWQI values provide compelling evidence of the success of these interventions. Moreover, the methodological framework employed in this study integrating morphometric analysis, RS-GIS techniques, and field-based validation can serve as a replicable model for similar assessments in other semi-arid and overexploited regions.

There is a critical need to ensure the long-term sustainability of these interventions through regular maintenance and community participation. Policy support should aim at scaling up such integrated approaches while promoting local capacity building and stakeholder engagement. The development of real-time GIS dashboards and mobile-based monitoring systems could further improve transparency and effectiveness. Future studies could incorporate climate data, socio-economic indicators, and machine learning models for predictive analysis and adaptive management. Overall, this study highlights the indispensable role of integrated watershed

management in achieving water security, agricultural resilience, and environmental sustainability.

**Plate 5.1 Project team**

# REFERENCES

# CHAPTER VI
# REFERENCES


Abbasnia, A., Yousefi, N., Mahvi, A.H., Nabizadeh, R., Radfard, M., Yousefi, M. and Alimohammadi, M. 2019. Evaluation of groundwater quality using water quality index and its suitability for assessing water for drinking and irrigation purposes: Case study of Sistan and Baluchistan province (Iran). *Human and Ecol. Risk Assess.: An Int. J.* 25(4): 988-1005.

Abijith, D. and Saravanan, S. 2022. Assessment of land use and land cover change detection and prediction using remote sensing and CA Markov in the northern coastal districts of Tamil Nadu, India. *Environ. Sci. and Pollut. Res. 29*(57): 86055-86067.

Agapiou, A. 2020. Estimating proportion of vegetation cover at the vicinity of archaeological sites using sentinel-1 and-2 data, supplemented by crowd sourced open street map geodata. *Appl. Sci. 10*(14): 4764- 4775.

Ahmed, S.A., Chandrashekarappa, K.N., Raj, S.K., Nischitha, V., and Kavitha, G. 2010. Evaluation of morphometric parameters derived from ASTER and SRTM DEM—a study on Bandihole sub-watershed basin in Karnataka. *J. Indian Soc. Remote Sens*. 38(2): 227-238.

Akyurek, Z and Yalçin, G. 2004, July. Analysing flood vulnerable areas with multicriteria evaluation. In *20th ISPRS congress.* 2(1): 359-364.

Al-Fahdawi, M.S. and Hassan, A.S. 2024. Quality evaluation for the life cycle of the construction project in Iraq. *J. of Al-Azhar Univ. Eng. Sector*, *19*(72): 905-925.

Al-Obaidy, A.H.M.J., Al-Janabi, Z.Z. and Al-Mashhady, A.A. 2016. Distribution of some heavy metals in sediments and water in Tigris River. *J. of Glob. Ecol. and Environ*. *4*(3): 140-146.

Arab, S., Bouchelouche, D., Hamil, S. and Arab, A.,2019. Application of water quality index for surface water quality assessment Boukourdane Dam, Algeria. In *Adv. in Sustain. and Environ. Hydrol., Hydrogeology, Hydrochemistry and Water Resour.: Proc. of the 1st Springer Conf. of the Arabian J. of Geosciences*. 2(1): 385-387

Araya, T., Nyssen, J., Govaerts, B., Deckers, J. and Cornelis, W.M. 2015. Impacts of conservation agriculture-based farming systems on optimizing seasonal rainfall partitioning and productivity on vertisols in the Ethiopian drylands. *Soil and Tillage Res. 148*: 1-13.

Ayers, R.S. and Westcot, D.W. 1985. Water quality for agriculture. Rome: Food and agriculture organization of the United Nations. 29(1): 174.

Bajirao, T.S., Kumar, P., Kumar, A., Tarate, C. and Bajirao, S. 2019. Application of remote sensing and GIS for morphometric analysis of watershed: A Review. *Int. J. Chem. Stud*. *7*(2): 709-713.

Baseri, M. and Mahjoobi, E. 2023. Evaluation of Different Spatial Interpolation Methods for IMERG Precipitation Zoning in Neyshabur Basin. *J. of Hydraulic and Water Eng.* 1(1): 89-98.

Bhandari, A.K., Kumar, A. and Singh, G.K. 2012. Feature extraction using NDVI: A case study of Jabalpur city. *Procedia Technol*. 6: 612-621.

Bhatt, S. and Ahmed, S. A. 2014. Morphometric analysis to determine floods in the Upper Krishna basin using Cartosat DEM. *Geocarto Int*. 29(8): 878–894.

Brown, R.M., McClelland, N.I., Deininger, R.A. and Tozer, R.G. 1970. A water quality index-do we dare. *Water and sewage works*, 117(10):32-76.

Chorley, R.J. 1957. A new standard for estimating drainage basin shape. Amer. *J. Sci*. 255: 138-141.

Choudhari, P.P., Nigam, G.K., Singh, S.K., and Thakur, S. 2018. Morphometric based prioritization of watershed for groundwater potential of Mula river basin, Maharashtra, India. *Geol. Ecol. Landsc*. 2: 256–267.

Dewana, B.R., Prasetyo, S.Y.J. and Hartomo, K.D. 2022. Comparison of IDW and Kriging Interpolation Methods Using Geoelectric Data to Determine the Depth of the Aquifer in Semarang, Indonesia. *J. Ilm. Tek. Elektro Komput. dan Inform*. *8*(2): 215-223.

Faniran, A. 1968. The index of drainage intensity: a provisional new drainage factor. *Aust. J. Sci. 31*(9): 326-330.

Gani, M.A., Sajib, A.M., Siddik, M.A. and Moniruzzaman, M. 2023. Assessing the impact of land use and land cover on river water quality using water quality index and remote sensing techniques. *Environ. Monitoring and Assess*. *195*(4): 449-455.

García-Ruiz, J.M., Beguería, S., Nadal-Romero, E., González-Hidalgo, J.C., Lana-Renault, N. and Sanjuán, Y. 2015. A meta-analysis of soil erosion rates across the world. *Geomorphology*. *239*: 160-173.

Gautam, A. and Rai, S.C. 2024. Groundwater zoning and sustainable management strategies for groundwater resources in the Bist-Doab region of Punjab, India. *Environ., Dev. and Sustain.* 26(4): 8421-8442.

Gautam, P.K. 2023. The significance of morphometric analysis of Shimsha River, Karnataka, India to understand the hydrological and morphological characteristics. *River*. 2(4): 490-505.

Gitelson, A.A., Viña, A., Arkebauer, T.J., Rundquist, D.C., Keydan, G. and Leavitt, B. 2003. Remote estimation of leaf area index and green leaf biomass in maize canopies. *Geophys. Res. Lett*. 30(5): 532-546

Goovaerts, P. 2008. Kriging and semivariogram deconvolution in the presence of irregular geographical units. *Math. Geosciences*. *40*: 101-128.

Gupta, S.K. and Shukla, D.P. 2020. Evaluation of topographic correction methods for LULC preparation based on multi-source DEMs and Landsat-8 imagery. *Spatial Inf. Res. 28*(1): 113-127.

Hengl, T. 2009. *A practical guide to geostatistical mapping*. Amsterdam, Netherlands: Hengl. 52(1): 15-20.

Horton, R.E. 1945. Erosional development of streams and their drainage basins; hydrophysical approach to quantitative morphology. *Geol. Soc. Am. Bull.* 56(3): 275-370.

Horton, R.E. 1932. Drainage-basin characteristics. *Transactions, Am. Geophys. Union*. *13*(1): 350-361.

Huan, V.D. 2022, May. Accuracy assessment of land use land cover LULC 2020 (ESRI) data in Con Dao island, Ba Ria–Vung Tau province, Vietnam. In *IOP Conf. Ser.: Earth and Environ. Sci.* IOP Publishing. 1028(1): 12010-12015.

Ibrahim, H., Yaseen, Z.M., Scholz, M., Ali, M., Gad, M., Elsayed, S., Khadr, M., Hussein, H., Ibrahim, H.H., Eid, M.H. and Kovács, A. 2023. Evaluation and prediction of groundwater quality for irrigation using an integrated water quality index, machine learning models and GIS approaches: A representative case study. *Water*. 15(4): 694-700.

Jensen, J.R. 2009. *Remote sensing of the environ.: An earth res. perspective*. Pearson Education India. 2(1): 5-24.

Jhariya, D.C., Kumar, T., Gobinath, M., Diwan, P. and Kishore, N. 2016. Assessment of groundwater potential zone using remote sensing, GIS and multi criteria decision analysis techniques. *J. of the Geol. Soc. of India*. *88*: 481-492.

Jiang, Q., He, X., Wang, J., Wen, J., Mu, H. and Xu, M. 2020. Spatiotemporal analysis of land use and land cover (LULC) changes and precipitation trends in Shanghai. *Appl. Sci. 10*(21): 7897-7905.

Kannan, R. and Venkateswaran, S., 2020. Drainage Morphometric Analysis of the Nagavathi Watershed of Dharmapuri District, Tamil Nadu, India Using SRTM Data and GIS. 2(1): 1-8.

Kato, T., Kuroda, H. and Nakasone, H. 2009. Runoff characteristics of nutrients from an agricultural watershed with intensive livestock production. *J. of Hydrol.* 368(1-4): 79-87.

Kılıç, E. 2020. Evaluation of Göksu River water quality using long-term monitoring data with water quality index method. *Mar. and Life Sci*. 2(1): 5-12.

Kiran, D.A. and Ramaraju, H.K. 2022. Evaluation and correlation analysis of surface water in and around Mangalore Coastal Belt, Karnataka, India. *Asian J. of Water, Environ. and Pollut. 19*(1): 27-32.

Knotters, M. and Brus, D.J. 2010. Estimating space-time mean concentrations of nutrients in surface waters of variable depth. *Water Resour. Res*. 46(8): 1-15.

Kumarasamy, P., Arthur James, R., Dahms, H.U., Byeon, C.W. and Ramesh, R. 2014. Multivariate water quality assessment from the Tamiraparani river basin, Southern India. *Environ. earth sci. 71*: 2441-2451.

Kuntamalla, S., Nalla, M., and Saxena, P.R. 2018. Morphometric Analysis of Drainage Basin through GIS: A Case Study from South Western part of Rangareddy District, Telangana State, India. *In 11th Int. Conf. on Res. in Sci., Technol. and Manag*. 2(1): 11-20.

Li, J. and Heap, A.D. 2008. A review of spatial interpolation methods for environmental scientists. 2(1): 1-7.

Liang, S. 2005. *Quantitative remote sensing of land surf*. John Wiley & Sons.1(2): 6-16.

Loghmari, I., Timoumi, Y. and Messadi, A. 2018. Performance comparison of two global solar radiation models for spatial interpolation purposes. *Renewable and Sustain. Energy Rev.* 82: 837-844.

Lou, C., Al-qaness, M.A., AL-Alimi, D., Dahou, A., Abd Elaziz, M., Abualigah, L. and Ewees, A.A. 2024. Land use/land cover (LULC) classification using hyperspectral images: a review. *Geo-spatial inf. Sci*. 3(1): 1-42.

Lu, G.Y. and Wong, D.W. 2008. An adaptive inverse-distance weighting spatial interpolation technique. *Comput. & geosciences*. 34(9): 1044-1055.

Mangan, P., Haq, M.A. and Baral, P. 2019. Morphometric analysis of watershed using remote sensing and GIS—a case study of Nanganji River Basin in Tamil Nadu, India. *Arabian J. of Geosciences*. 12: 1-14.

Masoumi, Z. and van Genderen, J. 2020. Artificial intelligence for sustainable development of smart cities and urban land-use management. *Geo-Spatial Inf. Sci.* 27(4): 1212-1236.

Melton, M. A. 1957 An Analysis of the Relations among Elements of Climate, Surface Properties, and Geomorphology. Columbia University, New York.

Miller, V.C. 1953. Quantitative geomorphic study of drainage basin characteristics in the Clinch Mountain area, Virginia and Tennessee. Technical report, Columbia University. Department of Geology, no. 3.

Mkhabela, M.S., Bullock, P., Raj, S., Wang, S. and Yang, Y. 2011. Crop yield forecasting on the Canadian Prairies using MODIS NDVI data. *Agri. and Forest Meteorol.*, 151(3): 385-393.

Nag, S.K. 1998. *Morphometric anal. using remote sensing Tech. in the Chaka sub-basin, Purulia district, West Bengal*. Indian Society of Remote Sensing. 26(1–2): 69–76.

Nedd, R., Light, K., Owens, M., James, N., Johnson, E. and Anandhi, A. 2021. A synthesis of land use/land cover studies: Definitions, classification systems, meta-studies, challenges and knowledge gaps on a global landscape. *Land*. *10*(9): 994.

Pandey, S., Kumari, N. and Al Nawajish, S. 2023. Land use land cover (LULC) and surface water quality assessment in and around selected dams of Jharkhand using water quality index (WQI) and geographic information system (GIS). *J. of the Geol. Soc. of India*. *99*(2): 205-218.

Pareta, K. and Pareta, U. 2011. Quantitative morphometric analysis of a watershed of Yamuna basin using ASTER (DEM) data and GIS. *Int. J. Geomat. Geosci*. 2(1): 248–269.

Pettorelli, N., Laurance, W.F., O'Brien, T.G., Wegmann, M., Nagendra, H. and Turner, W. 2014. Satellite remote sensing for applied ecologists: opportunities and challenges. *J. of Appl. Ecol.* 51(4): 839-848.

Ping, S.W., Wong, C., Chan, P., Khairul, N., Maulud, A., Syed, A., Fadhli, S., Syed, A.R., Kemarau, R.A., Hassan, M.I., Amri, F., and Mohd, A. 2024. Optimizing Hydrological Research: Comparative Analysis of DEMs for Enhanced Catchment Area Delineation. *J. Kejuruteraan.* 36(5): 1805-1812.

Rahmi, M., Parikesit, P. and Withaningsih, S. 2024. Vegetation change analysis using Normalized Difference Vegetation Index (NDVI) in Sumedang Regency. In *E3S Web of Conf.* EDP Sciences. 495: 2007-2013.

Ramesh, K. and Elango, L. 2012. Groundwater quality and its suitability for domestic and agricultural use in Tondiar river basin, Tamil Nadu, India. *Environ. monitoring and assess.* 184: 3887-3899.

Rawat, K.S. and Singh, S.K. 2018. Appraisal of soil conservation capacity using Normalized Difference Vegetation Index (NDVI) model-based C factor of RUSLE model for a semi-arid ungauged watershed: a case study. *Water Conserv. Sci. and Eng*. 3: 47-58.

Rekha, B.V., George, A.V. and Rita, M.J.E.R. 2011. Morphometric analysis and micro-watershed prioritization of Peruvanthanam sub-watershed, the Manimala River Basin, Kerala, South India. *Environ. Res. Eng. and Manag. 57*(3): 6-14.

Ren, J., Yang, J., Wu, F., Sun, W., Xiao, X. and Xia, J.C. 2023. Regional thermal environment changes: Integration of satellite data and land use/land cover. *Iscience*. *26*(2).

Richards, L.A. ed. 1954. Diagnosis and improvement of saline and alkali soils (No. 60). US Government Printing Office.

Robeson, S.M., 1997. Spherical methods for spatial interpolation: Review and evaluation. *Cartography and Geographic Inf. Syst. 24*(1): 3-20.

Rockström, J., Barron, J. and Fox, P. 2003. Water productivity in rain-fed agriculture: challenges and opportunities for smallholder farmers in drought-prone tropical agroecosystems. *Water productivity in agri.: Limits and opportunities for improv.*: 145-162.

Rouse Jr, J.W., Haas, R.H., Schell, J.A. and Deering, D.W. 1973, December. Paper a 20. In *Third earth Resour. Technol. satellite-1 Symp.: The Proc. of a Symp. held by Goddard space flight Cent. at Washington.* 351: 309-316.

Rudraiah, M., Govindaiah, S. and Vittala, S.S. 2008. Morphometry using remote sensing and GIS techniques in the sub-basins of Kagna river basin, Gulburga district, Karnataka, India. *J. of the Indian Soc. of remote sensing*. *36*: 351-360.

Schumm, S.A. 1956. Evolution of drainage systems and slopes in badlands at Perth Amboy, New Jersey. *Geol. Soc. Am. Bull.* 67(5): 597-646.

Schumm, S.A. and Hadley, R.F. 1961. *Prog. in the Appl. of landform anal. in studies of semiarid erosion*. US Department of the Interior, Geological Survey. 437(1): 1-7.

Seyam, M.M.H., Haque, M.R., and Rahman, M.M. 2023. Identifying the land use land cover (LULC) changes using remote sensing and GIS approach: A case study at Bhaluka in Mymensingh, Bangladesh. Case Studies *Chem. Environ. Eng*. 7: 100293-100298.

Sharma, R., Rimal, B., Baral, H., Nehren, U., Paudyal, K., Sharma, S., Rijal, S., Ranpal, S., Acharya, R.P., Alenazy, A.A. and Kandel, P. 2019. Impact of land cover change on ecosystem services in a tropical forested landscape. *Resour. 8*(1): 18-25.

Shekar, P.R. and Mathew, A. 2023. Morphometric analysis of watersheds: a comprehensive review of data sources, quality, and geospatial techniques. *Watershed Ecol. Environ.*

Singh, M.C., Satpute, S., and Prasad, V. 2023. Remote sensing and GIS-based watershed prioritization for land and water conservation planning and management. Water Sci. Technol. 88(1): 233-265.

Singh, P. and Verma, P. 2019. A comparative study of spatial interpolation technique (IDW and Kriging) for determining groundwater quality. *GIS and geostatistical tech. for ground. sci.* 43-56.

Smith, K.G. 1950. Standards for grading texture of erosional topography. *Am. J. Sci*. 248(9): 655-668.

Soni, S. 2017. Assessment of morphometric characteristics of Chakrar watershed in Madhya Pradesh India using geospatial technique. *Appl. Water Sci.* 7: 2089-2102.

Sowmya, D.R., Shenoy, P.D., and Venugopal, K.R. 2020. Watershed delineation using SRTM DEM for Bangalore South Region. *Int. J. Eng. Sci. Invention*. 9(3): 1-9.

Sreedevi, P.D., Sreekanth, P.D., Khan, H.H., and Ahmed, S. 2013. Drainage morphometry and its influence on hydrology in a semiarid region: using SRTM data and GIS. *Environ. Earth Sci.* 70: 839-848.

Strahler, A. N. 1964. Quantitative geomorphology of drainage basin and channel networks. Handbook of applied hydrology techniques. *Environ. Conserv. J.* 24(1): 71-81.

Subba Rao, N. 2006. Seasonal variation of groundwater quality in a part of Guntur District, Andhra Pradesh, India. *Environ. Geol. 49*: 413-429.

Sujatha, E.R., Selvakumar, R., Rajasimman, U.A.B., and Victor, R.G. 2015 Morphometric analysis of sub-watershed in parts of Western Ghats, South India using ASTER DEM. *Geomat. Nat. Hazards Risk.* 6(4): 326-341.

Sukristiyanti, S., Maria, R., and Lestiana, H. 2018. Watershed-based morphometric analysis: a review. In IOP conference series: earth and environmental science, IOP *Publ*. 118(1): 12028-12035.

Suresh, R. 2012. *Soil and water conserve. eng.* Standard Publishers Distributors. 6(2):34-67.

Thomas, J. and Prasannakumar, V. 2015. Comparison of basin morphometry derived from topographic maps, ASTER and SRTM DEMs: an example from Kerala, India. *Geocarto Int.* 30(3): 346-364.

Tiwari, R.N. and Kushwaha, V.K., 2021. Watershed prioritization based on morphometric parameters and PCA technique: A case study of Deonar River Sub Basin, Sidhi Area, Madhya Pradesh, India. *J. of the Geol. Soc. of India*. 97(4): 396

Todd, D.K. and Mays, L.W. 1980. Groundwater hydrology. John Wiley & Sons.

Tunas, I.G., Tanga, A. and Oktavia, S.R. 2020. Impact of landslides induced by the 2018 Palu Earthquake on flash flood in Bangga River Basin, Sulawesi, Indonesia. *J. of Ecol. Eng. 21*(2): 190-200.

Uddin, M.G., Nash, S., Rahman, A. and Olbert, A.I. 2022. A comprehensive method for improvement of water quality index (WQI) models for coastal water quality assessment. *Water Res. 219*: 118532.

Umrikar, B.N. 2017. Morphometric analysis of Andhale watershed, taluka Mulshi, district Pune, India. *Appl. Water Sci*. 7: 2231-2243.

United Nations Environment Programme. Division of Early Warning and Assessment, 2011. UNEP year book 2011: emerging issues in our global environment. UNEP/Earthprint.

Vasistha, P. and Ganguly, R. 2022. Water quality assessment in two lakes of Panchkula, Haryana, using GIS: case study on seasonal and depth wise variations. *Environ. Sci. and Pollut. Res. 29*(28): 43212-43236.

Venkatesan, A. 2014. Geoinformatics in fluvial geomorphological study of thoppaiyar sub basin Tamil Nadu India. Ph.D thesis, Periyar University, Salem: 195-200.

Vincy, M.V., Rajan, B., and Kumar, A. P. P. 2012. Geographic information system based morphometric characterization of sub-watersheds of Meenachil river basin, Kottayam district, Kerala, India. *Geocarto Int*. 27(8): 661-684.

Visharolia, U.S., Shrimali, N.J. and Prakash, I. 2017. Watershed delineation of Purna River using geographical information system (GIS). *Int. J. Adv. Eng. Res. Develop.* 690-695.

Vivekananda, G.N., Swathi, R. and Sujith, A.V.L.N. 2021. Retracted article: multi-temporal image analysis for LULC classification and change detection. *European J. of remote sensing*. *54*(2): 189-199.

Waikar, M.L. and Nilawar, A.P. 2014. Identification of groundwater potential zone using remote sensing and GIS technique. *Int.J. of Innovative Res. in Sci., Eng. and Technol.* 3(5): 12163-12174.

Wang, Y., Akeju, O.V. and Zhao, T. 2017. Interpolation of spatially varying but sparsely measured geo-data: A comparative study. *Eng. Geol.* 231: 200-217.

White, R.E. 2005. *Principles and practice of soil sci.: the soil as a natural resour*. John Wiley & Sons. 1(4): 1-13.

Yalcin G, Akyurek Z. 2004. Analysing flood vulnerable areas with multicriteria evaluation. Geo-imagery bridging continents, XXth ISPRS Congress. 2(1): 359–364.

You, H., Tang, X., Deng, W., Song, H., Wang, Y. and Chen, J., 2022. A study on the difference of LULC classification results based on Landsat 8 and Landsat 9 data. *Sustain.* 14(21): 13730-13739.

Zerihun, M., Mohammedyasin, M.S., Sewnet, D., Adem, A.A. and Lakew, M. 2018. Assessment of soil erosion using RUSLE, GIS and remote sensing in NW Ethiopia. *Geoderma regional.* 12: 83-90.

Zhang, X., Chen, X., Zhang, W., Peng, H., Xu, G., Zhao, Y. and Shen, Z. 2022. Impact of land use changes on the surface runoff and nutrient load in the Three Gorges Reservoir Area, China. *Sustain.* 14(4): 2023-2028.

Zhang, Z., Zhang, F., Zhang, Z. and Wang, X. 2023. Study on Water Quality Change Trend and Its Influencing Factors from 2001 to 2021 in Zuli River Basin in the Northwestern Part of the Loess Plateau, China. *Sustain.* 15(8): 6360-6375.

Zhou, J., Feng, K., Li, Y. and Zhou, Y. 2016. Factorial Kriging analysis and sources of heavy metals in soils of different land-use types in the Yangtze River Delta of Eastern China. *Environ. Sci. and Pollut. Res.* 23: 14957-14967.

# IMPACT OF SOIL AND WATER CONSERVATION MEASURES ON IRRIGATION WATER QUALITY AND LULC CHANGES IN PERUMATTY PANCHAYATH

**BY**

**MIDHUN S (2020-02-033)**

**ANN MARIA PETER (2021-02-014)**

**MEENAKSHI MADHUMOHAN (2021-02-031)**

**NASLA SHARIN P (2021-02-035)**

**ABSTRACT OF PROJECT REPORT**

Submitted in partial fulfilment of the requirement for the degree of

***BACHELOR OF TECHNOLOGY IN AGRICULTURAL ENGINEERING***

**Faculty of Agricultural Engineering and Technology**


**Kerala Agricultural University**

**DEPARTMENT OF SOIL AND WATER CONSERVATION ENGINEERING**

**KELAPPAJI COLLEGE OF AGRICULTURAL ENGINEERING AND FOOD TECHNOLOGY**

**Tavanur-679573, Malappuram**

**Kerala, India**

**2025**

## ABSTRACT

This study assesses the impact of soil and water conservation measures on irrigation water quality and LULC changes in Perumatty Panchayath, located in the Chittur block of Palakkad district, Kerala. The region, marked by groundwater overexploitation and shifting agricultural practices, faces critical challenges in sustaining water availability and soil productivity. The project aims to evaluate the effectiveness of conservation practices in addressing these issues using geospatial and analytical methods. A total of four microwatersheds, viz. Sarkarpathy, Mullanthodu, Kambalathara-Kalyanappetta, and Muthuswamy were delineated using SRTM data and ArcGIS tools. Morphometric parameters such as stream order, slope, and drainage density were computed to characterize watershed hydrology. Soil and water conservation measures like bunds, farm ponds, and centripetal terraces were documented to evaluate their impact on land stability and water retention. LULC changes over a decade (2014–2024) were analysed across three seasons, viz. Kharif, Rabi, and Zaid using Landsat 8/9 satellite imagery. Classification accuracy was ensured through supervised learning methods and validated training samples. NDVI was used to assess vegetative health, density, and seasonal dynamics. Results showed positive trends in vegetation recovery in regions with implemented conservation measures. For irrigation water quality assessment, 13 samples were collected and tested for parameters like pH, EC, sodium, chloride, calcium, and magnesium. IWQI was calculated and spatially mapped using IDW) and Kriging interpolation techniques. Comparative validation using statistical metrics such as $R^2$, MAE, ME, and PBIAS indicated Kriging with a Gaussian semi-variogram performed better in heterogeneous areas, while IDW showed reasonable accuracy in uniformly sampled zones. Furthermore, a strong correlation was identified between NDVI-based LULC changes and spatial IWQI variation, highlighting the influence of land cover on water quality. The findings confirm that integrated conservation strategies, when combined with continuous monitoring through remote sensing and GIS, significantly improve both land and water resource sustainability. This study underscores the importance of applying geospatial technologies in evaluating the effectiveness of conservation efforts and provides a scientific foundation for future planning and policy-making in similar agro-ecological settings.